THE UNIVERSITY OF CHICAGO

PALMITOYLATION MEDIATES NEURON-SPECIFIC BACE1 LOCALIZATION: IMPLICATIONS FOR APP PROCESSING USING A KNOCK-IN MOUSE MODEL

A DISSERTATION SUBMITTED TO

THE FACULTY OF THE DIVISION OF THE BIOLOGICAL SCIENCES

AND THE PRITZKER SCHOOL OF MEDICINE

IN CANDIDACY FOR THE DEGREE OF

DOCTOR OF PHILOSOPHY

COMMITTEE ON NEUROBIOLOGY

BY

CELIA GIULIETTA FERNANDEZ

CHICAGO, ILLINOIS

DECEMBER 2015

Dedication

I would like to dedicate this work to my family, especially my parents, Carlos Alejandro Fernandez and Ellen Louise Ekström, for always believing in me and encouraging me to do whatever it is that makes me happy, to keep a positive attitude and work hard to overcome whatever obstacles were in my path. My younger brothers, Nicolas Andrés and Carlos Rafael, have always been very close to me; in particular, Carlos, who has autism, inspired me from a very early age to pursue neuroscience, to try to understand what it means to be autistic or "normal." Finally, my loving & endlessly supportive husband, Zachary James Williams, who, since the first day we met, has encouraged me to push myself farther than I thought possible, without whom I never would have made it this far.

Table of Contents

List of Figures

Acknowledgements

First I would like to thank Dr. Gopal Thinakaran for his support and mentorship throughout this project. Dr. Thinakaran always challenges me and pushes me to stretch myself farther, to accomplish more than I honestly thought possible, and I am a far better scientist now than when I started in his lab because of it. For this I will always be very grateful. I would like to acknowledge my thesis committee, Drs. Sangram Sisodia, James Mastrianni, Robert Vassar, and William Green, for their patient guidance and support throughout this project. I also want to thank the Neuroscience graduate program and the Department of Neurobiology administration for their support, including Sharon Montgomery, Diane Hall, Keli Uhter, Jo DeGroot, and Holly Evans, all of whom I relied on heavily for getting through the practical aspects of working in a lab.

Several experiments would not have been possible without help of certain people. Dr. Angele Parent helped with managing the mouse colony and spent a significant amount of time helping me with the MetaMorph Image analysis software. Dr. Carole Deyts helped immensely with the lipid raft fractionations. I am very thankful for the help of members of Dr. William Green's lab, especially Dr. Okunola Jeyifous for guidance with primary neuronal tissue culture, and Dr. Sarah Antinone for guidance with the Acyl-RAC assay. I thank members of Dr. Sam Sisodia's lab for letting me use the lab's ultracentrifuge. Dr. Katherine Sadlier and members of Dr. Robert Vassar's lab provided me with BACEKO brain tissue and assisted me with culturing neurons from BACEKO mice and WT littermates, including performing the genotyping. Dr. Tong-Chuan He provided the pAdTrace plasmids and recombinant adenoviruses for BACE1 expression in neuron cultures. Dr. Masaki Fukata provided the miRNA constructs to knock-down

DHHC expression in neuron cultures. I am very thankful for the help of Dr. Vytas Bindokas at the University of Chicago Imaging Core Facility, for his patience and time spent teaching me how to use the confocal microscopes and imaging software for data analysis.

I also want to acknowledge all the members of the Thinakaran lab, past and present, for their support and for creating a fun, enjoyable work environment: Dr. Virginie Buggia-Prevot, whom I often referred to as my "mini-mentor" and worked very closely with on the first half of my project; Dr. Kulandaivelu Vetrivel, whose seemingly endless knowledge about everything helped me gain my footing in the lab and who never minded when I had a stupid question; Dr. Ping Gong, who helped me overcome many early cloning hurdles; Dr. Xavier Meckler, who first taught me how to culture neurons and gave me my very first glimpse of neurons under the microscope; Jelita Holland, who was not only an intensely organized lab manager who taught me everything I needed to know about staining brain slices, but was a source of happiness and joy for everyone in the lab; Dr. William Zeiger, who helped me navigate life as a graduate student during my first few years; Margaret Lefkow, with whom we created "the most supportive bench bay" in the lab; Dr. Pierre De Rossi, who helped coach me through the end of my thesis; and Casey Rice, who managed to take over the mouse colony duties very quickly and will no doubt have much success in the lab and beyond. I am thankful for the help provided by our extremely bright & talented undergraduate volunteers, particularly Shelly Thai, Nicholas Hernandez, Joshua Saucedo, Bianca Demara, and Elizabeth Woo. Despite being so young in their careers, their enthusiasm was a source of motivation, fulfillment and pride in the work we do in the lab.

I never would have thought I could seriously pursue a career in science without my very first job as a lab assistant, washing dishes, genotyping mice and analyzing RNA by Northern blots despite not even being old enough to vote; this was the opportunity of a lifetime, I am very grateful for Dr. Samuel Hawgood, Cynthia Brown, and especially Dr. Jennifer Akiyama for this first exposure to science. After college, I was very lucky to work as a technician in the lab of Dr. John Peters, present at my first international conference and publish my first, first-author publication; without this experience, I never would have had the confidence and drive to apply to graduate school. I am very grateful for the mentorship given by Dr. Grace Loredo, Dr. Chris Bradley, Dr. Nancy Lane and Dr. Mohammad Shahnazari.

Finally I want to acknowledge the support that I received from everyone here at the University of Chicago, from my friends in the graduate program with whom I commiserated many times, to the many people of various backgrounds throughout the school that I was lucky enough to cross paths with. It was an honor to be in the presence of such smart, funny, and interesting people over the last six years; in a way, I feel as though I "grew up" here thanks to their encouragement and support.

Abstract

Alzheimer's disease (AD) is a devastating neurodegenerative disease of aging characterized by the presence in the brain of neurofibrillary tangles and senile plaques, the latter being composed of amyloid beta (Aβ) peptides. Aβ is implicated in synapse dysfunction and neuronal cell death, ultimately leading to the cognitive decline seen in the disease. Significant research effort has therefore focused on studying the production and clearance mechanisms of Aβ. Sequential cleavage of Amyloid Precursor Protein (APP) by β- and γ-secretase activities releases the Aβ peptide. β-site APP-Cleaving Enzyme 1 (BACE1) was identified as the β-secretase over 15 years ago, and is an attractive therapeutic target for treatment of AD. Modulating BACE1 localization away from the intracellular compartment in which it encounters APP is one proposed strategy for specifically blocking APP cleavage, leaving the other functions of BACE1 intact. However, a detailed characterization of BACE1 transport, specifically in neurons, is incomplete. I set out to study the potential mediators of BACE1 localization in neurons, focusing on a type of post-translational modification, palmitoylation. I hypothesized that BACE1 mislocalization in neurons would alter APP processing and Aβ deposition. Using cultured hippocampal neurons expressing a non-palmitoylatable mutant, I have found that lack of palmitoylation prevents BACE1 localization in dendritic spines. While BACE1 normally enriches into the axonal versus the somatodendritic compartment over time in mature neurons, the non-palmitoylatable mutant does not. I have created a knock-in mouse model in which the non-palmitoylatable mutant is expressed under the control of the endogenous promoter, and while this mouse thus far has failed to demonstrate any striking differences in BACE1 localization or APP processing compared to mice expressing wild-type BACE1, an

Alzheimer's mouse model expressing this non-palmitoylatable mutant exhibits decreased Aβ plaque deposition. This mouse model therefore constitutes a valuable tool to study whether specific modifications of BACE1 affect transport in vivo and whether this transport is linked to APP processing.

CHAPTER I

Introduction

Alzheimer's disease and the Amyloid Cascade Hypothesis

Alzheimer's Disease (AD) is a devastating neurodegenerative disease of aging, the most common form of dementia worldwide and the 6th leading cause of death in the United States[1, 2]. While old age has historically been associated with dementia, AD was first characterized as a distinct disease over a hundred years ago by Dr. Alois Alzheimer, describing the clinical and histopathological features present in his patient, Auguste Deter, in a 1906 report[3]. Symptoms of AD include disruptive memory loss, especially in forming new memories; disorientation, changes in mood and personality, difficulty with communication, and eventually difficulty with swallowing and movement[1]. AD represents a huge burden on family and caregivers, and is one of the costliest diseases to society. Like other neurodegenerative diseases of aging, as the proportion of the population over the age of 65 increases, the number of cases of AD will also increase; yet there is currently no effective therapy or cure, making AD a major public health concern and underscoring the need for more basic research into the underlying etiology of the disease[1].

Histologically, AD is characterized by the presence in the brain of intracellular neurofibrillary tangles and extracellular senile plaques[3, 4]. Neurofibrillary tangles are aggregates of hyperphosphorylated tau, a cytoskeletal microtubule-associated protein, while senile plaques are aggregates composed of amyloid-beta (Aβ) peptide. Aβ can occur as peptides of varying length, with the two

major species occurring in brain being the 40- and 42-amino acid peptides, the latter of which is more hydrophobic and more easily aggregates to form plaques[5].

Senile plaques appear as a heterogenous population that can be described as two main types, the classic "dense-core" and "diffuse" plaques[6-11]. Dense-core plaques consist of a dense amyloid core surrounded by a clear halo and wisps of amyloid immunostaining at the periphery. These types of plaques tend to exhibit dystrophic neuritic processes, termed "dystrophic neurites", that are positive for tau protein, as well as a variety of lysosomal and synaptic proteins. Dense-core plaques are classically detectable using a variety of different histological staining techniques, including Congo red, thioflavin S, and two different silver-based methods, the modified Bielschowsky stain and Bodian stain. In contrast, diffuse plaques are "cotton wool-like" plaques that lack both the dense core and neuritic processes, and are stained by the modified Bielschowsky method, but not by the Bodian stain[9]. All of these plaques are detectable using Aβ immunostaining. In addition to these extracellular amyloid deposits, intracellular Aβ immunostaining can also be seen, although to a lesser extent[12, 13].

The isolation of Aβ from fibrils found in amyloid deposits in cerebral blood vessels and in plaques in both AD patients and Down's Syndrome patients[14-16] provided the first clues that overproduction of this peptide may lead to disease pathology. Given that the peptide was found to be identical in both AD and Down's Syndrome pathologies, it was predicted that the precursor protein to the Aβ peptide would be found on chromosome 21, and this was indeed found to be the case[17-20]. Pathogenic mutations were soon found in the sequence of Amyloid Precursor

Protein (APP) that codes for Aβ, associated with early-onset familial AD[21, 22]. Thus, understanding the genetics that caused inherited forms of AD provided insight into the molecular pathways underlying the disease as a whole, ultimately leading to the Amyloid Cascade Hypothesis of AD, which posits that increased production and decreased clearance of Aβ drives AD pathogenesis, including neurofibrillary tangle formation, synapse loss, and neuron cell death[23-25].

In addition to Aβ production and plaque formation, the process of Aβ clearance and degradation is also important. Most of the information regarding Aβ clearance mechanisms also comes from genetic association studies. Most notably, a common allele variant, ε4, of the *APOE* gene, encoding apolipoprotein E (ApoE), is a major risk factor for AD[26, 27]. ApoE is involved in cholesterol transport throughout the body, and can be found in senile plaques[28, 29]. In vivo microdialysis measurements of Aβ in brain interstitial fluid (ISF) of mice overexpressing both human AD-linked APP and one of the three ApoE isoforms revealed that Aβ was elevated in mice expressing the ε4 allele, and this elevation paralleled an increased Aβ plaque burden [30]; the elevated Aβ levels could not be accounted for by changes in APP processing/Aβ production. When mice were given an inhibitor to block Aβ synthesis, the level of remaining Aβ dropped compared to mice expressing the ε4 allele, providing compelling evidence for a role of ApoE, and the ε4 allele, in Aβ protein stabilization/degradation[30]. It has been suggested that ApoE may compete with soluble Aβ for uptake in astrocytes via Low-density lipoprotein Receptor-related Protein 1 (LRP1)[31], thereby providing a mechanism for ApoE-induced Aβ stabilization. Additionally, many Aβ-degrading enzymes have been identified in

vitro (reviewed in [32]). One of these enzymes, Neprilysin, was purified from rat brain and shown to degrade radiolabeled Aβ; furthermore, degradation of radiolabeled Aβ injected into hippocampus in anesthetized rats was blocked by administration of thiorphan, an endopeptidase inhibitor for which Neprilysin is a target [33]. The same group went on to demonstrate that Neprilysin-deficient mice exhibited both decreased degradation of exogenous, radiolabeled Aβ, as well as elevated steady-state levels of endogenous Aβ[34]. Another target of thiorphan, Neprilysin-2, was genetically ablated in mice, also resulting in elevated Aβ[35]. Along the same lines, genetic deletion of endothelin-converting enzyme leads to elevated Aβ[36]. Insulin-degrading enzyme is yet another degrading enzyme that, when knocked-down in mice, leads to elevation of Aβ[37, 38]. Degradation and clearance mechanisms of Aβ continue to be an intensely pursued area of research for AD therapeutics.

The role of Aβ at the synapse

Accumulating evidence suggests that Aβ plays a role in mediating synaptic plasticity, specifically by blocking Long-Term Potentiation (LTP), the persistent strengthening of synapses due to prior synaptic activity. An early study showed that Aβ oligomers, rather than Aβ peptide monomers or the larger fibrillar assemblies found in plaques, block LTP in rat hippocampal slices, before any signs of cell death and degeneration[39]. Secreted Aβ oligomers derived from cell culture media, which are resistant to detergent solubilization, blocked hippocampal LTP in anesthetized rats[40]. Importantly, pretreatment of culture media with insulin degrading enzyme, which should degrade any Aβ monomers, had no effect, demonstrating that

oligomers specifically were responsible for the LTP blockade. When extracts derived from AD brain or cerebrospinal fluid (CSF) were incubated with rat hippocampal neurons, Aβ oligomers could be seen in clusters along neurites by immunostaining, and overlapped with the postsynaptic marker PSD-95, suggesting a synaptic localization; in the same study, neurons treated with synthetic, purified Aβ oligomers resulted in upregulation of Arc, an immediate-early gene that is activated by synaptic activity[41]. Aβ treatment in cultured neurons decreases surface levels of NMDA receptor subunits NR2B and NR1, depresses NMDA receptor currents, and reduces NMDA-induced cAMP Response Element Binding protein (CREB) phosphorylation, a transcription factor activated by synaptic activity[42]. Aβ alters axonal transport kinetics and dendritic spines[43], decreases synapse size and number[44], and exerts Tau-dependent synaptic, network, and cognitive impairments[45, 46]. Thus, Aβ is found to depress excitatory synaptic activity. On the other hand, synaptic activity has been found to induce Aβ production, suggesting that Aβ may normally signal in a negative feedback loop to suppress neuronal hyperactivity[47]. This last point also suggests that the machinery required for Aβ production and release should be present at the synapse. The enzymes responsible for, and the contribution of their subcellular localization to, Aβ production, are discussed in the next sections.

Aβ production and BACE1

As mentioned above, the Aβ peptide is a product of a larger precursor protein, APP, generated by the sequential cleavage of two enzymatic activities, β- and γ-secretase (Fig. 1). A third secretase, α-secretase, cleaves APP within the Aβ

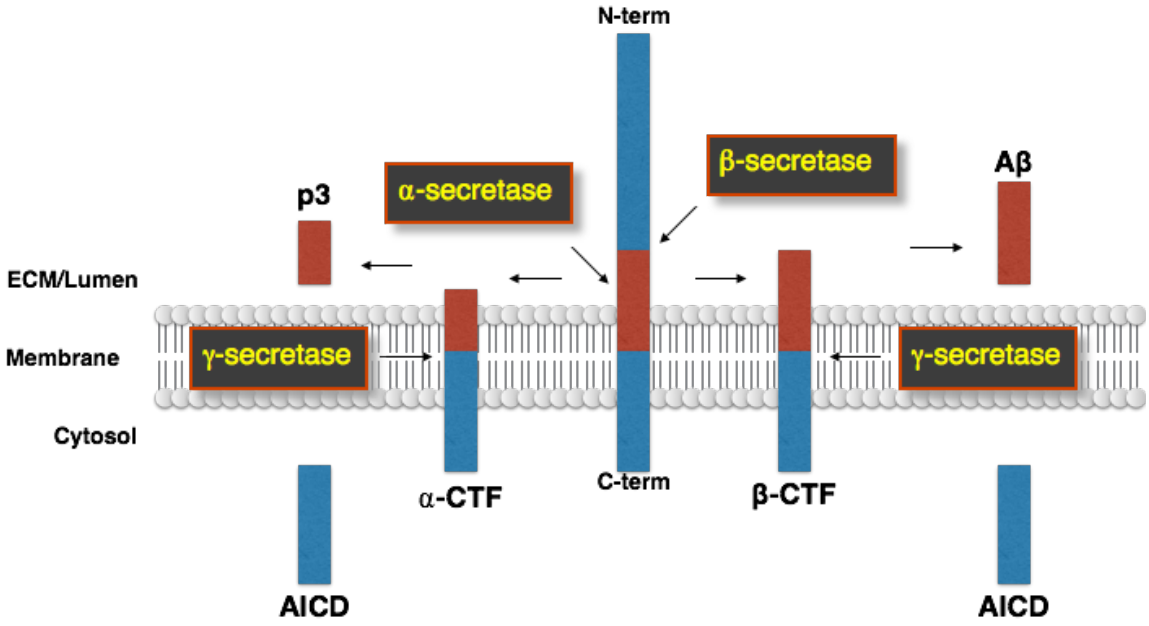

Figure 1: Schematic of APP processing. α-Secretase cleaves APP within the sequence coding for Aβ (red), and thus precludes Aβ generation to produce a truncated p3 fragment and APP Intracellular Domain (AICD). Alternatively, the β-secretase BACE1 cleaves APP at the start of the Aβ sequence, and subsequent cleavage by γ-secretase releases the Aβ peptide and AICD.

peptide sequence (Fig. 1). While the α-secretase activity has been ascribed to members of the A Disintegrin And Metalloproteinase (ADAM) family[48], and γ-secretase is known to be an enzymatic complex consisting of multiple proteins[49], the β-secretase consists of a single protein, β-site APP Cleaving Enzyme-1 (BACE1), identified 16 years ago[50-54]. BACE1 is a type I transmembrane aspartyl protease with a large extracellular/lumenal N-terminal region, a single transmembrane domain, and a short C-terminal cytoplasmic tail (Fig. 2). Two aspartyl residues in the N-terminus coordinate with water molecules to initiate proteolysis. The rather large active site of BACE1 has hampered efforts to create BACE1 inhibitors that are able to cross the blood brain barrier, although recent progress has been made (reviewed in [55]). The short C-terminus contains a multitude of protein targeting motifs and sites of post-translational modifications, which help mediate protein subcellular localization and stabilization.

BACE1 is an attractive therapeutic target for AD for numerous reasons. BACE1 knockout (KO) mice have low brain Aβ levels and do not accumulate amyloid plaques[56, 57], and BACE1 KO in transgenic mouse models of AD rescues cognitive decline[58-61]. Furthermore, while a mutation in APP that enhances BACE1 cleavage is associated with early-onset familial AD[22], a normal sequence variant that lowers BACE1 cleavage in transfected, cultured cells is associated with lower incidence of AD[62]. However, BACE1 has many other substrates besides APP, which are discussed in greater detail in the following section.

Additional substrates of BACE1 & implications for BACE1 inhibition

An unbiased quantitative proteomic analysis, using two different human cell

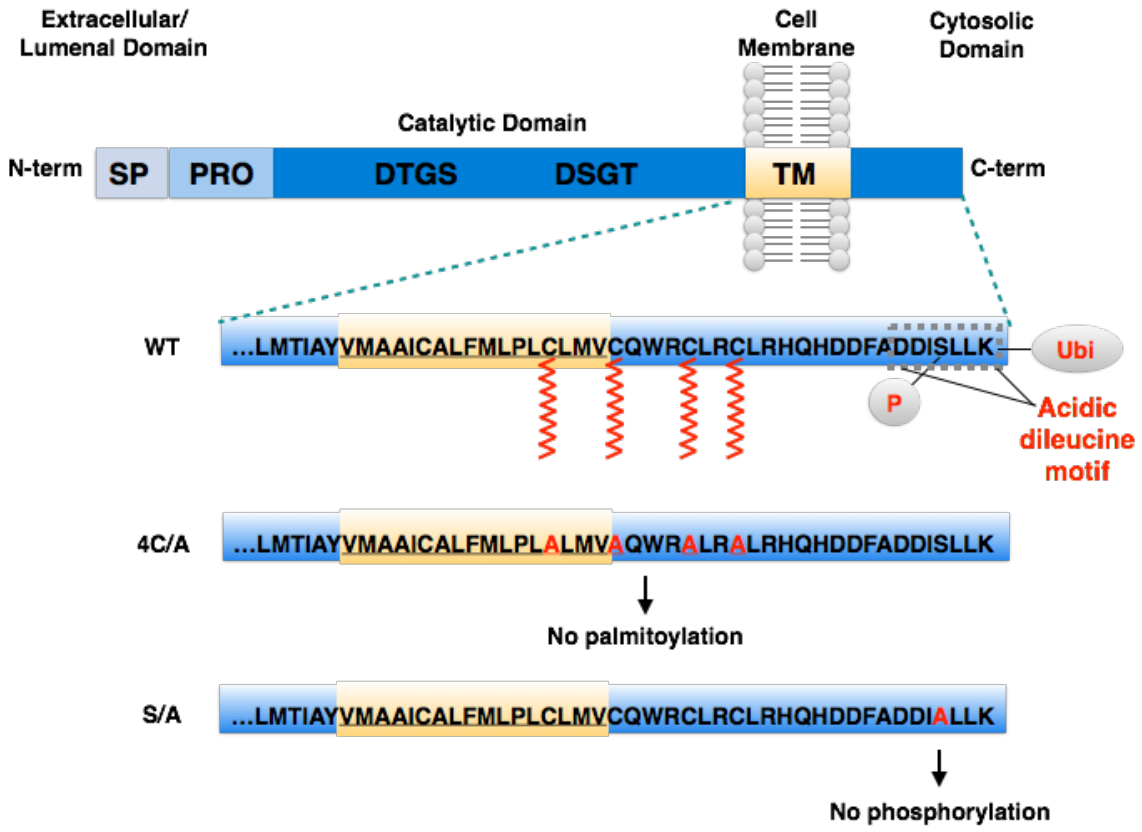

Figure 2: Schematic of the protein structure of BACE1 and point mutants used in the current study. BACE1 is a type I transmembrane protein with large N-terminal, extracellular/lumenal catalytic domain, one transmembrane domain, and a short C-terminal cytosolic domain. The N-terminus contains a signal peptide sequence (SP) and a pro-domain (PRO) that gets cleaved during protein processing. The C-terminus contains an acidic dileucine motif involved in internalization from the cell surface; a lysine residue, K501, that undergoes ubiquitination, and a serine residue, Ser498 that undergoes phosphorylation. Further upstream, in a juxtamembrane region of the C-terminus, are four cysteine residues that undergo palmitoylation. Mutation of these 4 cysteine residues (474, 478, 482, and 485) to alanine ("4C/A") blocks palmitoylation, while mutation of Ser498 to alanine ("S/A") blocks phosphorylation.

lines, HeLa and human embryonic kidney (HEK) cells, stably expressing human BACE1, revealed 68 putative substrates for BACE1[63]. Another proteomic approach focused on secreted proteins throughout the proteome (the "secretome") of both HEK cells and primary cultured mouse neurons, and identified additional BACE1 substrates, some of which were validated[64]. Given these other, non-APP substrates, even specific BACE1 inhibitors would be expected to exhibit off-site, rather than off-target, effects[65]. For instance, BACE1 has been implicated in myelination and ErbB4 signaling via processing of Neuregulin 1 (NRG1)[66-68], and has also been shown to cleave L1 and Close Homologue of L1 (CHL1), adhesion molecules that are critical for axonal guidance and maintenance of neural networks[69, 70]. The transmembrane domain of BACE1 was shown to interact with the signaling molecule adenylate cyclase, regulating the cAMP/PKA/CREB pathway[71]. Given these other, potentially vital, roles that BACE1 plays in normal physiology, global inhibition of BACE1 may have unintended negative consequences, particularly in a vulnerable aging population.

Clues to the possible negative effects of BACE1 inhibition come from studies of BACE1 knock-out (KO) mice, which were initially described as exhibiting a "mild" phenotype[56, 57]; since then, seizures, hyperactivity, specific memory deficits and axon guidance impairments have been reported[60, 70-74]. BACE1 KO mice display activity-dependent deficits in hippocampal synaptic transmission[75]; specifically, BACE1 KO mice exhibit impairments in excitatory input from mossy fibers to CA3 pyramidal cells, as well as inhibitory input from CA3 interneurons[76]. Finally, long-term treatment of adult mice with a BACE1 inhibitor led to deficits in motor

coordination, due to NRG1 isoform-dependent maintenance of muscle spindles[77]. BACE1 inhibition may therefore also block important physiological functions that are still being defined, and which need to be taken into consideration before employing BACE1-targeted therapeutics to treat AD.

Although there are many caveats to inhibiting BACE1 activity for treatment of AD, BACE1 still remains a viable therapeutic target, since BACE1 inhibition prevents the overproduction and deposition of Aβ. Effective AD therapies may only require ~50% BACE1 inhibition for a sufficient reduction of Aβ levels, although the stage of disease progression at the start of treatment will likely determine the level of BACE1 inhibition necessary for therapeutic efficacy[55].

BACE1 and APP intracellular transport

BACE1 inhibition will not only inhibit Aβ production, but will also inhibit the other, potentially vital, functions of BACE1. An alternative strategy for blocking Aβ production specifically is to influence BACE1 localization away from the cellular compartments in which BACE1 encounters APP (Fig. 3). This assumes that APP is localized in separate compartments distinct from other BACE1 substrates. BACE1 substrates localize to many compartments throughout the neuron, such as the axon (NRG1; Contactin-2; APP), the postsynaptic density (Semaphorin 4C (Sema4C)), Golgi (Golgi integral membrane protein 4 (GOLIM4)), endosomal/lysosomal trafficking pathway (Mannose-6-phosphate receptor (M6PR)), and plasma membrane (Ephrin-A5, L1, CHL1, APP)[64]. Multiple BACE1 substrates therefore should localize to the same compartment, complicating a strategy whereby localization is modulated to specifically inhibit processing of one substrate, namely,

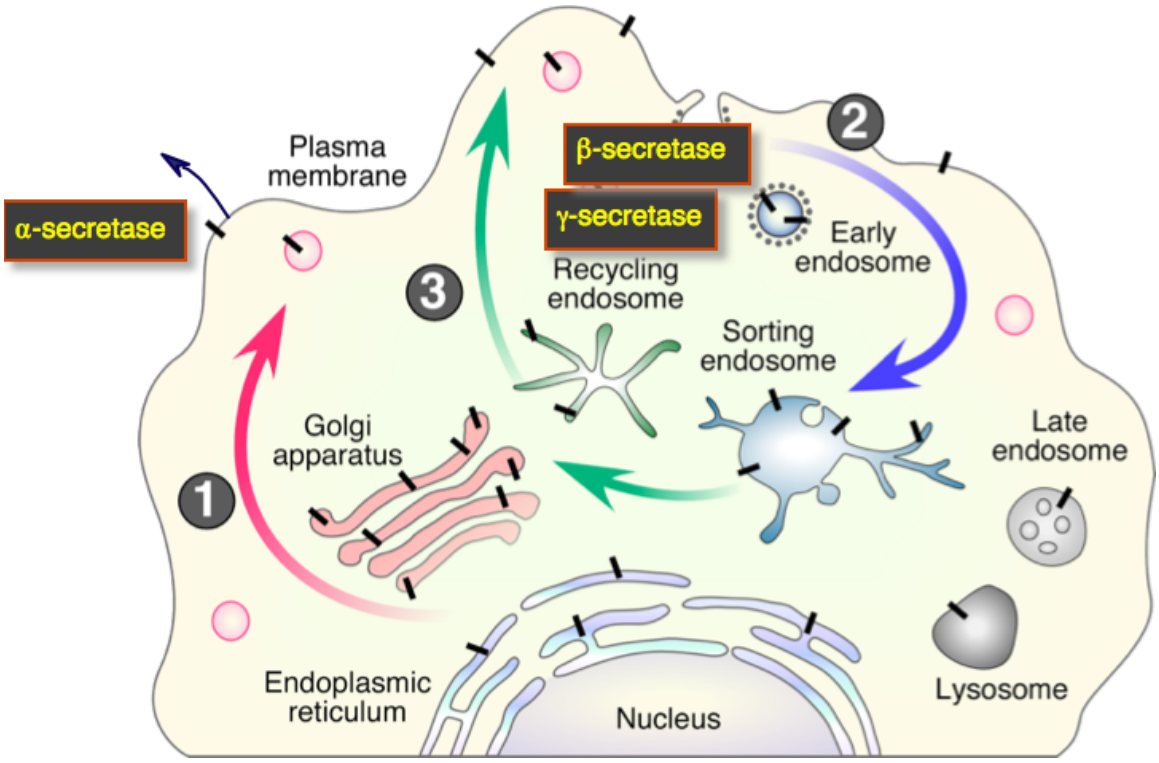

Figure 3: Schematic of protein trafficking pathways inside the cell. 1) Transmembrane proteins produced in the ER are trafficked to the Golgi where they are processed before transport to the plasma membrane via the constitutive biosynthetic pathway. At the plasma membrane, APP is thought to undergo cleavage by α-secretase. 2) Proteins are internalized from the cell surface in early endosomes and then are transported to recycling endosomal compartment, where they are sorted either back to the cell surface (3) or targeted to the late endosome and lysosome for degradation. While APP cleavage can occur anywhere it encounters secretases, it is thought that APP, BACE1 and γ -secretase converge in these post-Golgi transport compartments. Figure modified from Thinakaran & Koo, J Biol Chem, 2008[78].

APP. A more detailed understanding of how BACE1 localizes to certain compartments, and how this ultimately affects substrate processing, will reveal the therapeutic viability of this targeting strategy.

Much of the initial work characterizing the intracellular localization of APP and the secretases was conducted in non-neuronal cells. After synthesis in the ER and transport through the Golgi, APP is trafficked to the surface of the cell, where it encounters α-secretase (Fig. 3). Alternatively, APP is internalized from the surface of the cell into endosomes, where it encounters BACE1; ectodomain-cleaved APP C-terminal fragments (CTFs) are then processed by γ-secretase. Due to its acidic pH optimum and steady-state localization, BACE1 cleavage of APP is believed to occur inside the acidic organelles of the endocytic pathway[50, 51]. Along these lines, endocytosis of APP has long been proposed as a prerequisite for Aβ generation and release[79]. Experiments using cultured cells expressing APP mutants defective for O-glycosylation suggested that APP cleavage occurs after O-glycosylation in the secretory pathway[80]. APP lacking its cytoplasmic domain does not get internalized into endosomes, and subsequently undergoes less β-cleavage compared to full-length APP[81]. Recycling of endocytosed BACE1 to the trans-Golgi network (TGN) was found to account for a majority of Aβ generation in cultured HEK cells[82]. Sorting nexin 6 (SNX6), a component of the retromer complex involved in protein transport between endosomes and the TGN, was identified as a negative regulator of BACE1-mediated APP processing, presumably by altering subcellular localization[83]. Modulation of endocytic trafficking via Rab5, a small GTPase important for

endosomal transport, also modulates BACE1-cleaved APP CTFs and Aβ production[84]. Intriguingly, enlarged endosomes have been reported as another histopathological feature of AD and Down's syndrome brains[85, 86], and endocytosis is slower in older neurons in culture[87]. Thus, endosomal trafficking of both BACE1 and APP appear to be important for APP processing and Aβ production, particularly in the context of AD.

Subcellular localization of APP and APP processing in the brain

In the brain, many studies have suggested that the subcellular location, and specifically the axonal transport, of APP and APP processing are important for Aβ production. One study demonstrated that APP undergoes axonal transport by showing that sciatic nerve ligature caused accumulation of radiolabeled APP just proximal to the ligature after 6-24 hours[88]. In another study, radiolabeled methionine was injected into rat entorhinal cortex, and analysis of extracts from the dentate gyrus, to which entorhinal axons project, revealed that only fully-glycosylated, mature forms of full-length radiolabeled APP, as well as radiolabeled APP CTFs, were present[89]. The possibility that cells in the dentate gyrus may have upregulated APP due to any injury caused by injection was ruled out, since only the neuron-expressed isoform of APP was visible, not the KPI-domain isoform of APP, which was previously shown to be up-regulated by injury; also, the pattern of APP obtained by radiolabeling was indistinguishable from that of steady-state APP. Thus, the only way radiolabeled APP and APP CTFs could have appeared in the dentate gyrus was via axonal transport. From this study, it was still an open question as to whether APP cleavage to produce those accumulated APP CTFs had occurred in the

neuron cell body (i.e., the entorhinal cortex), during axonal transport or at the terminal fields. The importance of axonal transport to Aβ deposition was suggested by two studies showing that lesion of axonal inputs to the hippocampus significantly decreased both Aβ and full-length APP in that region[90, 91]. Furthermore, both BACE1 and BACE1-cleaved APP β-CTFs can be found prominently in mossy fibers, the hippocampal axon tract from dentate gyrus to CA3[92]. Arguing in favor of a synaptic localization of APP and BACE1, synaptic activity influences Aβ generation and release[45, 47, 93, 94], and APP, BACE1 and βCTFs are reported to be found in presynaptic vesicles, endosomes and presynaptic terminals[94-97]. In a somewhat unexpected demonstration of the importance of APP axonal transport to Aβ production and deposition, a transgenic mouse line overexpressing BACE1 exhibited a decrease in plaque burden and Aβ levels, despite exhibiting high levels of β-cleavage as evidenced by high βCTFs; the authors found that APP axonal transport in these mice was severely diminished, and attributed their findings to BACE1 cleaving APP early in the secretory pathway[98]. Similarly, transgenic mice overexpressing Reticulon-3 (RTN3), a protein involved in membrane trafficking in the early secretory pathway, exhibited BACE1 retention in the ER and a concomitant decrease in Aβ production[99]. Taken together, these studies suggest that the neuron-specific subcellular localization of APP processing by BACE1 is an important factor in Aβ production and deposition in mouse brain.

Transport and localization of BACE1 and APP in cultured neurons

Studies in cultured primary hippocampal neurons have further elucidated the cell biological mechanisms regulating neuronal trafficking of BACE1.

Endogenous and transfected, fluorophore-tagged BACE1 appears in both the somatodendritic and axonal compartment in primary cultured neurons[92, 100-104]. Overexpression of RTN3 in cultured neurons significantly decreases the overlap of fluorophore-tagged BACE1 with synaptophysin-positive puncta along the axon, which are likely to be presynaptic sites; BACE1 anterograde transport along axons was also significantly diminished[103]. The same study demonstrated that RTN3 overexpression had no effect on APP transport, indicating that the effect was specific to BACE1 transport. MicroRNA (miRNA)-mediated depletion of Vps35, a component of retromer, caused mislocalization of fluorophore-tagged BACE1 to a primarily dendritic, rather than somatic/perinuclear, distribution in cultured neurons; furthermore, miRNA-depletion of Vps35 significantly reduced the number of BACE1-positive vesicles moving in the retrograde direction, as revealed by live imaging[105]. Rab11, a GTPase involved in endosomal trafficking and recycling, was recently identified as a regulator of Aβ production in neurons[106], and expression of dominant-negative Rab11 in cultured hippocampal neurons expressing fluorescently-tagged BACE1 (BACE1-YFP) significantly decreases BACE1 localization in axons[102]. Rerouting BACE1 away from the lysosome, where it normally undergoes degradation, leads to accumulation of BACE1 and an increase in β-cleaved APP and Aβ production[107]. Similarly, stabilization of BACE1 by preventing transport to lysosomes also increased APP processing, while enhancing BACE1 turnover decreased BACE1 cleavage of APP[108].

BACE1 protein structure, targeting motifs and posttranslational modifications

Proteins are often targeted to specific intracellular sites by 1) amino acid motifs present in the protein sequence, and 2) reversible post-translational modifications. Both of these mechanisms mediate protein:protein interactions with certain adaptor molecules, which form the basis of cargo protein selection into particular transport vesicles and targeting of those transport vesicles to specific target organelles. For example, mGluR1a postsynaptic localization involves a two-step process involving first dendritic targeting, then sequestration at postsynaptic sites, with each step requiring distinct protein interaction motifs[109]. It has been shown than a "DDXXLL" acidic dileucine motif present at the C-terminus of the BACE1 protein sequence (Fig. 2) regulates binding to Golgi-localized, gamma adaptin ear-containing, ARF-binding (GGA) proteins, a family of clathrin adaptors that mediate transport in the endosomal system, and its distribution in endocytic organelles[110, 111]. Expression of a BACE1 mutant in which the two leucines are mutated to alanine, thus preventing dileucine motif-mediated endocytic transport, results in accumulation of BACE1 at the cell surface[92, 112, 113]. Adjacent to this motif is a phosphorylation site at serine 498[112, 114], which enhances binding to GGA[111, 115, 116] (Fig. 2). Mutation of Ser498 to an alanine residue prevents phosphorylation, and expression of this "S/A" mutant in both neurons and nonneuronal cells results in a punctate expression pattern, with very little to no surface localization at steady-state[112-115]. Despite these effects on BACE1 steady-state localization, neither of these mutants (LL/AA or S/A) was found to have any effect on BACE1 cleavage of APP[112, 114, 115, 117].

Palmitoylation and lipid rafts

Further upstream of the dileucine motif and phosphorylation site, BACE1 undergoes *S*-palmitoylation at four cysteines in a juxtamembrane region at the C-terminal tail[118, 119] (Fig. 2). Protein *S*-palmitoylation is the covalent, reversible addition of the 16-carbon saturated fatty acid palmitate to cysteine residues via thioester linkage; certain proteins, such as Sonic hedgehog, undergo irreversible *N*-palmitoylation via a stable amide bond[120]. Here, I will refer to *S*-palmitoylation simply as "palmitoylation." Palmitoylation is commonly found on proteins expressed by neurons and particularly on synaptic proteins in response to synaptic activity[120-123]. For soluble cytoplasmic proteins like PSD-95, palmitoylation is responsible for membrane tethering[121, 122]. For transmembrane proteins, however, palmitoylation can either alter protein conformation to regulate protein:protein interaction, and/or can mediate localization within different membrane microdomains that are enriched in cholesterol and sphingolipid, termed lipid rafts[120, 124].

Lipid rafts are dynamic, sterol- and sphingolipid-enriched domains within the lipid bilayer, ranging in diameter from 10-200nm, that are widely believed to facilitate certain cell signaling pathways by providing a platform for protein:protein and protein:lipid interactions[125, 126]. Lipid raft-associated proteins can be identified biochemically by their resistance to certain non-ionic detergents, such as Triton X-100 or Lubrol WX, in what are known as detergent-resistant membranes (DRMs). DRMs, like lipid rafts, are highly enriched in cholesterol and sphingolipids, and the high lipid-to-protein ratio leads to a low relative density when subjected to a

sucrose density gradient, allowing for separation between DRMs and soluble membrane proteins[126].

Lipid rafts and APP processing

Many lines of epidemiological evidence have suggested a role for cholesterol metabolism and lipid raft targeting in APP processing and Aβ production. High total cholesterol and LDL levels in serum correlates with elevated levels of Aβ42 in human AD cortex[127], and patients taking statins, which lower cholesterol by inhibiting its synthesis, were found to have a lower prevalence of AD[128]. In a transgenic mouse model of AD, which expressed familial AD-related mutants of human APP and human PS1, a high cholesterol diet accelerated amyloid pathology and increased levels of βCTF, correlating with elevated serum levels of cholesterol[129]. Changes in cholesterol metabolism alter cellular membrane transport and lipid raft targeting. Lipid raft isolation from early and late stage AD brain reveals not only a difference in lipid composition compared to control, but also a co-distribution of APP and BACE1, and BACE1 is specifically elevated in lipid rafts taken from the entorhinal and frontal cortices[130].

In vitro data on lipid rafts and APP processing echoes the epidemiological data. In cultured, transfected cell lines, BACE1 is found in Lubrol WX-soluble, low density DRMs positive for lipid raft markers alongside βCTFs, while full-length APP was enriched in the non-raft fractions[131]. Antibody co-patching is an additional method used to determine raft localization of proteins, useful in confirming findings from biochemical analysis of DRMs. Using co-patching with a known raft marker, glycosyl phosphatidylinositol (GPI)-anchored placental alkaline phosphatase

(PLAP), BACE1 and APP were shown to co-segregate into GPI-PLAP-positive lipid rafts[132]. BACE1 cleaves palmitoylated, lipid raft-targeted APP preferentially in CHO cells[133]. Interestingly, inducing neuronal activity by application of PTX to primary cultured neurons enhanced the association of APP with BACE1 in DRM fractions[134]. All of these studies beg the question: if BACE1 can be excluded from lipid rafts, will there be a concomitant decrease of β-secretase processing of APP? To address this question, my lab previously characterized a palmitoylation-deficient mutant, BACE 4C/A, in which the four cysteines have been mutated to alanine (Fig. 2). Lack of palmitoylation prevented BACE1 localization in lipid rafts when overexpressed in non-neuronal cells; however, there were no other obvious differences in subcellular localization, and there was no difference in Aβ levels or β-cleaved APP fragments[119].

In addition to, and perhaps due to, mediating lipid raft localization, palmitoylation is also implicated in controlling membrane protein trafficking throughout different compartments of the neuron. Two axonally-targeted proteins, GAP-43 and paralemmin, contain a C-terminal palmitoylated domain necessary and sufficient for axonal targeting[135]. Like BACE1, these palmitoylated motifs also mediated localization in detergent-insoluble lipid rafts in non-neuronal cells; but unlike BACE1, GAP-43 and paralemmin are peripheral membrane proteins, and might be regulated by different mechanisms than those governing a transmembrane protein such as BACE1. In polarized MDCK cells, ligand binding of pIgR induces distribution to DRMs, cholesterol-dependent internalization and subsequent transcytosis from basolateral to apical membranes[136]. Whether BACE1 also

undergoes raft-mediated transcytotic axonal targeting remains to be determined. Given that there are nuanced differences in protein transport mechanisms between cultured, non- polarized non-neuronal cells, and highly polarized neurons[137, 138], and given the importance of palmitoylation in neuron-specific compartment localization, particularly in response to synaptic activity[120], I decided to examine the role of palmitoylation in BACE1 localization in neurons. I found that palmitoylation appears to enhance the efficiency of BACE1 targeting to neuron-specific compartments, including dendritic spines and the axon, in cultured hippocampal neurons. I generated a knock-in mouse model, in which the wild type BACE1 is replaced with a mutant that does not undergo palmitoylation. I have confirmed that this mutant is not palmitoylated and is not targeted to lipid rafts, using brain lysates from these knock-in mice compared to wild type littermates. However, in the adult mouse, there does not appear to be any differences in localization. Despite this, I have found that expression of the non-palmitoylatable mutant in a mouse model of aggressive, early-onset Alzheimer's disease leads to a reduction in amyloid burden throughout the brain, and a decrease in BACE1 accumulation around amyloid deposits. Together, my data suggests that the palmitoylation-mediated neuronal targeting of BACE1 influences APP processing in the context of AD pathology, and supports the hypothesis that altering BACE1 localization at the neuronal level should interfere with APP processing and AD pathogenesis.

CHAPTER II

Materials and Methods

Antibodies and reagents

Rabbit monoclonal anti-BACE1 antibody EPR3956 was purchased from GeneTex. Mouse anti-Synapsin1 (Syn1)-biotin was purchased from Synaptic Systems. Mouse anti-PSD-95 antibody (clone K28/43) and mouse anti-AnkyrinG (AnkG) monoclonal antibody (clone N106/36) was purchased from NeuroMab. Rabbit anti-MAP2 polyclonal antibody was purchased from Millipore. Mouse anti-MAP2 monoclonal antibody (clone HM.2), mouse anti-phosphoneurofilament H (pNF; clone SMI31, Sternberger Monoclonals/Covance) and mouse anti-FLAG (clone M2) antibody were purchased from Sigma. Rabbit polyclonal anti-Flotillin-2 antibody IL408 was raised against a glutathione S-transferase-human Flotillin-2 (Flot2) fusion protein[139]. Rabbit polyclonal anti-BACE1 IL410 was raised against a synthetic peptide corresponding to the N-terminal residues 46-60 of BACE1[140]. Rabbit polyclonal anti-phosphoBACE1 PB7 and non-phosphoBACE1 B7 were custom generated against synthetic peptides corresponding to the last 15 amino acids at the C-terminus of BACE1, either phosphorylated or non-phosphorylated at Ser498, respectively (YenZym Antibodies). Rabbit polyclonal antiserum CTM1 was raised against a synthetic peptide corresponding to the C-terminal 15 amino acids of APP followed by the c-Myc epitope (MEQKLISEEDLN). Rabbit polyclonal anti-PS1Loop antibody, which recognizes the C-terminal fragment of PS1, was raised against residues 263-407[141]. Mouse monoclonal antibody 3D6 was raised against a synthetic peptide and recognizes amino acids 1-5 of the Aβ 1-42 sequence (Elan

Pharmaceuticals). Mouse monoclonal anti-LAMP1 antibody (clone 1D4B) was from Developmental Studies Hybridoma Bank. Streptavidin-DyLight- and Alexafluor-conjugated secondary antibodies were purchased from Invitrogen/Life Technologies. IR dye-conjugated secondary reagents for use on the Odyssey Imager were purchased from LiCOR. Unless otherwise indicated, all tissue culture reagents were purchased from Invitrogen/Gibco/Life Technologies.

Primary hippocampal neuron culture

Primary neuron cultures were generated from embryonic rat and mouse hippocampus. Rat neurons were cultured as a "co-culture" in which glia and neurons were grown on the same coverslip side-by-side, and mouse neurons were cultured as a "Banker" culture[142], in which neurons were cultured on coverslip inverted over a feeder layer of glia from P0-P2 mice. All animals used in this study were provided food and water *ad libitum*, maintained on a 12 hour light:dark cycle, and housed under conditions controlled for temperature and humidity. All animal procedures used in this study were reviewed and preapproved by the Institutional Animal Care and Use Committee at the University of Chicago.

Primary neuronal co-culture was generated as follows. Timed-pregnant female rats (at gestation day E17-18) were purchased from Charles River. After deep anesthetization with isofluorane followed by cervical dislocation and exsanguination, the embryo sac was dissected out into ice-cold CMF-HBSS-HEPES, pH 7.3 (1X Ca^{2+} & Mg^{2+}-free Hank's Buffered Salt Solution, 10mM HEPES, 100U/ml penicillin/streptomycin). Hippocampi were dissected out and incubated in 0.025% trypsin in CMF-HBSS-HEPES for 10 min. at 37°C. After washing three times in CMF-

HBSS-HEPES, hippocampi were dissociated by trituration in fire-polished, serum-coated glass Pasteur pipettes until a single-cell suspension was obtained. Cells were counted in a hemocytometer and plated at a density of ~1,750 cells per mm^2 onto poly-D-lysine (70-150kD, Sigma)-coated glass coverslips (Fisherbrand), and incubated at 37°C/5%CO^2. Coverslips were prepared first by rinsing in deionized water (dH2O) and incubating in fresh 70% w/v nitric acid for 18hrs. After washing 4 x 30 min. in dH2O on a rotator, coverslips were dried, autoclaved, and transferred to sterile 60mm dishes for storage. The day before culture, coverslips were incubated overnight 0.1mg/ml poly-D-lysine diluted in 0.1M borate buffer, pH 8.5. On the day of culture, coverslips were washed three times with sterile, autoclaved MilliQH_2O ("MilliQH_2O" is ultrapure water, which has been purified and deionized using Millipore Corporation water purifiers to achieve a purity characterized by resistivity of 18.2MΩ•cm at 25°C) and equilibrated in plating media (Neurobasal with 1X B27, 2mM GlutaMAX, 100U/ml penicillin/streptomycin, 1:20 heat-inactivated fetal bovine serum (FBS)) at 37°C/5%CO^2. 4 hours after plating cells, the media was changed completely to maintenance media (same as plating media but without FBS).

All experiments using neurons obtained from mice were prepared according to the procedure of Kaech and Banker[142]. Briefly, a confluent glial feeder layer, assumed to be primarily astrocytes[142], was first prepared in 60mm tissue culture-treated dishes. Cells were plated either directly from frozen stocks or split from confluent T75 flasks, and were originally derived from P0-P2 mouse cortices. Primary glial cultures were only split once before plating on 60mm dishes. On the

day of neuronal culture, hippocampi were dissected from E17 mice and dissociated as described above. Coverslips were prepared with small wax dots on the cell growth surface; after allowing hippocampal cells to adhere (4h after plating), coverslips were inverted over the glial feeder layer and incubated at 37°C/5%CO^2. 3 days after plating neurons (DIV3), cultures were treated with 5μM cytosine arabinoside (1-β-$_D$-arabinofuranosylcytosine; AraC) to inhibit glial growth, and maintained in maintenance media (Neurobasal with 1X B27, 2mM GlutaMAX, 100U/ml penicillin/streptomycin).

Immunostaining

Neurons were washed briefly in ice-cold neuroimaging medium ("NIM"; 119mM NaCl, 2.5mM KCl, 2mM $CaCl_2$, 2mM $MgCl_2$, 30mM D-Glucose, 25mM HEPES, pH 7.4) and fixed in 4% PFA/4% sucrose, pH 7.4, in PBS, washed in PBS, quenched in 50mM NH_4Cl, and permeabilized on ice for 8 min. in 0.2% TritonX-100 in PBS. After washing, nonspecific binding sites were blocked by incubation in 3% BSA in PBS. To stain for endogenous BACE1, neurons were incubated in anti-BACE1 rabbit monoclonal antibody EPR3956 for 36h at 4°C, then an additional 2h at 37°C. All other primary antibody incubations were performed either 18h at 4°C or for 2h at RT. After washing in PBS, secondary antibody incubations were performed for 1-2h @ RT. Syn1-biotin staining was performed after primary mouse and secondary anti-mouse incubations to avoid cross-reactivity of the mouse IgG, and was labeled with streptavidin-DyLight650. After final washes, coverslips mounted onto slides using Permafluor (Thermo) aqueous mounting media and sealed with clear nail polish.

Plasmids

To visualize transfected BACE1 in neurons, a C-terminally enhanced yellow fluorescent protein (EYFP)-tagged BACE1 with a 13-amino acid α-Bungarotoxin Binding Site ("WRYYESSLEPYPD") at the N-terminus ("BBS-BACEWT-YFP") was generated as described previously[92]. A BACE1 construct encoding an N-terminal FLAG-tag ("DYKDDDDK") was constructed by replacing the coding sequence for BBS with that for FLAG (5' GACTACAAAGACGATGACGACAAG 3'), using BamHI sites flanking the tag; presence of the FLAG tag was confirmed by sequencing. The BACE 4C/A mutant was generated as described previously[119]. The BACE S/A mutant was generated in the Thinakaran lab. Both C-terminal mutants were cloned into the same vector backbones as BACE1WT plasmids by swapping a BglII/NotI fragment that included the C-terminus.

To generate a Cerulean-tagged BACE1 WT construct, cDNA encoding Cerulean was first PCR-amplified from pCS2-Cerulean (generated in the Thinakaran lab), introducing a 5' AgeI site and spanning a 3' BsrGI site, with the following primers: Fwd 5' AGAACCGGTCGCCACCATGGTGAGCAAG 3'; Rev 5' TTACTTGTACAGCTCGTCCATGCC 3'. The AgeI and BsrGI restriction sites were then used to replace YFP with Cerulean (Cer) in pEYFP-N1 BACE1, creating BACE1-Cer in a pEYFP-N1 backbone. Presence of the Cerulean fluorophore was confirmed by sequencing.

To create a construct that simultaneously expressed BACE1-YFP and a separate Cerulean fluorophore under the control of a different promoter, a pS6-BBS-BACEWT-YFP_Cer construct was generated as follows. The pS6 BBS-BACEWT-YFP

vector was digested with ClaI and filled in with Klenow to create blunt ends. The sCMV IE94 promoter and Cerulean insert was excised out of pCS2-Cer by SalI/NotI digest and filled in with Klenow to create blunt ends before ligation into the vector. Proper insertion and orientation were confirmed by XbaI digest.

PSD-95-mCherry was generated from PSD-95-GFP in GW1 (Dr. Alaa El-Husseini, University of British Colombia, Canada) by replacing the GFP with mCherry cloned from pmCherry-ExpressN1 (Clontech), using unique HindIII/EcoRI restriction sites. Synaptophysin-mCherry was created from Synaptophysin-Cer (Karen O'Malley, Washington University) by replacing GFP with an EcoRI-blunted/NotI mCherry insert from PSD-95-mCherry into a BamHI-blunted/NotI site. A unique SpeI site was created from the blunt-end cloning and was used to confirm proper insertion of mCherry into the Synaptophysin-containing vector.

MicroRNA (miRNA) constructs expressing mCherry and directed against either LacZ, as a negative control, or DHHC-2 or -3, were a generous gift from Dr. Masaki Fukata (National Institute for Physiological Sciences, Japan)[121].

FM_{1-43} dye uptake experiments

To identify functional synapses and assess whether BACE1 localizes at those synapses, an FM dye uptake experiment was performed[143]. Neurons were equilibrated in live imaging medium (containing 119mM NaCl, 2.5mM KCl, 2mM $CaCl_2$, 2mM $MgCl_2$, 25mM HEPES pH 7.4, 30mM D-Glucose), followed by a 60 sec. dye-loading step during which neurons were incubated with 15μM FM_{1-43} (Molecular Probes/Life Technologies) in a high-KCl buffer (same as live imaging medium except with 31.5mM NaCl and 90mM KCl) to depolarize neurons and

stimulate uptake at functional presynaptic sites. Neurons were then washed three times in live imaging medium and time-lapse images were acquired within 10 min. A second depolarization step resulted in loss of FM_{1-43} puncta within 1 min., a time scale consistent with synaptic vesicle release, confirming that the FM_{1-43} puncta were functional presynaptic sites. To assess BACE1 overlap with these sites, DIV11 neurons were transfected with BACE1-Cerulean and the FM dye uptake was performed at DIV13.

Characterization of a phospho-BACE1-specific antibody, PB7

To demonstrate that the polyclonal antibody PB7 specifically recognizes phosphorylated forms of BACE1, and not just the serine residue itself that undergoes phosphorylation (Ser498), lysates were prepared from HEK293 cells stably expressing BACE1 WT in the presence of a serine phosphatase inhibitor, okadaic acid. Lysates were immunoprecipitated for BACE1 using an antibody that recognizes the N-terminus, IL410, immobilized on Protein A agarose beads. Immunoprecipitates were treated with 600 units of bacteriophage lambda phosphatase in a buffer containing 50mM TrisHCl, pH 7.8, 5mM DTT, 2mM $MgCl_2$, 100mg/ml BSA, for 1h @ 37°C. Immunoprecipitates were eluted by boiling in 2X Laemmli buffer for 3 min., subjected to SDS-PAGE in parallel and immunoblotted using either PB7 to detect phosphorylated BACE1, or B7 to detect total BACE1 (Fig. 4). To determine the usefulness of PB7 for fluorescence immunostaining, cultured hippocampal neurons were transfected with either FLAG-BACE1 WT or FLAG-BACES/A, in which Ser498 has been mutated to alanine and should therefore not undergo phosphorylation. Both of these constructs have an N-terminal FLAG tag,

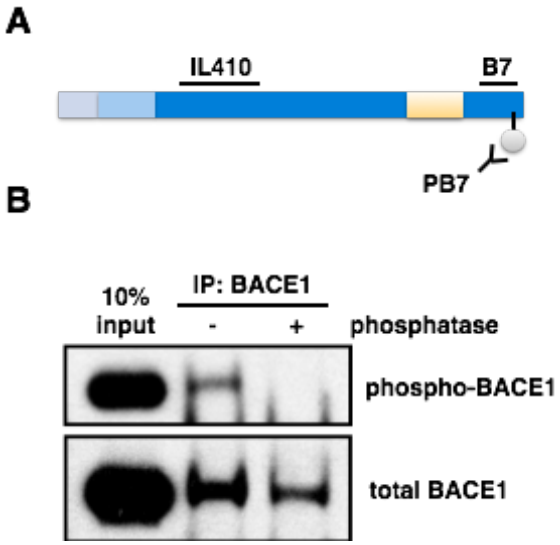

Figure 4: Characterization of the phospho-BACE1-specific antibody PB7. A, Schematic of BACE1 protein structure, illustrating the epitopes recognized by antibodies IL410, B7 and PB7. IL410 binds to the N-terminus of BACE1, while B7 binds to the C-terminus. PB7 specifically binds to phosphorylated Ser498. B, Lysates from were prepared from HEK cells stably expressing BACE1 and subjected to immunoprecipitation using an antibody that recognizes the N-terminal region of BACE1, IL410. Immunoprecipitates were subjected to phosphatase treatment to remove phosphate groups and eluted proteins were run in parallel and immunoblotted for phosphorylated and total BACE1. Immunoprecipitation was inefficient when comparing signal to 10% input. Phosphatase treatment abolished the phospho-BACE1 signal achieved with PB7 staining; therefore PB7 specifically recognizes the phospho-epitope, rather than simply the amino acid (Ser498) on BACE1.

instead of a C-terminal FLAG tag. Neurons were fixed, permeabilized, blocked and stained for total BACE1 using anti-FLAG antibody M2 (Sigma) and phosphorylated BACE1 using PB7. PB7 staining revealed punctate structures only in neurons transfected with BACE1 WT and not in those expressing BACES/A (Fig. 5a). Interestingly, the S/A mutant appeared to be enriched at the surface of the neuron, was barely visible along the axon, and appeared prominently in the growth cone (Fig. 5b, c). Phospho-BACE1 appeared few in puncta along the axon, and gave very bright staining in the distal tips of axons at the growth cone (Fig. 5b, c). Attempts to stain phosphorylated BACE1 in neurons expressing BACE1 with any C-terminal tags were unsuccessful (data not shown), possibly due to steric hindrance at the C-terminus blocking access of the antibody to the Ser498 epitope. Only PB7 staining in cells expressing BACE1 lacking a tag or with an N-terminal tag was successful.

Finally, to determine whether C-terminal mutants of BACE1 were capable of undergoing phosphorylation, I utilized cell lysates from HEK293 cells stably expressing BACE1 WT, BACE4C/A, BACES/A, BACES/D (a "phosphomimetic" in which the Ser498 has been mutated to Asp), and BACELL/AA (in which the two leucines of the dileucine motif, Leu499 & Leu500, have been mutated to alanine). Lysates were prepared in the presence of phosphatase inhibitors and subjected to SDS-PAGE and immunoblotting using PB7, followed by B7 for total BACE1. As expected, BACE1 WT gave a robust phospho-BACE1 signal and the non-phosphorylatable mutant, BACES/A, did not (Fig. 6). BACE4C/A gave a signal comparable to BACE1 WT, indicating that lack of palmitoylation does not change phosphorylation state, at least in cultured HEK cells. The BACES/D

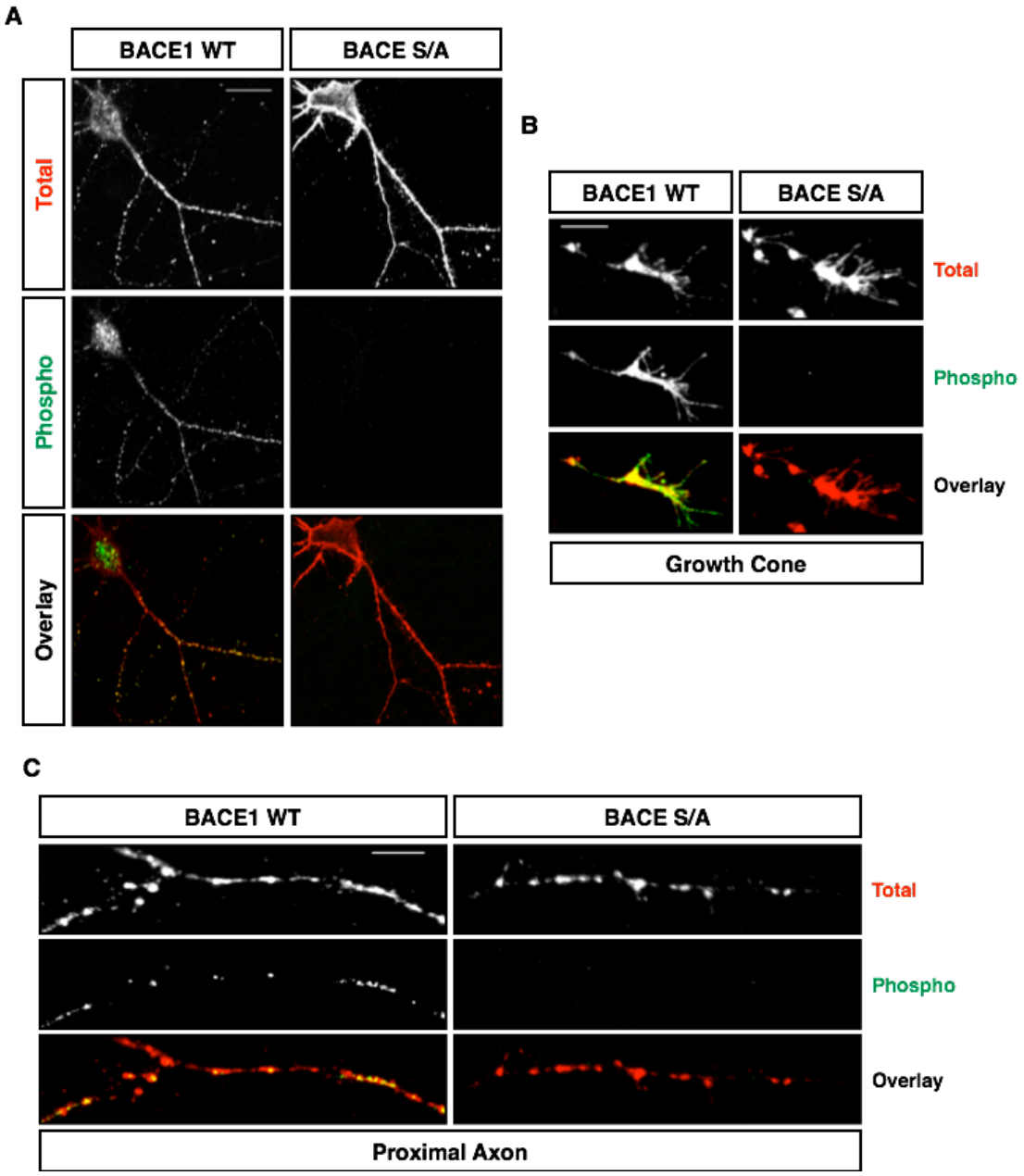

Figure 5: Neuronal staining with the phospho-BACE1-specific antibody PB7. A, Neurons transfected with FLAG-BACE1 WT or FLAG-BACE S/A were stained for phospho-BACE1 using PB7 and total BACE1 using anti-FLAG M2. PB7 staining is absent in neurons expressing BACE S/A. Scale bar, 30µm. B & C, PB7 staining in puncta along the proximal segment of axon is somewhat diminished; in contrast, PB7 staining is bright in growth cones. Scale bar, 5µm.

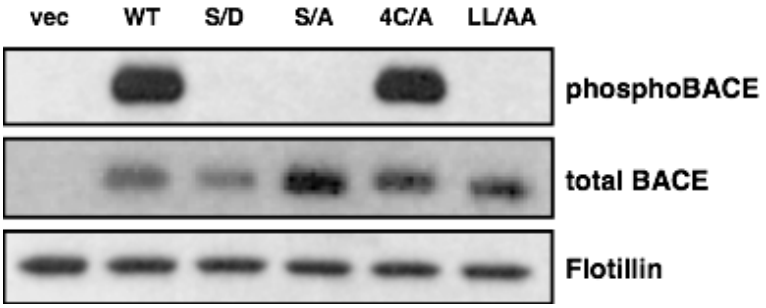

Figure 6. Detection of phosphorylated BACE1 in HEK293 cells stably expressing BACE1 WT and C-terminal mutants. HEK293 cells stably expressing pCDNA3.1 vector or the indicated BACE1 constructs were grown to confluence in a 6-well plate and lysates prepared in the presence of okadaic acid. 10% lysates were subjected to SDS-PAGE and probed for phospho-BACE1 using antibody PB7 and Flot2 as a loading control. The membrane was then stripped and re-probed for total BACE1 using antibody IL410, which recognizes the N-terminus of BACE1 (Fig. 2).

"phosphomimetic" did not exhibit a PB7 signal, emphasizing the specificity of PB7 for a phospho-group, and not just ionic charge. Interestingly and unexpectedly, the BACELL/AA mutant also did not exhibit a PB7 signal; our lab and others have previously shown that BACELL/AA is retained at the surface of the cell, and so this result would seem to suggest that phosphorylation occurs after internalization. However, this is in contrast to the results obtained in neurons transfected with BACES/A, showing that lack of phosphorylation appears to retain BACE1 at the cell surface. An alternative explanation for the PB7 staining results is that the LL residues are part of the PB7 antibody epitope. Antibodies directed to phosphorylated serine residues might help to answer this question.

Lipid raft analysis of forebrain extracts

Mice were deeply anesthetized with isofluorane and the forebrain immediately dissected, frozen on dry ice and stored at -80°C. All subsequent steps were carried out at 4°C. Lysates were prepared from frozen forebrains in homogenization buffer A (25mM TrisHCl, pH 7.4, 50mM NaCl, 250mM sucrose, 1mM DTT; 1mM PMSF + protease inhibitors added just before use), homogenized in a glass-teflon homogenizer and passed through a 25-gauge needle 10 times on ice. Homogenates were spun at 1000xg 10 min. The supernatant (S1), representing post-nuclear material, was transferred to a fresh tube and kept on ice. The pellet (P1), representing nuclear material, was resuspended in buffer A to wash, passed through a 25-gauge needle 5 more times and spun again at 1000xg 10 min. The washed pellet (P1') was resuspended in buffer A and stored at -20°C, and the supernatant pooled with the first (S1'). For time course experiments, forebrains

from 10 (E15, P0), 5 (P7), or 2 individual nontransgenic mice (P14) were pooled to have enough material to visualize by immunoblotting; one forebrain was collected individually for mice older than P30. To compare WT and 4C/A knock-in mice, tissue was harvested individually from mice at P7, tails were simultaneously collected for genomic DNA (gDNA) extraction, and genotyping was performed within 24h of collection. To allow for detection of BACE1 using material from individual mice, brain extracts were enriched for membrane proteins by centrifuging S1' at 12,000xg 20 min. The supernatant (S2), representing cytoplasmic proteins, was transferred to a fresh tube and stored at -20°C. The pellet (P2), representing the crude membrane fraction, was washed twice by resuspension in buffer B (0.32M sucrose, 4mM HEPES, pH 7.4; 1mM PMSF + protease inhibitors added just before use) and centrifuged at 12,000xg for 20 min. The final pellet (P2") was resuspended in 500µl buffer C (20mM HEPES, pH 7.4, 100mM NaCl; 1mM PMSF + protease inhibitors added just before use), mixed with 500µl 0.5% Lubrol WX (Lubrol 17A17, Serva; in 25mM TrisHCl, pH 7.4, 150mM NaCl, 5mM EDTA) plus 1ml of buffer B, and subjected to ultracentrifugation on a sucrose density step gradient (45%-35%-5%) at 39,000rpm for 21h at 4°C. 1ml fractions were collected from the top, and SDS was added to a final concentration of 0.25% before sonication for 30 sec. on ice. 20µl aliquots were fractionated on SDS-PAGE and immunoblotted for Flot2, a protein enriched in lipid rafts, to assess the reliability of the fractionation procedure. To compare raft vs. non-raft fractions, equal parts of fractions #4-6 (100µl each; identified as raft) and #8-12 (60µl each; identified as non-raft) were

combined, and 20µl of these combined fractions were fractionated on SDS-PAGE and analyzed by immunoblotting to assess relative BACE1 distribution.

Detection of BACE1 palmitoylation by acyl-RAC

Protein palmitoylation was detected in mouse brain lysate using a modified version of the Acyl-Resin Assisted Capture (Acyl-RAC) assay[144]. Mice were deeply anesthetized with isofluorane, immediately decapitated and the forebrain immediately dissected, frozen on dry ice and stored at -80°C. For tissue harvested from mice younger than weaning age (i.e., before ear tagging for identification and tail clipping for genotyping), tails were collected for gDNA extraction and genotyping was performed within 24h of collection. Frozen forebrains were homogenized in 500µl lysis buffer (25mM HEPES, 25mM NaCl, 1mM EDTA, pH 7.5; 1mM PMSF + protease inhibitors added just before use) using 15 strokes of a glass-teflon homogenizer and passed through a 25-gauge needle 15 times on ice. Homogenates were spun at 800xg for 5 min. The supernatant (S1), representing post-nuclear material, was transferred to a fresh microtube and spun again at 20,000xg for 30 min. The supernatant (S2), representing cytosolic proteins, was removed and the pellet (P2), representing the crude membrane fraction, was quantified for total protein by BCA assay (Pierce/Thermo). 2mg of protein was diluted to 1ml final volume with blocking buffer (100mM HEPES, 1mM EDTA, 2.5% SDS, 10mM N-ethyl maleimide (NEM); 1mM PMSF + protease inhibitors added just before use) and incubated at 40°C for 10 min. with frequent vortexing, to block any free cysteine residues on proteins. The first time I performed this assay, I also treated a separate set of parallel samples with a blocking buffer containing methyl

methanethiosulfonate (MMTS) instead of NEM, to determine which reagent was more efficient at blocking free cysteine residues. I found that the NEM treatment was better, and so performed all subsequent assays using NEM. The blocking reagent was removed by methanol/chloroform precipitation[145], and the proteins were resuspended in binding buffer (100mM HEPES, 1mM EDTA, 1% SDS, pH 7.5; 1mM PMSF + protease inhibitors added just before use). Half of the sample was treated with 2M NH_2OH to remove acyl groups from cysteine residues, while the other half was treated with 2M NaCl as a negative control, and each was rotated on a nutator with pre-washed thiopropyl sepharose (Sigma) beads for 3h at room temperature to pull-down proteins via the newly-liberated cysteines. Beads were washed 5 times with binding buffer, and eluted in binding buffer + 50mM DTT. Laemmli loading buffer was added to samples, which were then boiled and subjected to SDS-PAGE and immunoblotting for BACE1, PSD-95 Flot2.

Spine localization analysis

At DIV11, neurons were co-transfected with cDNA constructs encoding mApple-Actin (Margaret Gardel, University of Chicago) and either pS6 BBS-BACE1WT-YFP or BBS-BACE4C/A-YFP using Lipofectamine 2000. At DIV15, coverslips were rinsed briefly in ice-cold CMF-HBSS-HEPES, followed by fixation in ice-cold 4% PFA/4% sucrose in PBS, pH 7.4, at room temperature for 20 min. After three washes in PBS, residual PFA was quenched by a wash in ice-cold 50mM NH_4Cl for 10 min. at room temperature. Coverslips were washed 3 times in PBS and mounted onto slides in Permafluor mounting medium (Thermo). 200-nm-thick optical sections were acquired using a Leica SP5 Tandem Scanner Spectral 2-Photon

confocal microscope with 100X objective (NA 1.46, zoom 1.7; University of Chicago Light Microscopy Core Facility).

For consistency, spine analysis was performed at the proximal region of the apical dendrite, in the area of the first bifurcation. Dendritic spines were identified by enrichment with mApple-Actin and were separated into two different morphologically distinct categories: "mushroom" and "stubby." Mushroom spines are those with a clearly defined neck region emanating from the dendritic shaft, with a clearly defined, bulbous head region that is wider than the neck. Stubby spines lack a neck, and represent a more immature type of synapse. Manual quantifications of BACE1 spine localization were performed using the cell counter plugin in ImageJ (NIH), and included both spine types. Quantifications of fluorescence intensity in different spine regions were performed using MetaMorph Image Analysis Software (Molecular Devices). After subtracting background fluorescence using statistical correction, regions were manually created around spine head, neck (for mushroom spines), and at the base of the dendrite immediately below the spine head, using the mApple-Actin fluorescence as a reference. Regions were transferred to the YFP image and integrated intensity was measured. Statistical significance was determined by using the Kruskal-Wallis Rank-Sum t-test.

Axon-dendrite ratio analysis

At DIV5 or DIV11, neurons were transfected with either BBS-BACE1WT-YFP_Cer or BBS-BACE4C/A-YFP_Cer, in which two separate promoters drive expression of the BACE-YFP fusion protein and the Cerulean fluorophore.

Transfected neurons were fixed 1, 3, or 5 days after transfection and double-stained for AnkG and MAP2 to identify axons and dendrites, respectively. Wide-field epifluorescence images of fixed neurons were acquired as single in-focus planes using a Nikon TE2000 microscope and 60X (NA 1.49) objective. Images were analyzed using ImageJ (NIH). Briefly, 1-pixel-wide lines were drawn along the axon and three dendrites (apical and basal) to measure the mean fluorescence intensity in YFP and Cer images and averaged. Regions were drawn around the soma to measure the mean fluorescence intensity in the soma. A small circle was drawn in an empty region in each image to measure the background fluorescence. Background-subtracted axon, dendrite, and soma fluorescence intensities were used for all calculations.

Normalized axon-dendrite ratios (ADRs) for each individual neuron were calculated as follows:

$$ADR = \frac{\left(\frac{axon_{YFP}}{dendrite_{YFP}}\right)}{\left(\frac{axon_{Cerulean}}{dendrite_{Cerulean}}\right)}$$

Assuming that soluble cytoplasmic Cerulean distributes throughout the neuron randomly, this normalized ratio means that an ADR greater than 1 indicates a preference for axonal targeting, while an ADR equal to 1 indicates random distribution. This normalization method takes into account a higher fluorescence value associated with the larger geometry of the dendrite versus the axon.

Retroviral infections and axon-dendrite ratio analysis

Recombinant adenoviruses generated from pAdTrace BACE1 WT and 4C/A plasmids were generously provided by Dr. Tong-Chuan He (Department of

Orthopedics, University of Chicago). These adenoviruses express both monomeric red fluorescent protein (mRFP), as a morphological marker, and either FLAG-BACE1 WT or FLAG-BACE4C/A. DIV6 rat hippocampal neurons were transduced with adenoviruses using a 1:100 dilution of concentrated virus stock; at this dilution, ~10% of N2a cells were found to be infected in a test experiment (not shown), and ~30 neurons per 18mm coverslip were infected, much higher than the typical 10 neurons per 18mm coverslip using Lipofectamine 2000 tranfection. Neurons were then fixed at either DIV12 or DIV15 and stained for BACE1 using anti-FLAG antibody M2 (Sigma) and for dendrites using rabbit anti-MAP2. Axons were identified by mRFP fluorescence and lack of MAP2 staining. Axon-dendrite ratios were calculated as described above, using mRFP for normalization.

DHHC miRNA knockdown experiments

Hippocampal neurons were co-transfected at DIV11 with BBS-BACE1 WT-YFP and miRNA constructs to knockdown the expression of LacZ (as a negative control) DHHC-2, or DHHC-3. miRNA constructs also encode mCherry to verify expression and as a morphological marker. After 4 days of expression, neurons were fixed and subjected to ADR analysis as described above, using mCherry for normalization and AnkG staining to identify axons versus dendrites. In a parallel set of experiments, neurons were fixed and subjected to dendritic spine analysis as described above, using mCherry as a marker for dendritic spines.

FLAG antibody uptake & surface staining assay

The FLAG uptake and surface staining assay was developed in PT67 cells stably expression FLAG-BACE1 WT before performing the assay on neurons (Fig. 7,

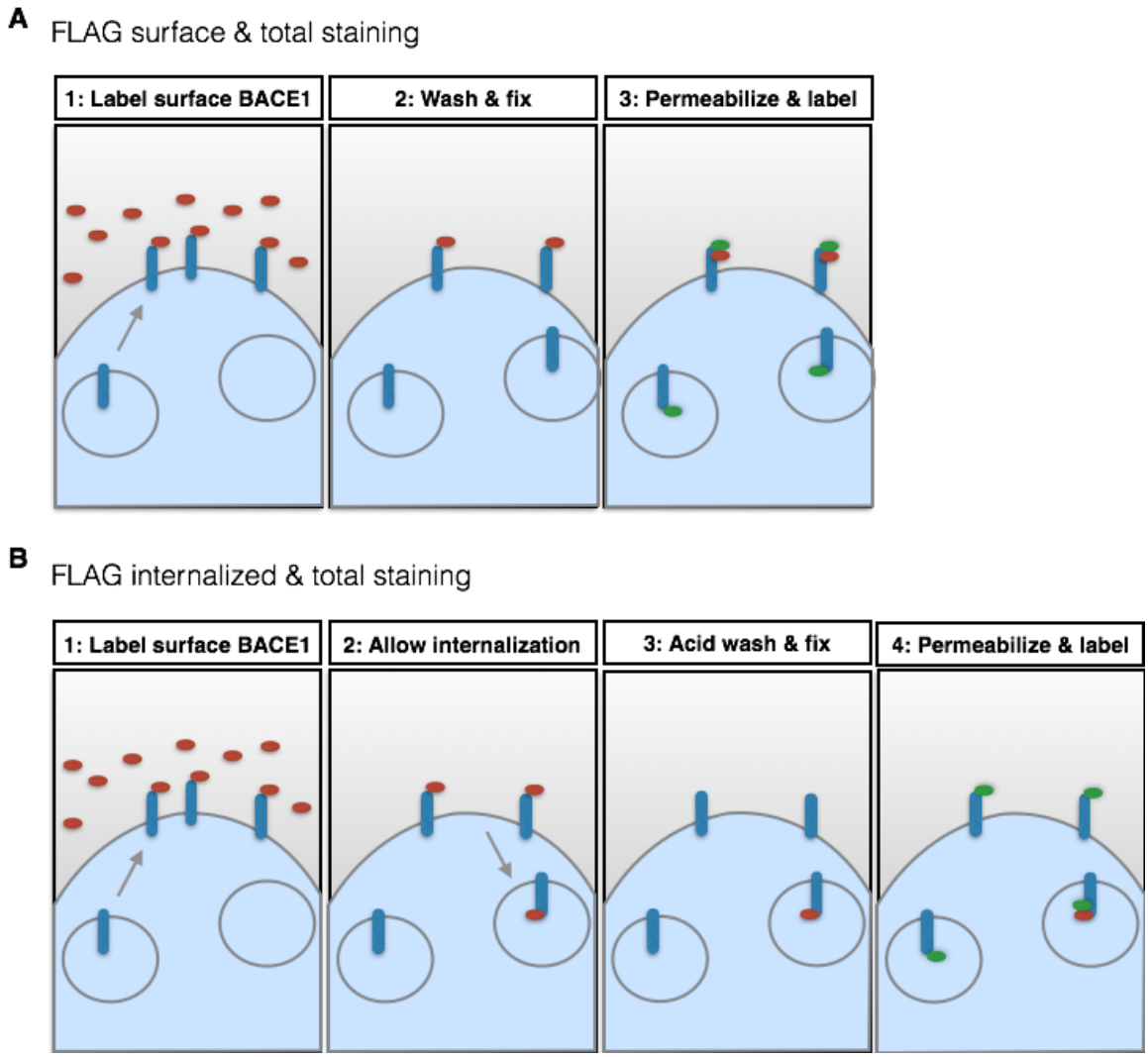

Figure 7. Schematic describing the FLAG-tag staining assay. A, Surface and total FLAG-BACE1 staining. B, Internalized and total staining, utilizing an acid wash step to eliminate residual FLAG antibody staining at the surface after the labeling and internalization period (20 min.). The second round of labeling in both steps will label total FLAG-BACE1, since the first round of labeling is not saturating, i.e., the second application of secondary labels all FLAG-BACE1, while the first application only labels either surface of internalized.

8). Coverslips were washed briefly on ice in ice-cold NIM, and surface-localized FLAG-BACE1 was labeled for 20 min. on ice with anti-FLAG antibody (M2, Sigma) in NIM + 20mg/ml BSA, to block non-specific binding sites. After the surface labeling, coverslips were washed 3X on ice and either fixed (for surface labeling) or returned to conditioned media at 37°C to allow internalization of FLAG-tagged BACE1. Coverslips were washed, fixed in 4% PFA/4% sucrose, pH 7.4, in PBS, and quenched in 50mM NH_4Cl. For surface labeling, cells were incubated in anti-mouse conjugated to AlexaFluor555 in 3% BSA in PBS. For internalized BACE1 labeling, cells were permeabilized on ice for 8 min. in 0.2% Triton in PBS, washed and blocked in 3% BSA in PBS, then incubated in anti-mouse conjugated to AlexaFluor555 in 3% BSA in PBS. To label total BACE1, permeabilized cells were then incubated with a second round of anti-FLAG antibody and anti-mouse secondary conjugated to AlexaFluor488. To perform the staining in neurons, transfection with BACE1 constructs encoding a FLAG-tag at the N-terminus was performed at DIV11, and staining was performed at DIV14-16, a stage during which there is an obvious difference in ADRs between WT- and 4CA-expressing neurons.

Generation of BACE4C/A knock-in mice

The BACE4C/A gene-targeted knock-in mouse, which expressed BACE1 in which the four palmitoylated Cys residues were substituted with Ala residues, was generated as follows. The gene-targeting vector was initially obtained from a large bacterial artificial chromosome (BAC) covering the mouse chromosomal sequence encoding the BACE1 gene (Children's Hospital Oakland Research Institute). I employed a gap repair/homologous recombination "recombineering" strategy to

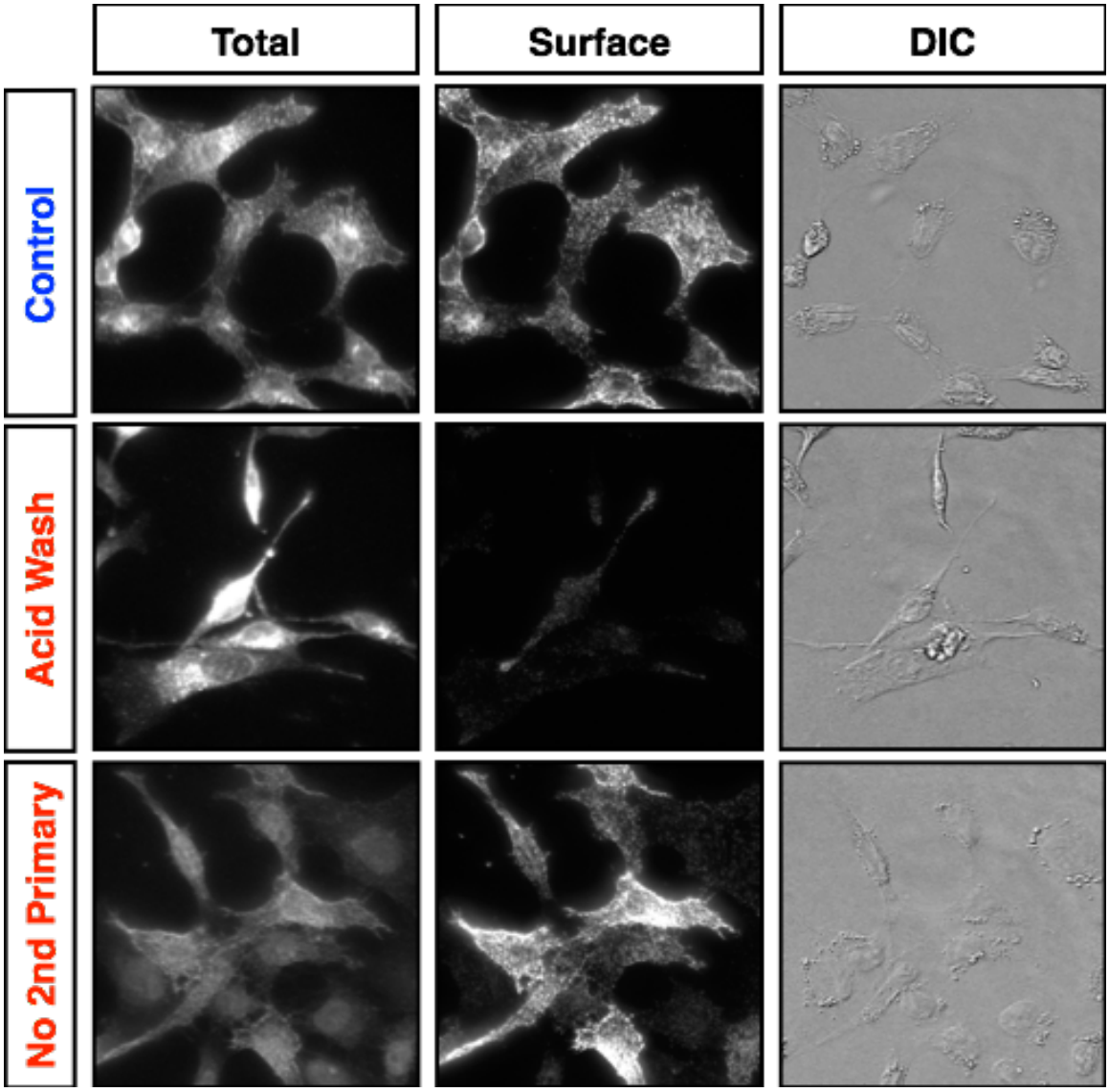

Figure 8. Development of FLAG staining assay to visualize surface FLAG-BACE1. PT67 cells stably expressing BACE1WT with an N-terminal, extracellular/lumenal FLAG tag were incubated with anti-FLAG antibody on ice for 20 min., washed and incubated with either PBS or an acid wash to strip away surface-bound FLAG antibody. Cells were then washed, fixed, and stained with secondary antibody to label surface-bound FLAG, and then permeabilized and subjected to a second round of FLAG antibody staining to label total FLAG-BACE1. Middle panel, the acid wash efficiently strips away surface signal. Bottom panel, cells in which the acid wash was omitted to leave surface staining intact, but in which the second round of FLAG antibody was also omitted, to visualize residual staining of the secondary. While total fluorescence in this condition was diminished, it was not completely absent and appeared to stain residual surface FLAG-BACE1, thus demonstrating that the first round of FLAG staining is not saturating, and that this second round of staining reveals total, not just intracellular, FLAG-BACE1.

retrieve ~9kb of chromosomal DNA into a smaller targeting vector (pGEM 7zf(+)). The 4 Cys-to-Ala mutations (C474A, C478A, C482A, C485A) were introduced into the vector using overlap-extension PCR and mutations were confirmed by sequencing. The targeting vector was altered and refined by GenOway (Lyon, France) for creation of the mouse line, to have a short 5' 3kb arm and a long 3' 4.2kb arm of homologous sequence flanking the 4C/A mutation site, allowing for homologous recombination of the targeting vector into the endogenous chromosomal locus (Fig. 9). A diphtheria toxin (DTA) cassette was engineered at the end of the 3' homology arm, to allow for negative selection against non-homologous recombined embryonic stem cell clones. A neomycin cassette flanked by *lox*P sites was also engineered in the intron 150bp upstream of exon 9, in a region that is not implicated in either gene regulation or mRNA splicing. The final targeting vector was linearized and transfected into mouse embryonic stem (ES) cells via electroporation. Out of 970 ES cell clones, 6 were identified and confirmed PCR, Southern blot and sequencing. These validated clones were injected into blastocysts, which were re-implanted into pseudo-pregnant females and allowed to develop to term. 14 highly chimeric (above 50%) males were generated and bred to Cre recombinase-expressing mice to excise the neo cassette, resulting in the final recombined locus. Genotyping by PCR was performed using tail DNA as a template and a set of two primers: "90548cof-TH1," 5' CTGGTGGGGAAAGCACTATTGGAAA 3' and "90549cof-TH1," 5' AACTTGGACAGAGCGAGCAGTAGGC 3'. The primers amplified a 334kb fragment from the wild-type allele, and a 444kb fragment from the knock-in allele.

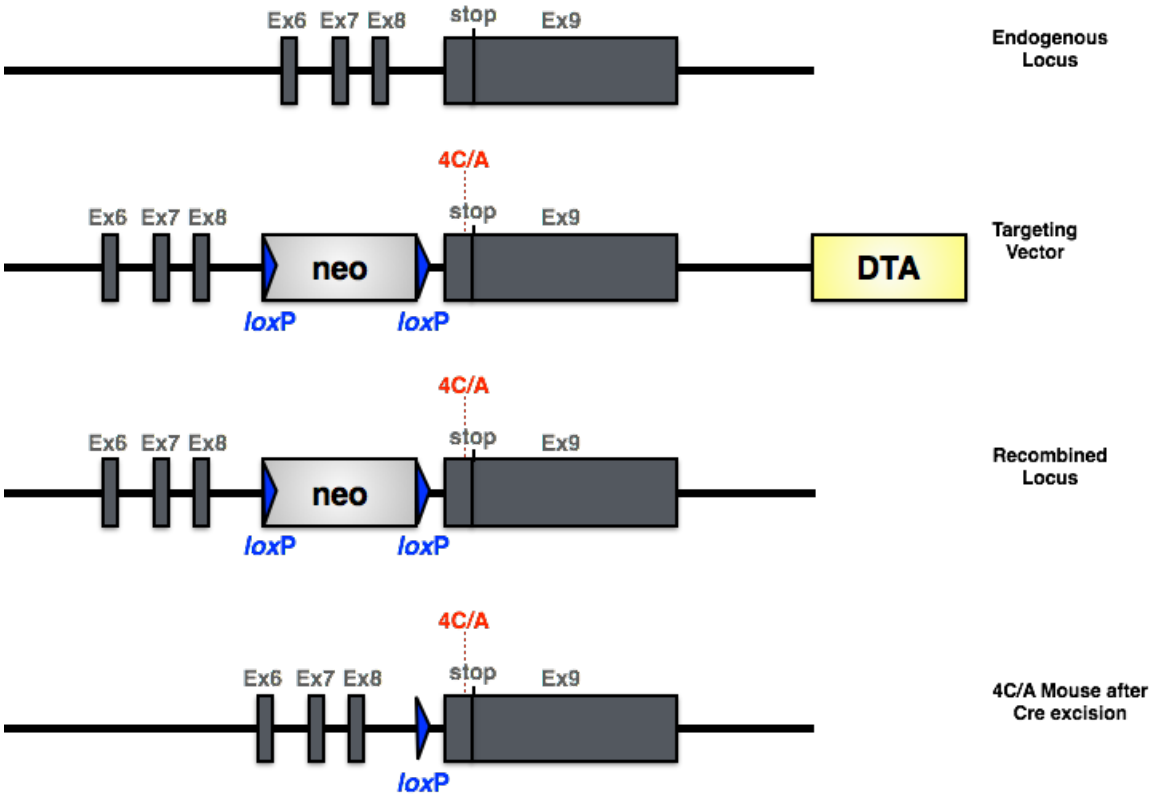

Figure 9. Gene-targeting strategy for creation of the BACE4C/A knock-in mouse. The palmitoylation site of BACE1 is located in exon 9 just upstream of the stop codon. An initial cloning vector spanning exon 8 and 9 was created in which the codons for the four cysteine residues that undergo palmitoylation were mutated to code for alanine residues instead (C474A, C478A, C482A, C485A). The knock-in targeting vector was comprised of a short 5' 3kb arm and a long 3' 4.2kb arm of homologous sequence flanking the BACE4C/A mutation site to allow for homologous recombination of the targeting vector into the endogenous locus. A diphtheria toxin (DTA) cassette was engineered at the end of the 3' homology arm, and a neomycin cassette flanked by *lox*P sites was also engineered in the intron 150bp upstream of exon 9. BACE4C/A chimeras were mated to Cre recombinase-expressing mice to excise the neo cassette, resulting in the final recombined locus.

Analysis of whole brain lysate by Western blot

Whole forebrain homogenates were prepared from adult mice that were first deeply anesthetized with isofluorane, rapidly decapitated into a methylbutane/dry ice slurry to quickly freeze the tissue, and the brain was immediately dissected and weighed. Immunoprecipitation (IP) buffer (150mM NaCl, 50mM Tris HCl pH 7.4, 0.5% Nonidet P-40, 0.5% sodium deoxycholate, 5mM EDTA) was added to get 20% weight/volume, and tissue was homogenized on ice with a tissue tearor. An equal volume of IP buffer +2% SDS was added to each sample to get 10% weight/volume in 1% SDS final concentration, and homogenates were sonicated at room temperature for 30 sec. to reduce viscosity by breaking down DNA.

Analysis of APP CTFs by immunoprecipitation

Forebrain lysates were prepared in IP buffer as described above. 500μg of lysate was immunoprecipitated with a polyclonal antibody to the C-terminus of APP, CTM1, and Protein A agarose beads. Immunoprecipitates were treated with 600 units of bacteriophage lambda phosphatase in a buffer containing 50mM TrisHCl, pH 7.8, 5mM DTT, 2mM $MgCl_2$, 100mg/ml BSA, for 1h @ 37°C. After washing in IP buffer without SDS, immunoprecipitates were eluted by boiling in 2X Laemmli buffer for 3 min., subjected to SDS-PAGE on a 16.5% Tris/Tricine gel and transferred to PVDF. Blots were probed for APP CTFs and full-length APP with antibody CTM1.

Histology

Mice were deeply anesthetized with isofluorane and intracardially perfused with ice-cold PBS for 5 min., followed by perfusion with ice-cold 4% PFA/4%

sucrose for 20 min. The brain was quickly removed and post-fixed in 4% PFA/4% sucrose for an additional 24h at 4°C, then switched to 30% sucrose for at least 48h at 4°C. The fixed brain was then frozen on dry ice, and serial 20µm-thick coronal sections through the olfactory bulb, and 40µm-thick sections through the forebrain, were collecting using a Leica Cryostat. Serial sections were collected in 6 wells of a 24-well plate per animal for olfactory bulb, and in 12-wells of a 12-well plate per animal for the forebrain, such that each well contained sections that were spaced at regular intervals apart. Sections were stored at -20°C in a "cryopreserve" buffer (30% ethylene glycol, 30% glycerol, 0.25M Tris-HCl, pH 7.5) until staining.

Immunofluorescence staining of coronal brain sections

Coronal brain sections were rinsed in Tris-buffered saline (TBS) 3x10 min. to remove cryopreserve, followed by an epitope retrieval step in citrate buffer (10mM trisodium citrate, 0.05% Tween-20, pH 6.0) for 30 min. at 90°C. After 3 x 5 min. washes in TBS, sections were quenched of any residual PFA in 10mM glycine, 0.25% Triton in TBS for 1h. After 3 x 5 min. washes in TBS, sections were then blocked in 5% horse serum, 0.25% Triton in TBS for 2h, followed by two 10 min washes in 1% BSA, 0.25% Triton in TBS. Sections were incubated with primary antibody diluted in 1% BSA, 0.25% Triton in TBS for 36h at 4°C; for BACE1 staining, fresh BACE1 antibody was added and sections were incubated at 37°C for an additional 2h. After 3 x 10 min. washes in 1% BSA, 0.25% Triton TBS, sections were incubated in secondary antibodies diluted in 1% BSA, 0.25% Triton in TBS for 2h; for Synapsin1 staining, sections were then washed and incubated with Synapsin1 antibody conjugated to biotin for 2h, washed, incubated with a streptavidin secondary

reagent conjugated to DyLight650 for 2h, then washed 3 x 15 min. in TBS. After antibody staining, sections were incubated in 0.25µg/ml Hoechst 33342 diluted in TBS for 20 min., washed and mounted on Superfrost plus slides with VectaShield mounting medium.

Quantification of BACE1 staining in brain sections

Wide-field epifluorescence images were acquired as single in-focus planes using a 4X objective on a Nikon TE2000 microscope. For quantifications of BACE1 staining in the hippocampus, the mossy fiber pathway in the dentate and CA3 areas were defined using Syn1 staining; the region was then transferred to the BACE1 image, and fluorescence intensity was quantified. The BACE1 fluorescence intensity was also measured along the infrapyramidal and suprapyramidal bundles, connecting the dentate and CA3 regions of the mossy fibers. The lengths of these bundles were measured using the Syn1 image, and to avoid confounding variables due to regional variance in bundle length, the same region of hippocampus was used between different animals. For all histological analyses, the Allen Brain Atlas was consulted to verify specific brain regions (http://atlas.brain-map.org).

Generation of 5XFAD-BACE4C/A transgenic/knock-in mice

For amyloid deposition studies, 5XFAD transgenic mice, which express five mutations associated with familial AD (APP K670N/M671L (Swedish) + I716V (Florida) + V717I (London), PS1 M146L + L286V) and generate high levels of Aβ42 specifically[146], were crossed with BACE4C/A mice (Fig.10). The 5XFAD mice are in a B6/SJL hybrid background, and it has been observed that 5XFAD mice in a congenic C57BL/6J background exhibit a less robust phenotype

(http://jaxmice.jax.org/strain/006554.html), which would potentially mask any effect of the BACE4C/A mutation on amyloid deposition. Therefore we employed a breeding strategy that would maintain the 5XFAD+BACE4C/A ("5X4CA") mice in an equivalent C57Bl6/SJL hybrid background (Fig. 10). 5XFAD males were first mated to BACE4C/A heterozygotes, producing nontransgenic and transgenic offspring heterozygous for BACE4C/A. From these offspring, 5XFAD BACE4C/A heterozygotes were mated with nontransgenic heterozygotes, producing an "F3" generation of 5XFAD mice expressing either BACEWT or BACE4C/A. These mice were used to study amyloid deposition by histological analysis and Aβ production by ELISA (described below).

Quantification of amyloid deposition in 5XFAD and 5X4CA mice

3 month-old 5XFAD mice and 5XFAD littermates expressing BACE4C/A were deeply anesthetized with isofluorane and intracardially perfused with ice-cold PBS for 5 min. The brain was quickly removed and split down the midline into two hemispheres; one hemisphere was postfixed in 4% PFA/4% sucrose for histological amyloid deposition analysis, while the other hemisphere was immediately frozen in a labeled microtube in a methanol/dry ice slurry and stored at -80°C for ELISA analysis (see below).

To quantify amyloid deposition analysis by histology, 3,3'-diaminobenzidine (DAB) staining was performed. Serial 40μm-thick coronal sections of post-fixed hemibrain, spaced 480μm apart, were stained by DAB immunohistochemistry using the mouse monoclonal antibody 3D6, which recognizes the first 5 amino acids of Aβ. Images were acquired using the same settings on a Cambridge Research and

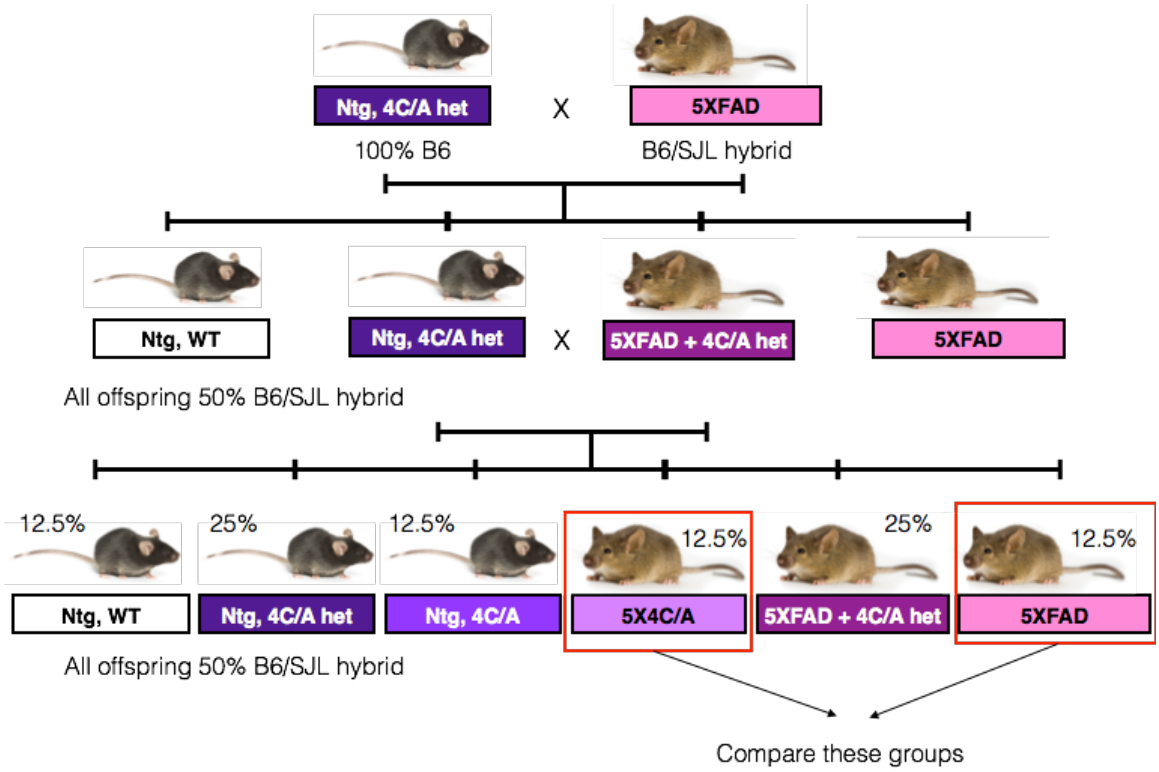

Figure 10. Crossing BACE4C/A knock-in mice with 5XFAD transgenic mice. To ensure that 5XFAD and 5XFAD+BACE4C/A mice ("5X4CA") were in equivalent backgrounds, nontransgenic mice heterozygous for the BACE4C/A mutation ("Ntg, 4C/A het"), which are in a 100% C57/Bl6 background, were first mated to transgenic 5XFAD mice ("5XFAD"), which are in a C57/Bl6/SJL hybrid background. Offspring from this cross resulted in nontransgenic mice homozygous for wild-type BACE1 ("Ntg, WT") or heterozygous for BACE4C/A, and transgenic mice expressing the 5XFAD transgenes either homozygous for wild-type ("5XFAD") or heterozygous for BACE4C/A ("5XFAD+4C/A het"). All offspring from this cross should have an equivalent B6/SJL hybrid background. Nontransgenic and transgenic heterozygotes from this generation were mated to produce 5XFAD and 5X4CA animals used for experiments, to compare the effects of wild-type BACE1 versus BACE4C/A in the 5XFAD Alzheimer's mouse model. All offspring thus have an equivalent B6/SJL hybrid background, to account for any differences in phenotype due to background. Expected allele frequencies are indicated in the figure; for actual allele frequencies, see Fig. 27.

Instrumentation (CRi) Pannoramic Scan Whole Slide Scanner (University of Chicago Light Microscopy Core Facility). After converting images to .tif format, a region of interest was drawn in ImageJ and the total area was measured; a threshold was then created around the amyloid deposits, using the negative staining of two WT brains as negative controls, and regions were created around the thresholded area and measured. The area of amyloid staining was divided by the total area for each region of interest analyzed to get the % area of amyloid burden. For all histological analyses, the Allen Brain Atlas was consulted to verify specific brain regions (http://atlas.brain-map.org).

Quantification of BACE1 elevation near amyloid deposits in 5XFAD and 5X4CA mice

Coronal brain sections from 5XFAD and 5X4CA mice were stained for BACE1 (EPR3956) and amyloid deposits (3D6) using immunofluorescence as described above. Wide-field epifluorescence images were acquired as single in-focus planes using a 10X objective on a Nikon TE2000 microscope. Image analysis was performed using MetaMorph software. After background subtraction using statistical correction, a threshold was set around amyloid deposits using the 3D6-stained image. A circular center filter with a diameter of 5 pixels was applied, followed by dilation by 5 pixels, to create a region around the amyloid deposits that included the surrounding dystrophic structures that might include BACE1. These regions were then transferred to the BACE1-stained image. The integrated intensity of the 3D6 and BACE1 signals were measured, to account for both fluorescence intensity and size of the deposits.

Statistical analysis

All statistical analyses and graphs were performed using Prism (GraphPad Software). The Mann-Whitney rank-sum t-test was used for comparisons between two groups, while comparisons across larger groups were performed using the Kruskal-Wallis test. Statistical tests used and n's are indicated in the corresponding figure legends. Post-hoc power analysis was used to determine whether the sample size was large enough to confidently make conclusions about the data, and was conducted using Statistical Solutions Power & Sample Size Calculator (http://www.statisticalsolutions.net/). Effect size, or the degree to which a difference was detected between two groups, was calculated as Cohen's *d*, using the formula

$$d = \frac{{M_1}^2 + {M_2}^2}{\sqrt{\frac{{S_1}^2 + {s_2}^2}{2}}}$$

where *M* is the mean and *s* is the standard deviation. All data are represented as mean ± SEM.

CHAPTER III

BACE1 targeting in neurons: Palmitoylation as a mediator

Normal BACE1 localization throughout the neuron and at synaptic sites, in transfected and non-transfected neurons

The subcellular localization of BACE1 may impact its ability to cleave APP and initiate Aβ production near the synapse; however, evidence supporting this hypothesis in neurons is lacking. Furthermore, the mediators of BACE1 localization in neurons are not well understood. To first characterize BACE1 localization at the cellular level, I cultured primary hippocampal neurons from BACEKO and wild type littermates and used immunofluorescence staining to visualize endogenous BACE1. I used the rabbit monoclonal antibody EPR3956 (GeneTex), which has its epitope at the intracellular C-terminus of the BACE1 protein sequence. BACE1 staining with this antibody was highly specific, as staining was virtually absent in cultures from BACEKO mice (Fig. 11a). Furthermore, staining cultured rat hippocampal neurons in the absence of primary antibody resulted in an absence of signal, demonstrating the specificity of this staining protocol (Fig. 11b). BACE1 staining in neurons from both mouse and rat brain reveals a somewhat diffuse pattern, suggestive of surface localization. BACE1 staining was also found in discrete puncta along neurites and in the cell body (Fig. 11, 12). A portion of BACE1 puncta overlapped with Synapsin1, a synaptic vesicle protein enriched at presynaptic sites. BACE1 puncta also overlapped with the postsynaptic marker PSD-95 (Fig. 12). A closer examination of BACE1 staining revealed BACE1 was present in puncta that were both positive and negative for synaptic markers (Fig. 12). I have assisted in immunostaining and

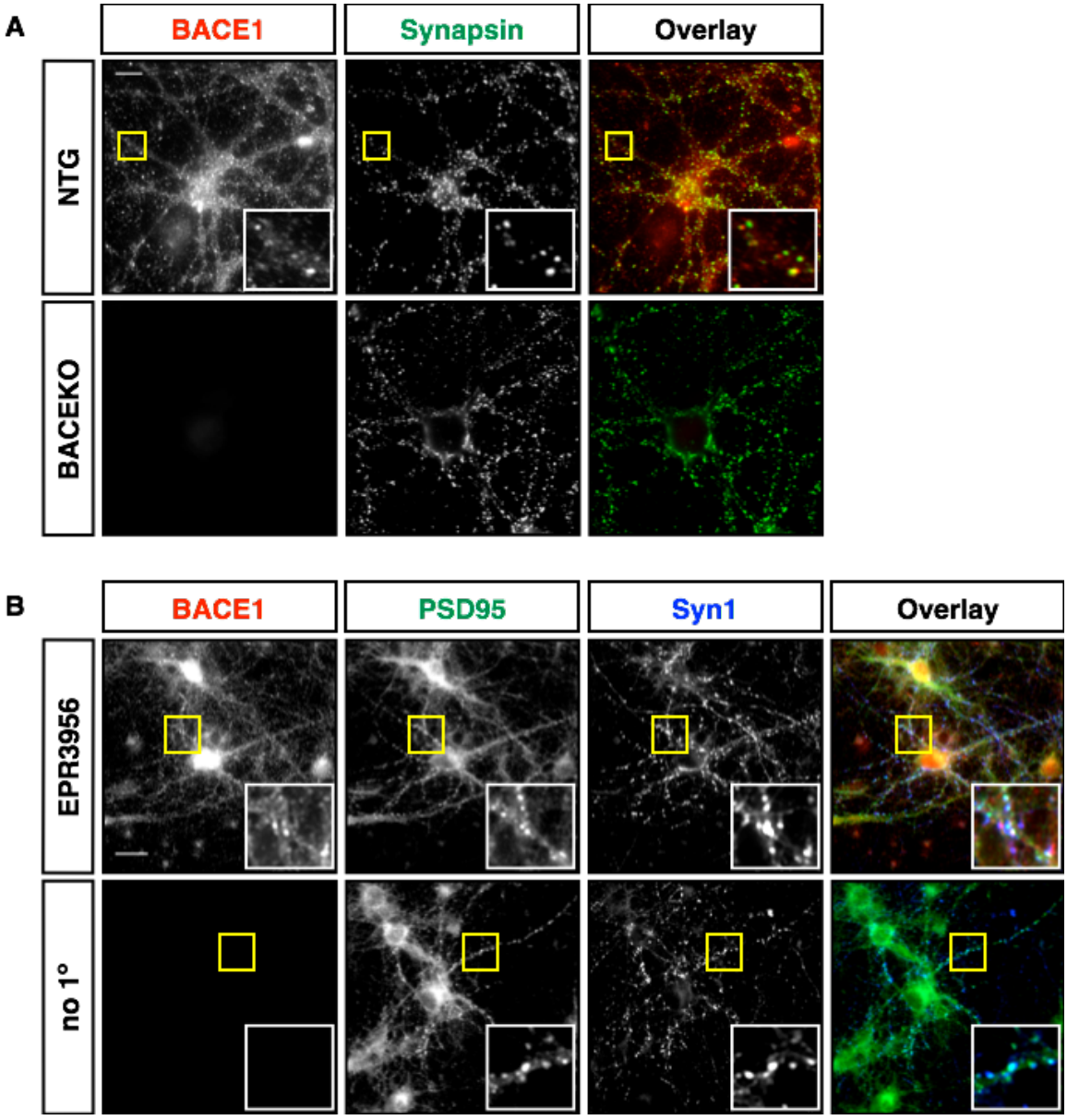

Figure 11. Specificity of antibody EPR3956 for endogenous BACE1 staining in cultured rat hippocampal neurons. A, Neurons from BACEKO E18 mice were cultured alongside BACE1-expressing nontransgenic ("NTG") litter mates at a control for antibody specificity. BACE1 staining using rabbit monoclonal antibody EPR3956 (GenTex) reveals specific staining along neurites, which is absent in BACEKO neurons, and partially overlaps with Syn1, a presynaptic marker. Scale bar, 10µm. B, BACE1 is present in synaptic puncta positive for PSD-95 and Syn1, and in non-synaptic puncta negative for those markers. BACE1 can also be seen throughout the soma, consistent with localization in a perinuclear compartment. Neurons that were not stained with EPR3956 but with only the secondary anti-rabbit AlexaFluor 555 antibody were devoid of staining. Scale bar, 20µm.

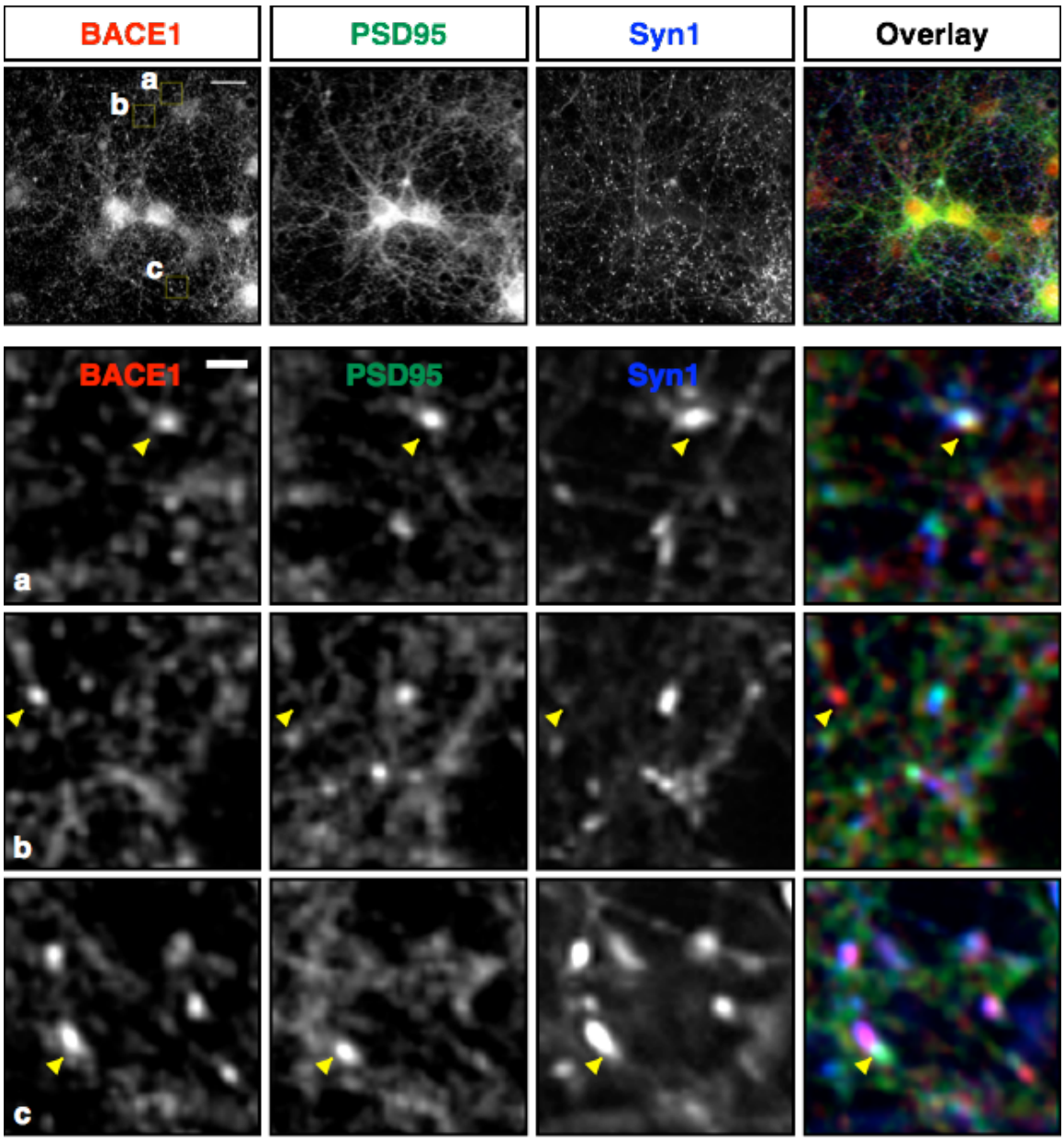

Figure 12. Endogenous BACE1 staining in cultured rat hippocampal neurons. BACE1 is present in synaptic sites positive for (a & c) and non-synaptic puncta negative for (b) PSD-95 and Syn1. Scale bar, 20µm (upper panel) and 2µm (lower panel).

colocalization experiments in my lab to show that overexpressed, fluorophore-tagged BACE1 colocalizes with markers of recycling endosomes in my cultured neurons[92, 102]. The pattern of overexpressed BACE1 localization (Fig. 13) matches endogenous BACE1 in my neuron culture system (Fig. 11, 12), with BACE1-positive puncta scattered throughout somatodendritic and axonal compartments, and is consistent with previous studies[97, 103, 104].

Previously my lab developed cDNA plasmids encoding BACE1 with an enhanced YFP (EYFP) tag fused to the C-terminus, to track real-time BACE1 localization in transfected cells by fluorescence microscopy. I used this construct and a cerulean-tagged BACE1 construct (BACE1-Cer) to further characterize synaptic BACE1 localization in neurons. In agreement with other reports on BACE1 localization in cultured neurons[103, 104], BACE1-YFP can be prominently seen in the soma, in MAP2-positive dendrites, and in MAP2-negative neurites, which are axons (Fig. 13). BACE1-YFP can also be seen in bulbous protrusions extending from the dendrite shaft, which I will refer to as dendritic spines. BACE1 also appears in discrete puncta along the axon, echoing the synaptic localization seen previously for endogenous BACE1. To determine if any of the axonal puncta were bona fide presynaptic sites, I performed $FM_{1\text{-}43}$ dye labeling[143] (Fig. 14). The $FM_{1\text{-}43}$ dye is a lipophilic styryl compound that is water-soluble and nonfluorescent in aqueous media; when the dye is inserted into the outer leaflet of the cell membrane, it becomes intensely fluorescent and will become internalized into recycled synaptic vesicles, staining active nerve terminals. Subsequent depolarization, causing massive synaptic vesicle fusion at synapses, will release the dye back into the

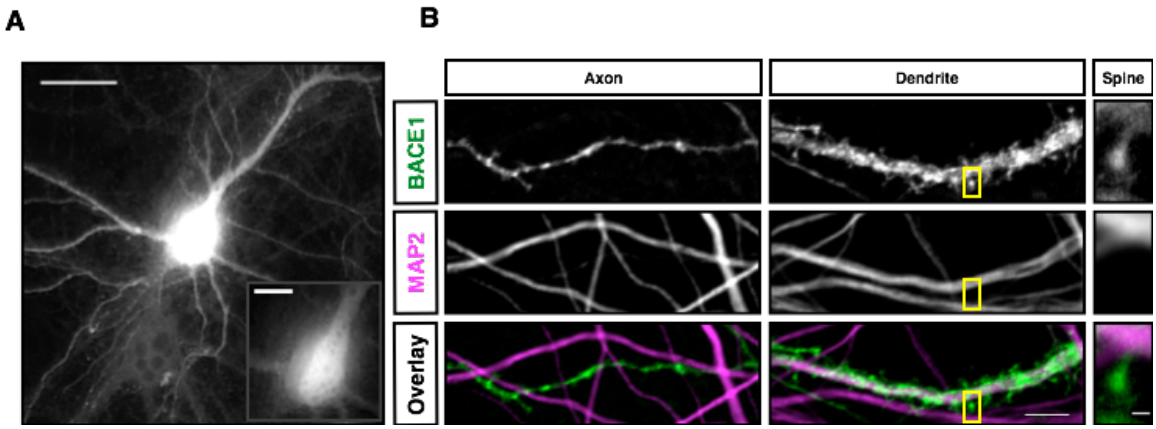

Figure 13. BACE1 can be found in both axons and dendrites in cultured hippocampal neurons. Mouse hippocampal neurons transfected at DIV11 with BACE1WT-YFP, fixed and stained at DIV12 for MAP2 to identify dendrites. A, Example of a neuron expressing BACE1-YFP; brightness is enhanced to show fine axonal and dendritic processes. Scale bar, 30µm. Inset, soma with lower brightness to show detail. Scale bar, 10µm. B, BACE1 is clearly seen in axons, which are negative for MAP2 (left) and also in dendrites, which are positive for MAP2 and have spine-like structures protruding out, which are also positive for BACE1 (right). Scale bar, 5µm (left) and 0.5µm (right).

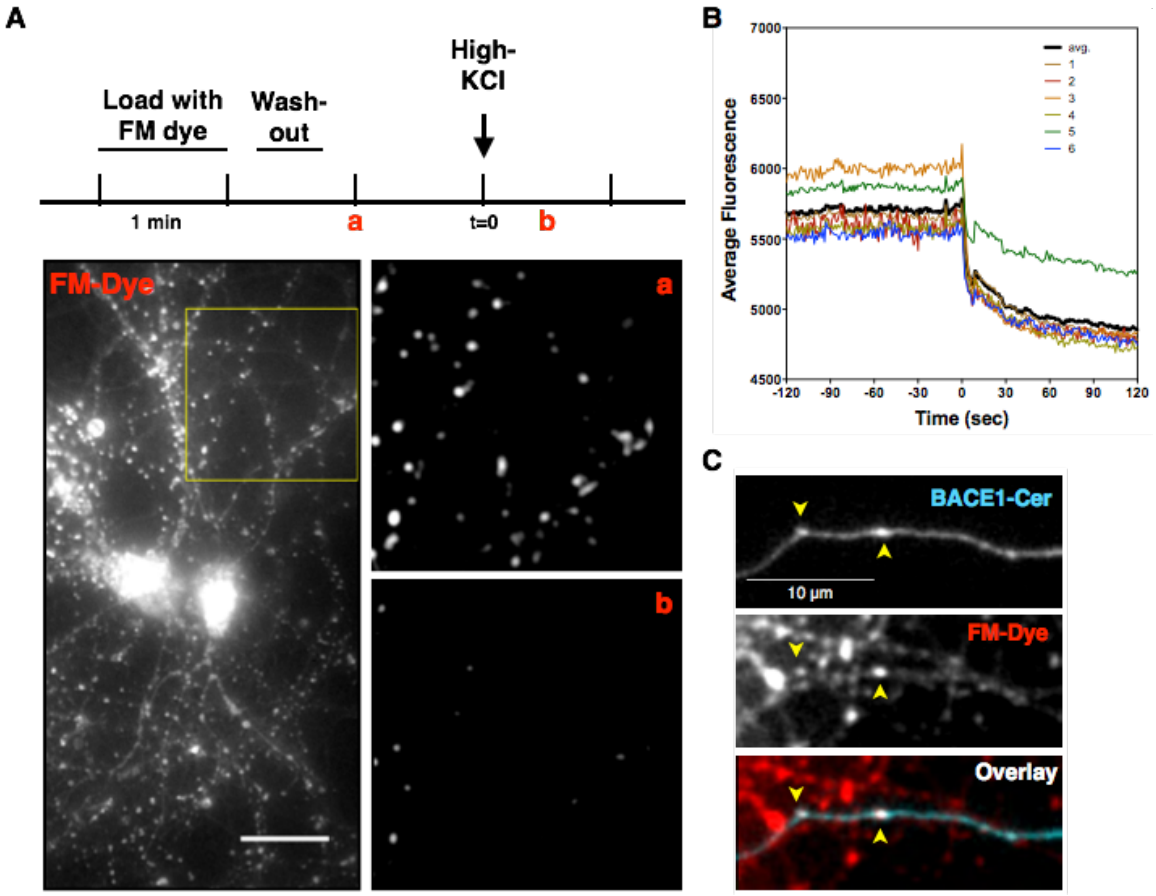

Figure 14. BACE1 is present at functional presynaptic sites. A, Demonstration that FM_{1-43} is taken up at presynaptic sites. Neurons were equilibrated in live imaging medium, followed by a 1 min. dye-loading step during which neurons were incubated with 15µM FM_{1-43} in a high-KCl buffer to depolarize neurons and stimulate uptake at functional presynaptic sites. Neurons were then washed three times in live imaging medium and time lapse images were acquired within 10 min. A second depolarization step resulted in loss of fluorescence at the vast majority of FM_{1-43}-positive puncta within 30 sec., a time scale consistent with synaptic vesicle release. Scale bar, 20µm. B, Plot of the average fluorescence and individual fluorescence of 6 representative FM_{1-43}-positive puncta from the neuron shown in A. For all but one of the puncta, fluorescence intensity drops within the first ~10 sec. after the second depolarization step. C, DIV11 neurons were transfected with BACE1-Cerulean and the FM dye uptake was performed at DIV13 as described to label presynaptic sites. BACE1-Cer can be found to overlap with FM_{1-43}-positive sites along the axon.

medium; active synapses are therefore identified by very rapid (~1 sec) loss of fluorescent signal upon depolarization, vs. nonsynaptic areas along the neuron that had endocytosed the dye during the dye loading step, which should not undergo rapid exocytosis upon depolarization (Fig. 14a)[143]. Because the FM_{1-43} dye was detected using a filter that normally detects YFP, I created a plasmid in which BACE1 was fused to Cerulean instead of YFP at the C-terminus (BACE1-Cer). BACE1 overlapped with FM_{1-43} dye-positive puncta in cultured transfected neurons, and the majority of these puncta lost FM_{1-43} dye fluorescence within ~1 sec, demonstrating that these were functional presynaptic sites (Fig. 14b, c). Taken together, these data show that both endogenous and expressed BACE1 is found throughout the neuron, in both synaptic and non-synaptic sites.

BACE1 enrichment into axons over time

Over the course of our experiments, I, and others in the lab, made the observation that, in transfected neurons, BACE1-YFP could be seen more clearly in the axons than the dendrites with time after transfection and in more mature (older than DIV12) neurons. To quantify this observation, I designed an experiment to measure the relative distribution of BACE1 in the axons versus the dendrites at three different time points after transfection, 1, 3 or 5 days (Fig. 15). To determine whether the age of the neurons in culture might also affect this distribution, which would be a reflection of the number of mature, fully functional synapses in the culture, I examined neurons transfected at either a younger (DIV5) or older (DIV11) age. In order to visualize all of the structures in the neuron, I co-transfected with a separate plasmid, pCS2-Cerulean; Cerulean is non-specifically targeted to all

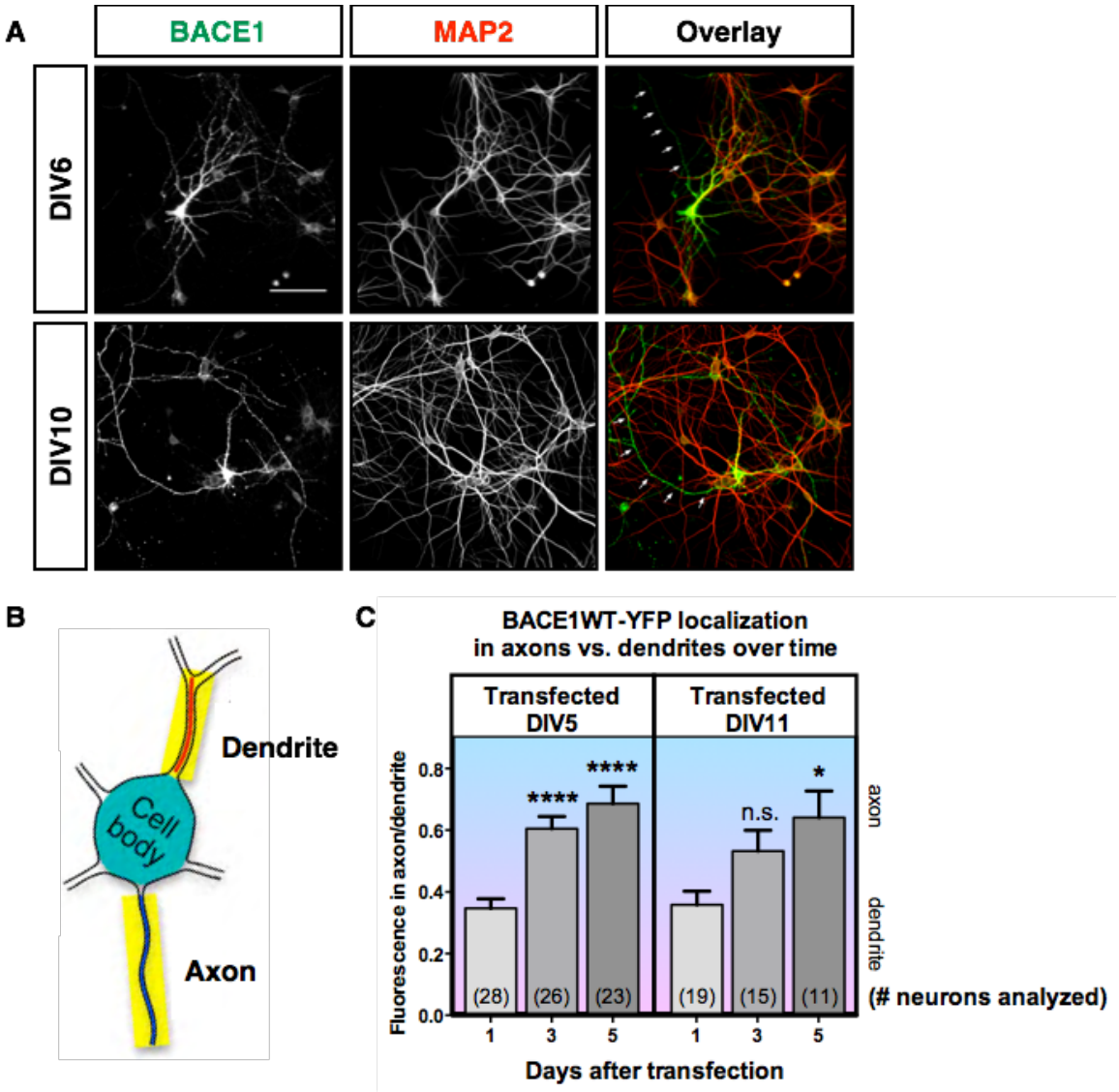

Figure 15. BACE1 appears to enrich into axons over time in culture. A, Mouse hippocampal neurons were transfected at DIV5 (shown) or DIV11 (not shown) with BACEWT-YFP and fixed and stained for MAP2 1, 3, or 5 days later. BACE1 can be seen more clearly in the axon at later time points. Scale bar, 100µm. B, To quantify BACE1 fluorescence in different neuronal compartments, lines were traced along the YFP fluorescence in MAP2-positive dendrites and MAP2-negative axons, and the mean fluorescence intensity was measured. C, BACE1 is significantly higher in the axon at 3 (DIV5 transfections) and 5 (DIV5 and DIV11 transfections) days after transfection. *, $p<0.05$; ****, $p<0.0001$, Kruskal-Wallis test.

compartments of the neuron and is thus useful and a morphological "fill" to identify axons and dendrites. Neurons were fixed and stained for MAP2 to identify dendrites, and Cerulean-positive, MAP2-negative neurites were identified as axons. I found that the ratio of BACE1 fluorescence in the axon vs. dendrites significantly increased at 5 days after transfection for both transfection time points, and even at 3 days after transfection for the DIV5-transfected neurons (Fig. 15).

BACE1 undergoes palmitoylation in vivo

Previously, our laboratory found that BACE1 undergoes palmitoylation at four cysteine residues in a juxtamembrane region of the cytosolic tail, and that mutation of all four cysteines to alanine ("4C/A" mutant) abolished palmitoylation and displaced BACE1 from lipid rafts in cultured non-neuronal cells[119] (Fig. 3). BACE1 also undergoes phosphorylation at serine 498 (Fig. 3), a few amino acids downstream of the palmitoylation sites. Phosphorylation has been suggested to enhance GGA1 binding and thus endosomal transport, in studies using non-neuronal cells[111, 114]. For other neuronal proteins, including AMPA and NMDA receptor subunits and GAP43, it has also been suggested that both phosphorylation and palmitoylation may generally influence each other to modulate localization, likely by affected the availability of the modification site or by restricting the protein to a domain that either contains or lacks the enzyme mediating the modification[147-149]. However, the relevance of either of these modifications to BACE1 transport or activity in neurons and in vivo is largely unknown. To begin to address how either phosphorylation or palmitoylation affect BACE1 in vivo, I analyzed BACE1 in mouse brain extracts at different stages of development. In agreement with a previous

report[66], BACE1 protein levels peak during periods of synaptogenesis, from P0 to P30 (Fig. 16a). Given the importance of lipid raft targeting in neuronal protein localization, and the fact that BACE1 expressed in cultured cells can be found prominently in lipid rafts[119], I also analyzed extracts enriched for lipid raft proteins versus non-raft localized membrane proteins to see if BACE1 is found in lipid rafts in the brain (Fig. 16b). BACE1 distribution in lipid rafts mirrored the pattern of BACE1 levels, peaking at P7 and dropping after 1 month (Fig. 16c). Using an antibody specific for phosphorylated forms of BACE1, PB7 (Fig. 4-6; described in Chapter II), phospho-BACE1 was only detectable in the raft fraction of P7 mice, and in the non-raft fractions of P0-P14 mice, and was barely detectable in the non-raft fraction of P30 and older mice (Fig. 16c). This signal was only detectable after a 30min. exposure to film. Phosphorylated BACE1 was not detectable in whole brain homogenates (attempted many times; data not shown), even in the presence of a cocktail of phosphatase inhibitors and a serine phosphatase-specific inhibitor, okadaic acid. Thus, although phosphorylation has been implicated in BACE1 endosomal transport in non-neuronal cells and is detectable in transfected neurons (Fig. 5), endogenous phosphorylated BACE1 was not readily detectable using antibody PB7, in my hands. I therefore focused my attention on palmitoylation as a post-translational modification regulating BACE1 localization.

To determine the relative level of palmitoylated BACE1 in mouse brain, I performed a modified version of the Acyl-RAC assay[144] (Fig. 17). To enhance detection of palmitoylated BACE1 and validate the assay, I prepared a crude membrane fraction from P7 mouse forebrain (Fig. 17a). The reliability of the Acyl-

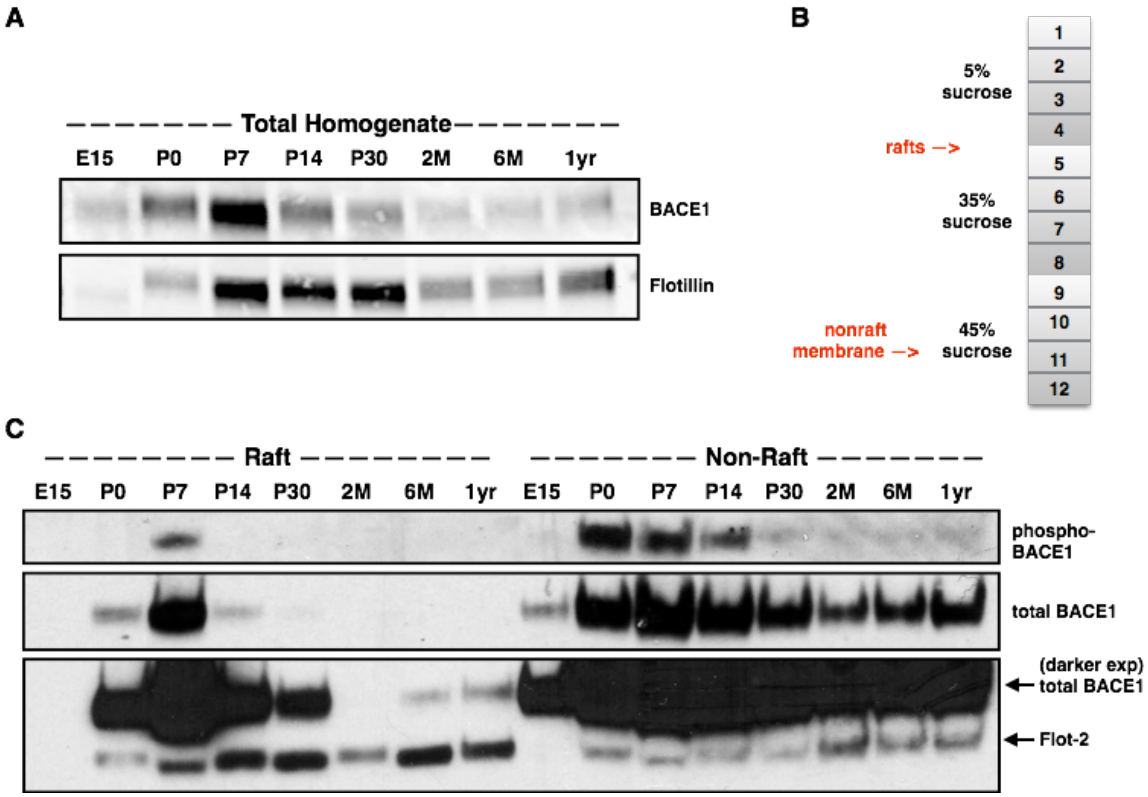

Figure 16. BACE1 protein levels and distribution in lipid rafts in mouse forebrain extracts at different developmental stages. A, Total BACE1 protein from forebrain extracts from mice at the indicated ages. BACE1 expression is elevated from P0 to P30, peaking at P7. BACE1 protein levels drop after 1 month. B, Sucrose density gradient used to separate raft proteins from non-raft membrane proteins in Lubrol-soluble extracts. C, BACE1 distribution in lipid rafts largely follows total protein expression, peaking at P7. A longer exposure is shown to demonstrate BACE1 raft distribution even at 1 month. Flot2 enrichment is found in the raft fractions relative to non-raft, with the exception of the 2 month-old sample, indicating that, overall, the raft fractionation was efficient. Phosphorylated BACE1 also appears to follow total BACE1 protein levels, and appears to be higher in the non-raft versus raft fractions.

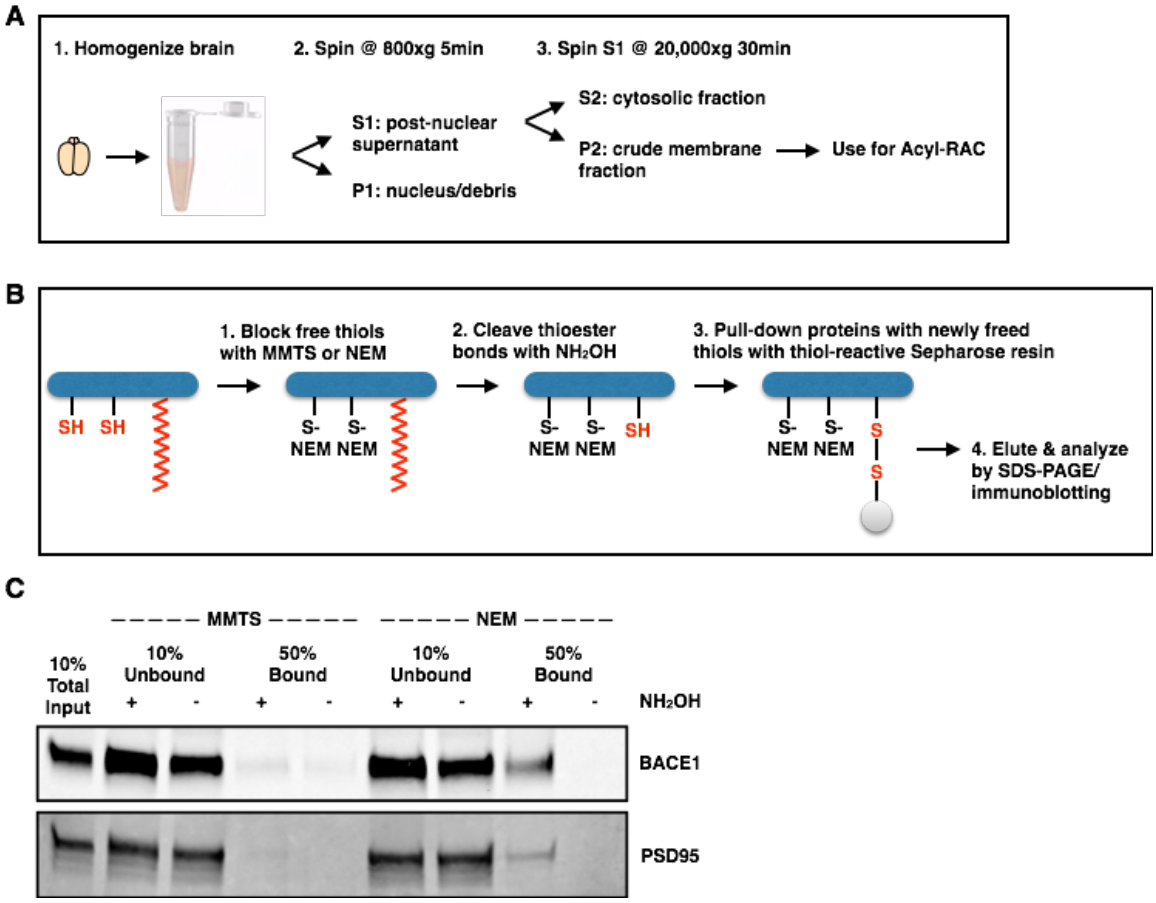

Figure 17. Acyl-RAC assay to determine levels of palmitoylated protein in brain homogenate. A, Preparation of membrane fraction from brain homogenates. B, Schematic outlining the Acyl-RAC assay. Membrane fractions of brain homogenates are treated with either MMTS or NEM to block free thiol groups. Thioester bonds are then cleaved with NH2OH and proteins with newly-liberated thiols (i.e., were previously palmitoylated) are captured with thiopropyl Sepharose resin. Unbound proteins are saved, and bound proteins are eluted in reducing buffer. C, A significant fraction of BACE1 is palmitoylated in mouse brain. MMTS and NEM were compared for blocking efficiency; NEM was found to completely block binding in the absence of NH_2OH, and therefore was used as blocking reagent in subsequent Acyl-RAC assays. 10% input, 10% unbound, and 50% bound (Acyl-RAC) fractions were analyzed by immunoblotting for BACE1 and PSD-95.

RAC assay depends on efficient blockade of any free thiols before removal of acylated thiol groups (plus NH_2OH treatment) and subsequent pull-down via thiol-reactive thiopropyl Sepharose resin (Fig. 17b). Efficient blocking can be tested by checking if the protein of interest is bound to thiopropyl Sepharose without removal of acylated thiol groups (minus NH_2OH treatment). In my hands, use of methyl methanethiosulfonate (MMTS) was inefficient at blocking free thiol groups, while N-ethylmaleimide (NEM) resulted in complete block of thiols (Fig. 17c). Furthermore, I found that NH_2OH treatment gave a clear, specific BACE1 signal that was at least as strong as the signal for PSD-95, a protein for which palmitoylation plays a well-defined role in targeting to post-synaptic sites in the brain. Therefore, endogenous palmitoylated forms of BACE1 are readily detectable at steady state and are found in lipid raft fractions in the mouse brain.

Palmitoylation mediates BACE1 spine localization

In transfected hippocampal neurons, BACE1 can be found prominently in dendritic spine-like protrusions. Palmitoylation plays a well-documented role in mediating protein localization in neuron-specific compartments, most notably at the synapse in cholesterol-rich dendritic spines[120, 150]. The observation that BACE1 localizes to dendritic spines suggested a possible role for palmitoylation in protein targeting to this compartment. Given the neuron-specific function of palmitoylation, and the fact that neurons are a relevant model system for studying the cell type-specific mechanisms of Alzheimer's disease, I chose to test the hypothesis that palmitoylation is important for localization of BACE1 in dendritic spines. Thus, I set out to first study the localization of the BACE4C/A non-palmitoylatable mutant in

cultured hippocampal neurons. As mentioned above, this mutant lacks the sites of palmitoylation and is excluded from lipid rafts in cultured cells[119].

I transfected neurons at DIV11 with constructs encoding either BACEWT-YFP or BACE4C/A-YFP, along with mApple-Actin as a marker of dendritic spines; dendritic spines are highly enriched in actin, providing a highly dynamic cytoskeleton that respond to changes in synaptic activity, and actin can be used as a morphological marker of spines[151-154]. BACE1 WT can clearly be seen to overlap with these actin-enriched spines; the 4C/A mutant, however, was conspicuously absent from these spines (Fig. 18a). For all spine analyses, I focused on the area of the first bifurcation of the apical dendrite, to ensure that there were no differences in spines due to proximity to the soma. BACE 4C/A expression did not alter the density of actin-positive spines in these neurons, and spine density corresponded to previous reports[155-157] (Fig. 18b). While BACE1 WT was present in ~80% of these spines, the 4C/A non-palmitoylatable mutant was present in only ~30% of actin-positive spines (Fig. 18c). To explore BACE1 localization at the spine in greater detail, I measured YFP fluorescence in each compartment of the spine, as defined by actin fluorescence: the head, the neck, and at the base of mushroom-type spines, and in the head and base of stubby-type spines (Fig. 19). I chose to focus on these two spine types for two reasons: first, they are easily identifiable, as mushroom-type spines have a characteristic bulbous head with a diameter that is at least 1.5 times wider than the diameter of the thinner neck extending from the dendrite shaft; while stubby-type spines lack such necks. Second, these two spine types represent a more mature and immature form of postsynaptic site, respectively, and I wanted to

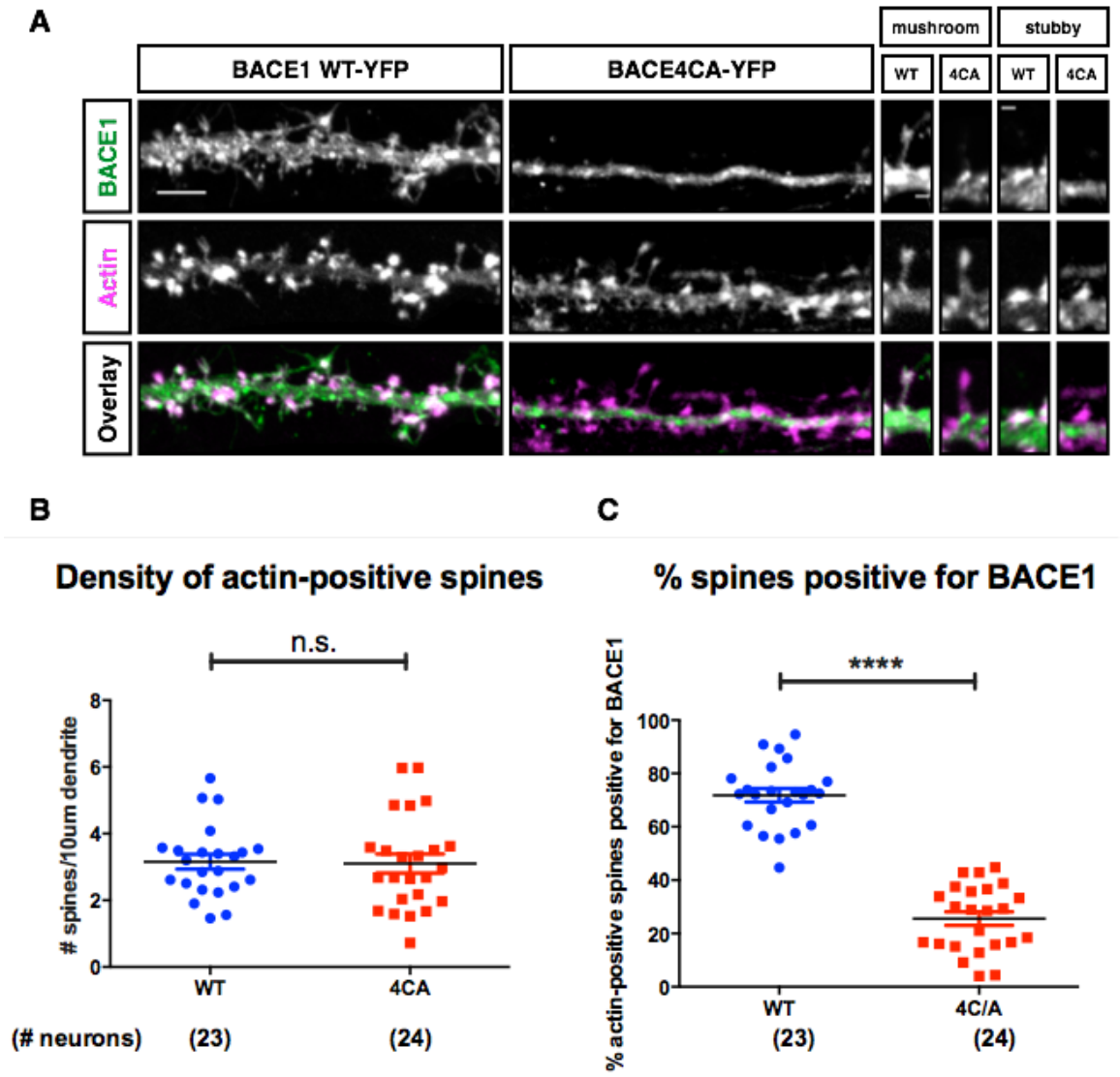

Figure 18. BACE1 localization in dendritic spines is mediated by palmitoylation. A, BACE1 WT can be found prominently in dendritic spines, while the non-palmitoylatable mutant 4C/A is not. Rat hippocampal neurons were co-transfected at DIV11 with mApple-Actin (to identify spines) and either BACE1WT-YFP or BACE4C/A-YFP and fixed at DIV15, a stage when dendritic spines are numerous. Scale bar, 5µm (left), 1µm (right). B, The density of actin-positive spines is not different between neurons expressing either BACE1 WT or the 4C/A mutant. C, The percentage of actin-positive spines containing the BACE4C/A mutant is significantly lower than that of BACE1 WT (post-hoc power analysis: 1.000; effect size r = 3.75). WT, 23 neurons; 4C/A, 24 neurons, from 2 different cultures. ****, $p<0.0001$ by Mann-Whitney Rank-Sum t-test.

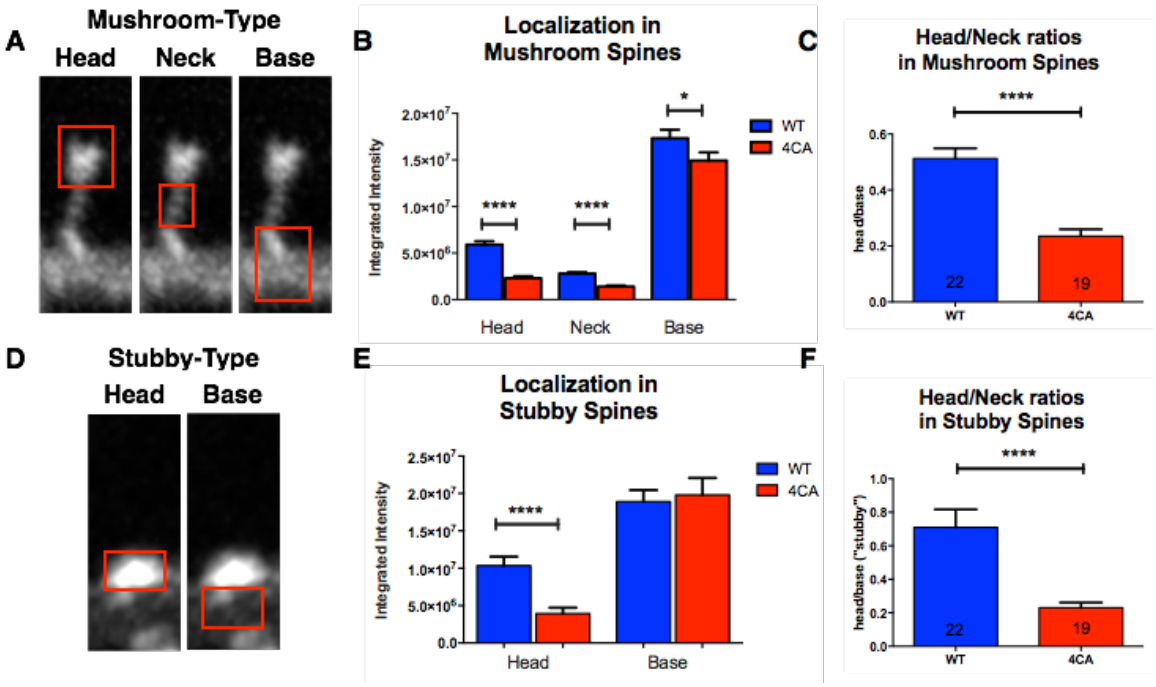

Figure 19. Lack of palmitoylation specifically affects BACE1 localization at the head of the spine. A, The palmitoylation-deficient 4C/A mutant of BACE1 is restricted from the actin-enriched heads of both mushroom and stubby dendritic spines. A & D, BACE-YFP fluorescence was measured in the head, neck and base compartments of mushroom and stubby dendritic spines, using the mApple-Actin signal to define each region. B, BACE4C/A-YFP is significantly less in the head and neck of mushroom-type dendritic spines compared to WT, and somewhat decreased at the base of the spine as well (post-hoc power analysis: 1.00, 1.00, and 0.55 for the head, neck, and base of mushroom-type spines, respectively; effect size: 0.68, 0.58, 0.12, respectively). Despite the decrease at the base of the spine, the effect size for this difference is very low. C, Normalizing BACE-YFP fluorescence intensity in the head of dendritic spines by dividing by the fluorescence at the base of the spine reveals a significant and specific decrease in the spine head (post-hoc power analysis: 1.00; effect size: 0.53), as opposed to an equivalent decrease throughout the spine apparatus. E, BACE4C/A-YFP is also significantly less in the head of stubby spines compared to WT (post-hoc power analysis: 1.00; effect size, 0.81). F, BACE4C/A-YFP is significantly less in the dendritic spine head specifically, when normalized to fluorescence at the base of the spine (post-hoc power analysis: 0.99; effect size: 0.78). Mushroom type spines: WT, n=279 spines 4C/A, n= 300 spines; stubby type spines: WT, n=61 spines, 4C/A, n=67 spines; all data collected from 22 WT-expressing neurons and 19 4C/A-expressing neurons, from 3 separate cultures. *, $p<0.05$; ****, $p<0.0001$, Mann-Whitney Rank-Sum t-test.

take into account any possible differences in trafficking mechanisms in spines that have more or less established signaling machineries. There was a significant decrease of 4C/A fluorescence at the head of each type of spine, and no change at the base of stubby type spines and a more modest decrease at the base of mushroom type spines (Fig. 19). I considered the possibility that lack of palmitoylation may generally decrease BACE1 protein levels in the neuron, leading to an apparent but not specific decrease in the spine. To assess the relative amount of BACE1 in the head of the spine compared to the base of the spine, the fluorescence in the head of each spine was divided by the fluorescence at the base of the same spine. This revealed a clear decrease of 4C/A specifically in the head of the spine for both types (Fig. 19).

Palmitoylation Mediates BACE1 Targeting to the Axon

In mouse neurons transfected with BACE1 WT, I observed a steady increase of BACE-YFP fluorescence in the axon over time (Fig. 15). However, when I transfected with BACE4C/A, I had difficulty visualizing BACE1 in the axons of older (DIV12-16) neurons (Fig. 20 & 21). To quantify this difference in axonal localization, I calculated a normalized axon:dendrite ratio (ADR), in which the BACE-YFP fluorescence in the axon was divided by the average fluorescence in the three largest dendrites; this "raw" YFP axon:dendrite ratio was then normalized to the axon:dendrite ratio of Cerulean, a soluble fluorophore produced on the same expression plasmid as the BACE-YFP fusion protein but under the control of a separate promoter (BACE-YFP_Cer). Assuming random distribution of Cerulean throughout the neuron, an ADR of 1 would indicate random distribution of BACE-

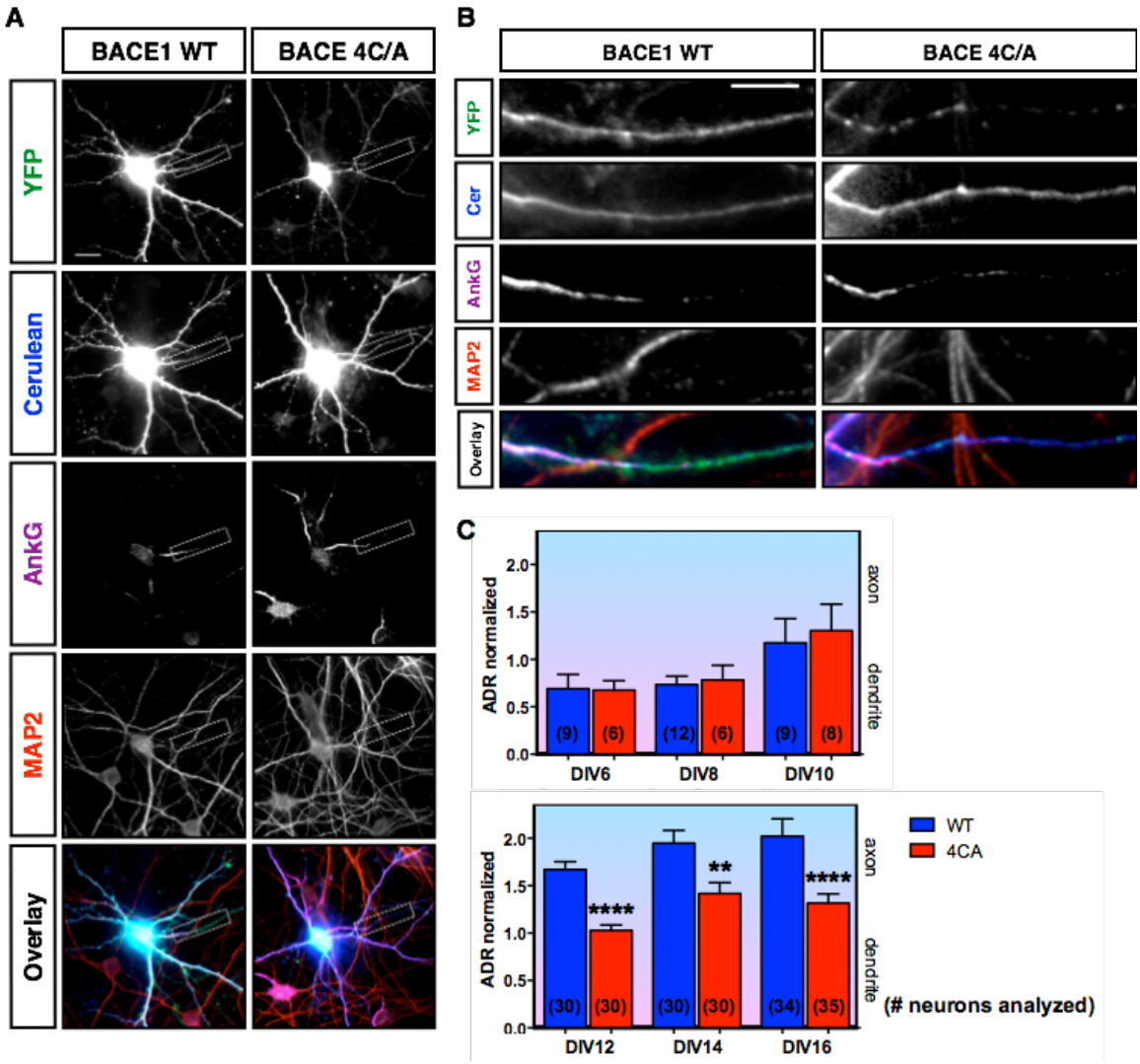

Figure 20. BACE1 WT enriches in the axon in mature neurons, while the palmitoylation-deficient 4C/A mutant does not. A, Neurons transfected with BACE-YFP-Cer constructs were fixed & stained 5 days later for AnkG, a marker for the axon initial segment, and MAP2. Scale bar, 20µm. B, Enlarged view of the axon from the neurons in A. Scale bar, 10µm. C, BACE1 ADR normalized to Cerulean ADR. At later time points (older than DIV11), the ADR of BACE4C/A was significantly diminished compared to the WT (post-hoc power analysis: 1.00, 0.97, and 0.97 for DIV12, DIV14, and DIV16, respectively; effect size r = 1.64, 0.77, and 0.81, respectively), whereas at all earlier time points, the relative distribution of WT and 4C/A in the axon versus the dendrites was no different (post-hoc power analysis: 0.03, 0.08, and 0.07 for DIV6, DIV8, and DIV10, respectively; effect size r = 0.04, 0.14, and 0.17, respectively). Number of neurons quantified per condition are indicated in the graph. Results are from at least 3 separate cultures, each performed on all time points in parallel. **, p<0.01; ****, p<0.0001, Kruskal-Wallis test.

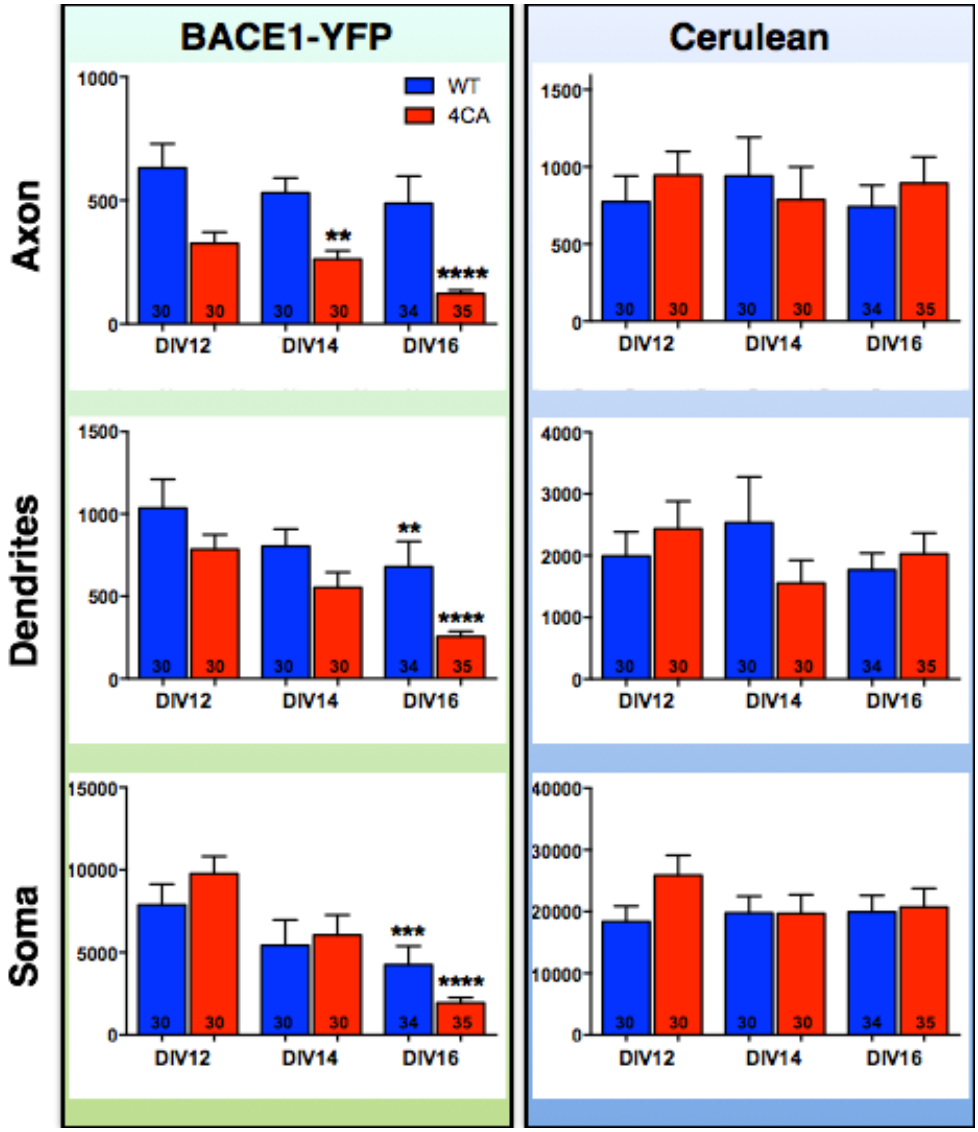

Figure 21. Raw fluorescence of neurons analyzed in Figure 20c demonstrates that BACE1 WT is retained in the axon in older neuronal cultures, while the 4C/A is diminished throughout the neuron. The panel on the right shows that cerulean levels remain unchanged throughout the neuron at all the time points analyzed; however, BACE1WT-YFP fluorescence in the soma, and to a lesser extent in the dendrites, begins to decrease at DIV16 compared to DIV12, yet stabilizes in the axon (post-hoc power analysis: 0.83 and 0.53 in the soma and dendrites, respectively; effect size, 0.54 and 0.38, respectively). In contrast, BACE4C/A-YFP fluorescence was significantly decreased in the axon compared to the WT, especially at later time points (post-hoc power analysis: 0.88, 0.99, and 0.87 for DIV12, DIV14, and DIV16, respectively; effect size, 0.73, 0.99, and 0.79, respectively). At DIV16, BACE4C/A-YFP was also diminished in the dendrites, and to a lesser extent in the soma, compared to WT (post-hoc power analysis: 0.79 and 0.53 for dendrites and soma, respectively; effect size, 0.67 and 0.48, respectively). Results are from at least 3 separate cultures, each performed on all time points in parallel. **, $p<0.01$; ***, $p<0.001$; ****, $p<0.0001$, Kruskal-Wallis test.

YFP; an ADR greater than 1 would indicate a preference for axonal localization, and an ADR less than 1 a preference for dendritic localization. This method controls for differences in fluorescence intensity based on both the geometry of the neurite and plasmid expression from cell to cell. ADRs were calculated at 1, 3, and 5 days after transfection at DIV5 or DIV11, to compare any differences in protein expression based on time after transfection. For the DIV11 transfected neurons, the 4C/A ADR was significantly less than the WT ADR at every time point tested (Fig. 20C). An analysis of the raw fluorescence demonstrated that, while the 4C/A mutant tended to decline in all compartments of the neuron with time after transfection, the WT only decreased in the dendrite and soma, while remaining constant in the axon (Fig. 21). Furthermore, Cerulean fluorescence was stable at all time points tested. These results provide evidence that BACE1 undergoes palmitoylation-dependent targeting to axons.

To address whether the axonal enrichment of BACE1 may be an artifact of the transfection system I used (e.g., to rule out that the lipids present in the Lipofectamine transfection reagent might have influence BACE1 trafficking), neurons were infected with an adenovirus that expressed either BACE1 WT or BACE4C/A with an N-terminal FLAG tag ("FLAG-BACE) for detection by immunostaining. Unfortunately, the vast majority of transduced cells at later time points were MAP2-negative cells with a glial morphology (>95% at DIV16), but among the few MAP2-positive neurons at DIV15, there was a significant lack of BACE 4C/A in the axon in older cultures (Fig. 22).

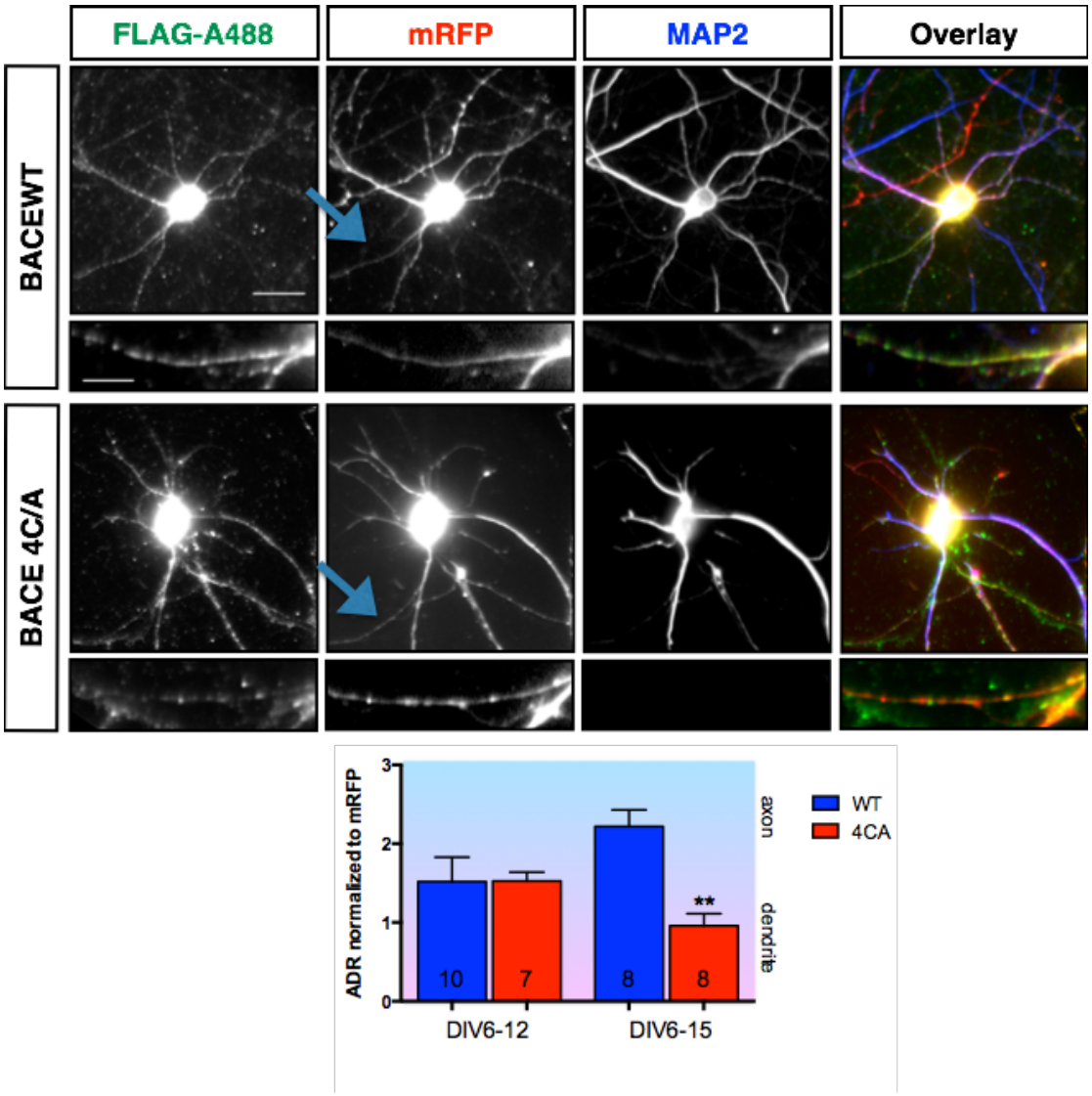

Figure 22. Using a viral transduction strategy, BACE4C/A localization in the axon is repressed in older neurons in culture. DIV6 rat hippocampal neurons were transduced with retrovirus encoding both mRFP to mark neuronal morphology and BACE1WT or BACE4C/A with a FLAG tag at the extracellular N-terminus. Neurons were fixed at either DIV12 or 15 and stained for for BACE1 using an anti-FLAG antibody, and for dendrites using an anti-MAP2 antibody. Axons (arrows, and lower panel) were identified by mRFP fluorescence and lack of MAP2 staining. BACE4C/A localization in the axon was significantly diminished at DIV15, but not DIV12 (post-hoc power analysis: 0.03 and 1.00 for DIV12 and DIV15, respectively; effect size, 0.01 and 2.43, respectively). Scale bar, 30µm (upper), 10µm (lower). Results are from at least 2 separate cultures, each performed on all time points in parallel. **, $p<0.01$, Kruskal-Wallis test.

BACE1 WT and 4C/A surface localization and internalization

The differences in neuronal localization, but not non-neuronal localization[119], of BACE1 WT and 4C/A suggested a neuron-specific, palmitoylation-dependent pathway of protein transport and targeting. We previously found that recycling endosomes are a major targeting compartment for BACE1 transcytosis, whereby a majority of axon-targeted BACE1 is retrogradely transported from dendrites to the soma, where it is routed to the axon in a Rab11-dependent manner[92, 102]. I therefore reasoned that palmitoylation might also play a crucial role in this pathway. In order to visualize internalized BACE1 exclusively, and simultaneously compare with total BACE1 to normalize for differences in protein expression levels, I developed a FLAG-based surface labeling and internalization assay (Fig. 7, 8; described in Chapter II).

Before exploring any differences in BACE4C/A internalization, I first wanted to know whether the BACE4C/A mutant is able to get to the surface of the neuron. I therefore performed surface staining on neurons expressing FLAG-BACE1WT or FLAG-BACE4C/A. There was some individual variation among neurons expressing either the WT or the 4C/A; however, BACE4C/A could clearly be seen at the surface, to the same extent as the WT (Fig. 23a) when taking the total signal into account. I next asked whether BACE4C/A is capable of undergoing internalization in neurons by performing a 15 min. uptake of FLAG antibody after a 20 min. labeling period on ice; excess FLAG antibody was removed by a brief acid wash. Unfortunately the acid wash was not well tolerated by the neurons; however, I was still able to see internalized BACE1 present in puncta throughout the soma and dendrites for both

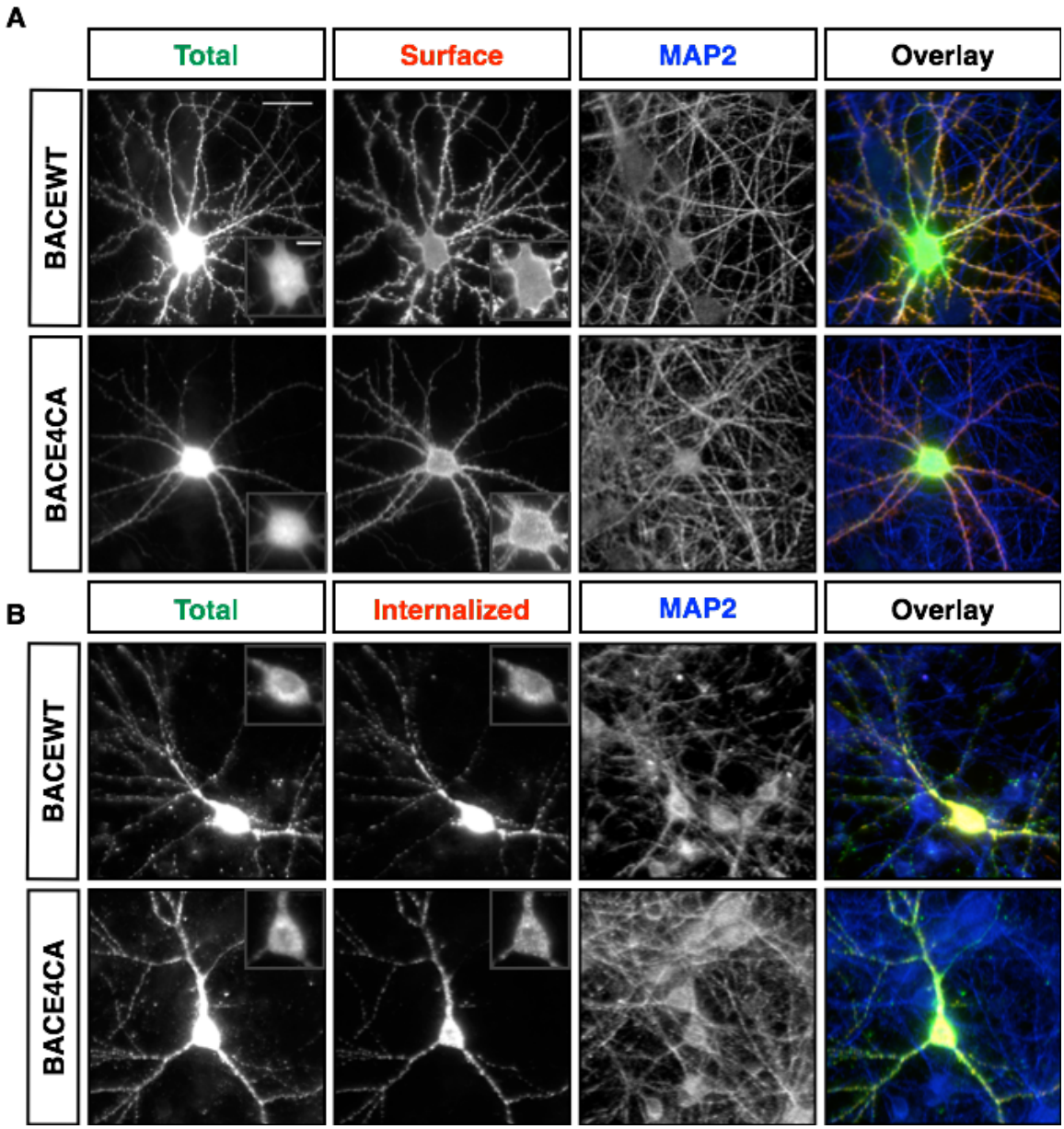

Figure 23. FLAG antibody staining in neurons expressing N-terminally FLAG-tagged BACE1 constructs. A, Neurons were stained with the FLAG antibody under nonpermeabilizing conditions to label surface-localized BACE1. After labeling with secondary, neurons were fixed, permeabilized and stained a second time with the FLAG antibody to label total BACE1. Neurons were also stained for MAP2 to identify dendrites. Both WT and 4C/A BACE1 can be seen at the surface of the neuron. B, 15 min. FLAG uptake assay to identify internalized BACE1 in neurons. After a FLAG antibody labeling period on ice, neurons were returned to 37°C for 15 min. to allow internalization of surface-labeled BACE1. Neurons were fixed, permeabilized and labeled with secondary, followed by a second round of FLAG labeling to identify total BACE1. Both WT and 4C/A can be seen internalized throughout the soma and dendrites. Scale bar, 30µm; Inset scale bar, 10µm.

constructs (Fig. 23b). In agreement with my previous findings, internalized BACE1 was present in puncta along the axon, while there was little to no BACE4C/A detectable along the axon. While the 4C/A mutant was quantitatively decreased in the axon, there were still occasional puncta seen along the axon.

We previously found BACE1 WT in stationary puncta along the axon that overlap with Synaptophysin (Syp), a marker of presynaptic terminals[102]. This suggests that BACE1 may be present in vesicles at the presynaptic terminal, and that it may cycle to and from the presynaptic surface, yet appear stationary during live imaging. To determine whether BACE1 WT is internalized at these putative presynaptic sites, and whether the few 4C/A-positive axonal puncta overlap with Syp, a brief (5 min.) FLAG antibody internalization assay was performed on neurons co-transfected with Syp-mCherry and BACE1 constructs in which a FLAG tag is fused to the extracellular/luminal N-terminus. While a majority of the Syp-positive puncta were positive for internalized BACE1 WT, there was virtually no overlap between Syp and BACE 4C/A (Fig. 24).

DHHC miRNA-mediated knock-down in neurons expressing BACE1WT

The experiments I performed thus far utilized a non-palmitoylatable mutant; I therefore extrapolated that the phenotype I had seen for the mutant was due to the lack of the modification itself and no other factor. To see if I could recapitulate the 4C/A phenotype in neurons expressing BACE1 WT by affecting its palmitoylation state, I co-transfected neurons with miRNA constructs targeting either LacZ (negative control), or one of the putative palmitoyl transferase enzymes mediating BACE1 palmitoylation, DHHC-2 or DHHC-3[119, 121]. DHHC-2 is present at the synapse

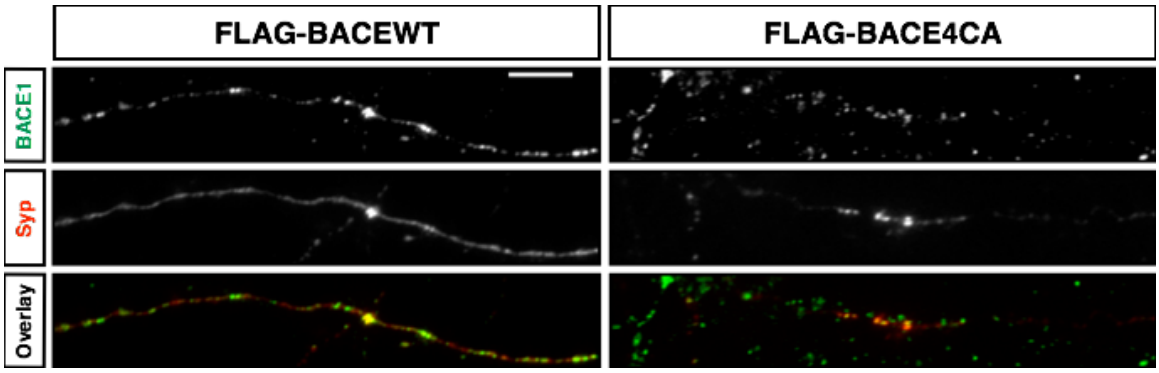

Figure 24. Axonal puncta positive for the presynaptic marker synaptophysin are also positive for internalized BACEWT, but not BACE4C/A. A 5 min. uptake of FLAG antibody was performed as described. Over this short time frame, internalized BACEWT can clearly be seen in Syp-positive puncta, which are likely presynaptic sites, while there is virtually no internalized BACE4C/A staining. Scale bar, 10µm.

and mediates PSD-95 palmitoylation in response to synaptic activity, whereas DHHC-3 is a Golgi-resident enzyme[121]. In a previous study from my lab, both of these enzymes were shown to elevate BACE1 palmitoylation when over-expressed in non-neuronal cells[119]. Furthermore, DHHC-2 was reported to colocalize with Rab11 in perinuclear vesicles in non-neuronal cells[158], and we found that Rab11 mediates BACE1 axonal targeting[102], raising the hypothesis that DHHC-2 palmitoylation in this compartment may be necessary for efficient axonal targeting in a Rab11-dependent manner. The miRNA constructs that I used for knock-down also expressed the mCherry fluorophore, which I used to visualize neuronal morphology and identify axons, along with AnkG immunostaining. To be sure that I allowed enough time for the constructs to knockdown their targets, I transfected at DIV11 and waited 4 days, until DIV15, to fix and stain the neurons. This was also a stage at which a difference in ADR between WT and 4C/A was clear, and when mature mushroom-type spines become more prevalent. When I knocked-down either DHHC-2 or DHHC-3, I observed a striking but not significant decrease of BACE1 WT-YFP fluorescence in both the axons and dendrites, and even a reduction of BACE1 WT-YFP fluorescence in the soma of neurons in which DHHC-3 was knocked down (Fig. 25). Because the fluorescence was decreased in all compartments, there was no way to tell if there was a selective decrease in axonal enrichment, as all the ADRs were equivalent. In a separate set of experiments, using different neuron cultures, I co-transfected neurons with BACEWT-YFP and the miRNA knockdown constructs and analyzed the spine localization of BACE1 (Fig. 26). In these experiments, I identified spines by their morphology alone, using the

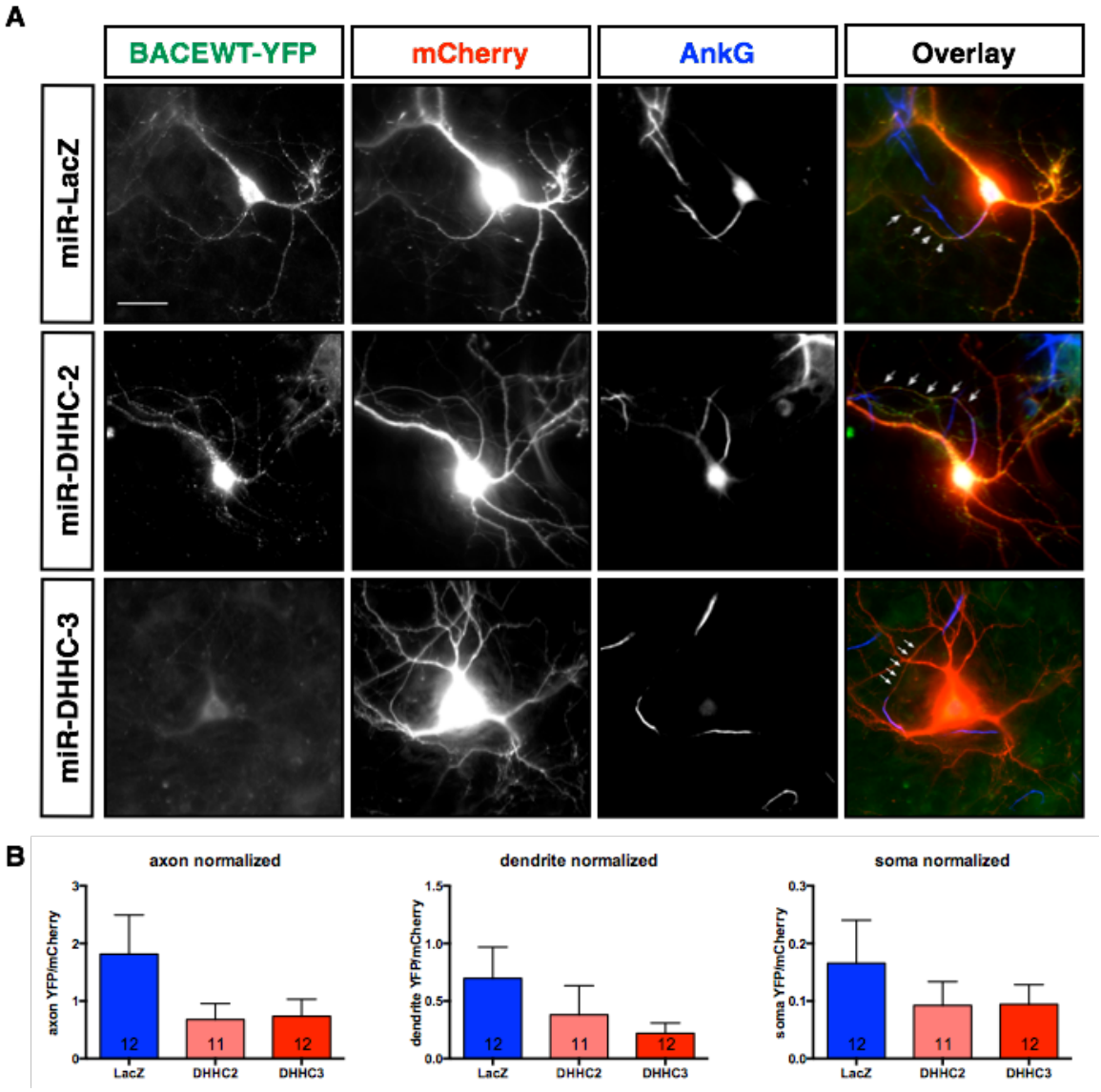

Figure 25. DHHC-2 and DHHC-3 miRNA-mediated knock-down decreases BACE1WT-YFP fluorescence in all compartments of the neuron, axonal and somatodendritic. A, Neurons were co-transfected with BACE1WT-YFP and miRNA constructs to knock down expression of either LacZ (negative control), DHHC-2 or DHHC-3. At DIV15, 4 days after transfection and a time at which BACE1WT-YFP is observed to be preferentially targeted to the axon, neurons were fixed and stained with an antibody to the axon initial segment marker, AnkG, to identify the axon. Scale bar: 30um. B, BACE1WT-YFP luorescence in the axon, dendrite and soma were normalized to the fluorescence of mCherry as a control. BACE1WT-YFP fluorescence tended to be decreased in all compartments analyzed in the DHHC-2 and -3 knockdown neurons, although this did not reach significance (by Kruskal-Wallis ANOVA).

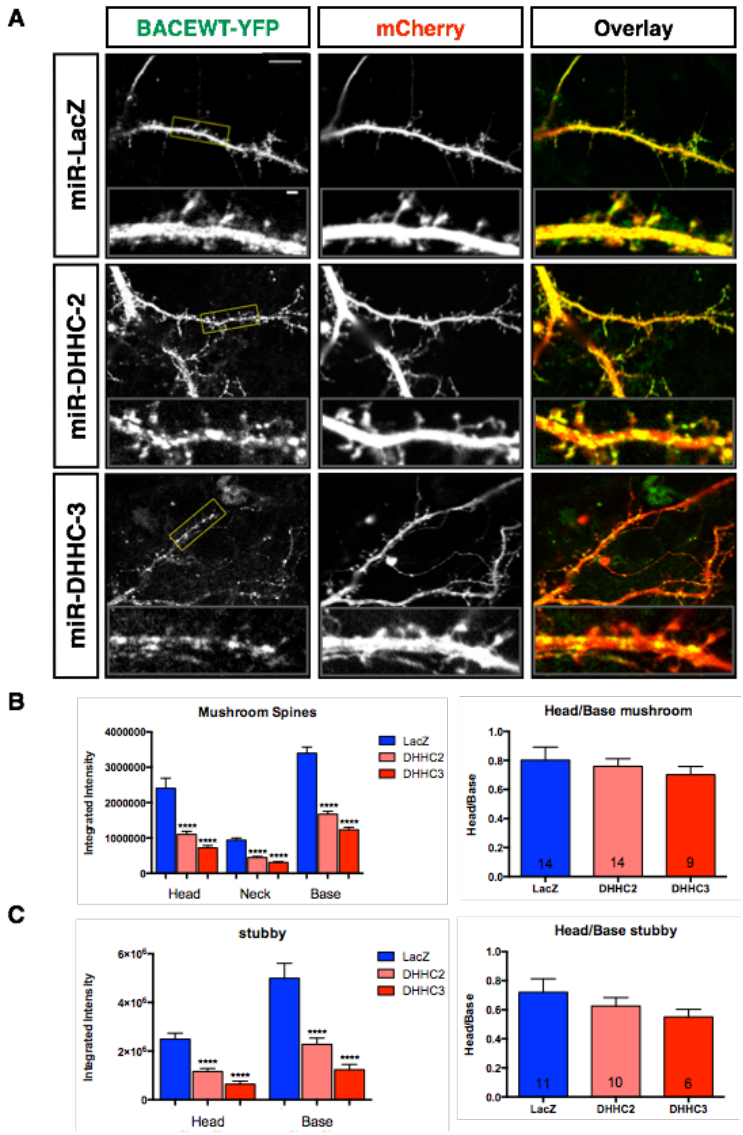

Figure 26. DHHC-2 and DHHC-3 miRNA-mediated knock-down decreases BACE1WT-YFP fluorescence in dendrites and dendritic spines. DIV11 hippocampal neurons were co-transfected with BACE1WT-YFP and a miRNA plasmid directed towards either LacZ (negative control), DHHC-2, or DHHC-3. The same plasmid expresses the mCherry fluorophore to fill the neuron and reveal morphology. 4 days after transfection, neurons were fixed and imaged by confocal microscopy. Images were acquired at the first bifurcation of the apical dendrite and spines were identified by their characteristic morphology (enlarged head and a thinner neck protruding from the dendrite shaft with a length approximately equal to or less than the diameter of the head). BACE1WT-YFP fluorescence was clearly dampened in the DHHC-2 knock-down neurons, and was barely detectable in the DHHC-3 knock-down neurons. Scale bar, 10µm; Scale bar, 1µm. Data collected from two independent cultures. For mushroom-type spines, LacZ: 153 spines, 14 neurons; DHHC2, 245 spines, 14 neurons; DHHC3, 217 spines, 9 neurons. For stubby-type spines, LacZ: 47 spines, 11 neurons; DHHC2: 77 spines, 10 neurons; DHHC3, 30 spines, 6 neurons.

mCherry fluorescence as a marker. I found that, when either DHHC-2 or DHHC-3 was knocked down, there was a highly significant decrease of BACE1WT-YFP fluorescence in all compartments analyzed (Fig. 26). Unlike in neurons expressing BACE4C/A, in which there was a moderate reduction of BACE1 fluorescence overall and a specific reduction of in the spine head, I found no specific reduction of BACE1 WT in the spine head, for either mushroom-type or stubby-type spines, when either DHHC was knocked down (Fig. 26b, c). Unfortunately, the neurons did not tolerate the miRNA expression very well, and it was difficult to get data from more than 2 different cultures. Also, I noticed a severe lack of dendritic spines in neurons expressing the DHHC miRNA constructs, which is expected given the importance of these enzymes in maintaining spine structure and function.

Altogether, my experiments in cultured neurons show that BACE1 is normally targeted to both synaptic and non-synaptic puncta throughout the neuron, enriches into axons with time after transfection, and suggests that palmitoylation mediates efficient BACE1 targeting to dendritic spines and axons. BACE4C/A is still transported to the cell surface and undergoes internalization. Palmitoylated BACE1 can be found in rodent brain; additionally, BACE1 can be found in lipid rafts in rodent brain. The in vivo significance of BACE1 palmitoylation is not known, and is the focus of the following chapters.

CHAPTER IV

Development and Characterization of the BACE4C/A Knock-In Mouse

Generation of the BACE4C/A knock-in mouse

The results described in the previous chapter suggested that palmitoylation-dependent trafficking of BACE1 mediates neuron-specific targeting, which may be important for BACE1 function in normal brain and during AD pathogenesis. To unequivocally determine the in vivo effect of BACE1 palmitoylation on amyloid beta production and amyloid deposition, the creation of a BACE 4C/A knock-in mouse was necessary (Fig. 9, 10). A knock-in strategy was preferable over a transgenic strategy, as gene targeting would result in the mutant completely replacing the wild type, and expression would be under the control of the endogenous promoter, thus eliminating any confounding variables due to overexpression. Creation of the BACE4C/A gene-targeting construct is described in greater detail in Chapter II. I started with a "recombineering" methodology to retrieve a large portion of the 3' region of the BACE1 gene from a bacterial artificial chromosome (BAC) into a smaller, more manageable cloning vector. Subsequent cloning steps produced a targeting construct with 5' and 3' homologous arms for homologous recombination into the endogenous BACE1 gene, along with mutations in the cysteine codons, resulting in the 4C/A mutant protein (Fig. 9). The targeting vector was further modified and refined by the experts at GenOway (Lyon, France) to finally generate 4C/A heterozygous knock-in mice. For all studies described here, heterozygous mice were mated to each other to produce homozygous knock-ins (referred to as "BACE4C/A mice") and homozygous wild-type littermate controls (referred to as

"BACE1 WT mice"). Initial assessments find that BACE4C/A mice are healthy, viable and fertile, and mating of heterozygotes results in the expected Mendelian frequency of the different genotypes: 24% WT, 55% heterozygote and 21% 4C/A homozygous knock-in (215 pups analyzed from 35 matings, average litter size = 7 pups; Fig. 27).

Biochemical characterization of BACE4C/A mice

Analysis of steady-state BACE1 protein levels by Western blot analysis in 1.5-2 month old forebrain lysates revealed no significant differences between WT and 4C/A littermates (Fig. 28). Probing for full-length APP also revealed no significant differences, suggesting that there may be no change in APP processing, which is discernable in the brain lysates of BACEKO mice (Fig. 28A). To assess levels of APP cleavage products, forebrain lysates were immunoprecipitated with an antibody that recognizes the C-terminus of APP, CTM1. Because APP CTFs are present in brain lysates as phosphorylated forms, the phospho-CTFs can overlap with the non-phospho-CTFs on Western blot, confounding analysis[89]. Therefore, immunoprecipitates were treated with bacteriophage lambda phosphatase to clearly see the β-, +11-, and α-CTFs. The +11-CTF is an alternative BACE1 cleavage product, whereby cleavage occurs 11 amino acids downstream of the start of the Aβ sequence[140]. Quantification of the bands by densitometry revealed no difference in APP cleavage products between WT and 4C/A mice (Fig. 29).

To observe palmitoylation of endogenous BACE1 in mouse brain and to confirm that the BACE4C/A mutant protein expressed in KI mouse does not undergo palmitoylation, I performed an Acyl-RAC assay (Fig. 30). I used a membrane fraction

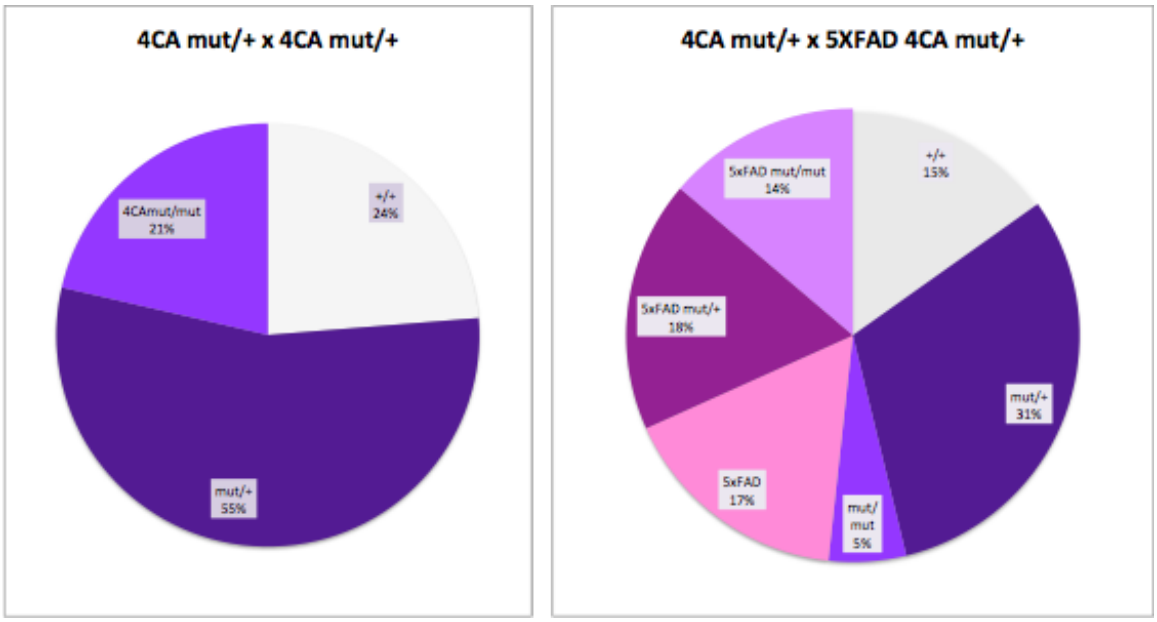

Figure 27. BACE4C/A and 5XFAD+4C/A birth ratios. Crossing BACE4C/A heterozygotes produces offspring in roughly the expected Mendelian ratios (24% WT, 55% heterozygote, and 21% homozygous knock-in). Crossing a nontransgenic BACE4C/A heterozygote to a 5XFAD BACE4C/A heterozygote produces offspring in roughly the expected Mendelian ratios, with the exception of nontransgenic BACE4C/A homozygous knock-in, which appears in 5% of pups.

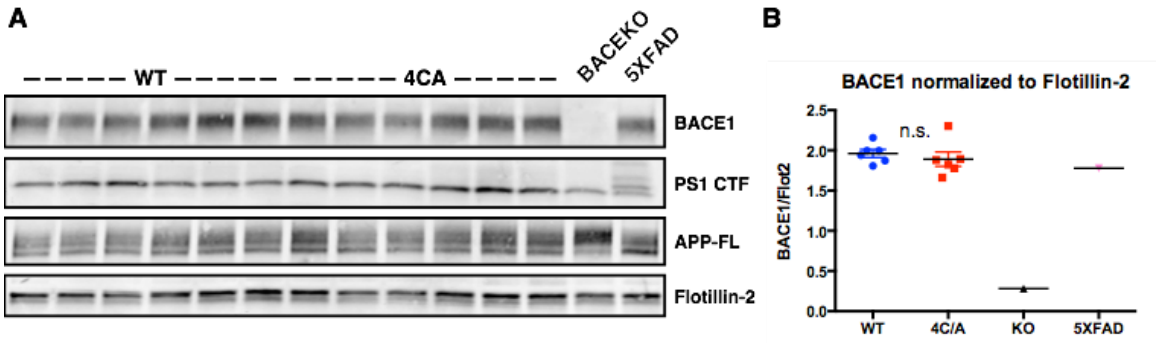

Figure 28. Steady-state levels of BACE1 protein are unchanged in 4C/A mice compared to WT. A, Forebrain lysates from 6 WT and 6 4C/A mice between P45-P60 were analyzed alongside lysates from BACEKO and 5XFAD mice and probed by Western blot for BACE1, PS1 CTF, full-length APP, and Flot2 as a loading control for membrane proteins. Lack of BACE1 signal in the BACEKO lysates demonstrates antibody specificity. B, Quantification of the blot in A. There were no significant differences between WT and 4C/A brain lysates in any of the proteins analyzed.

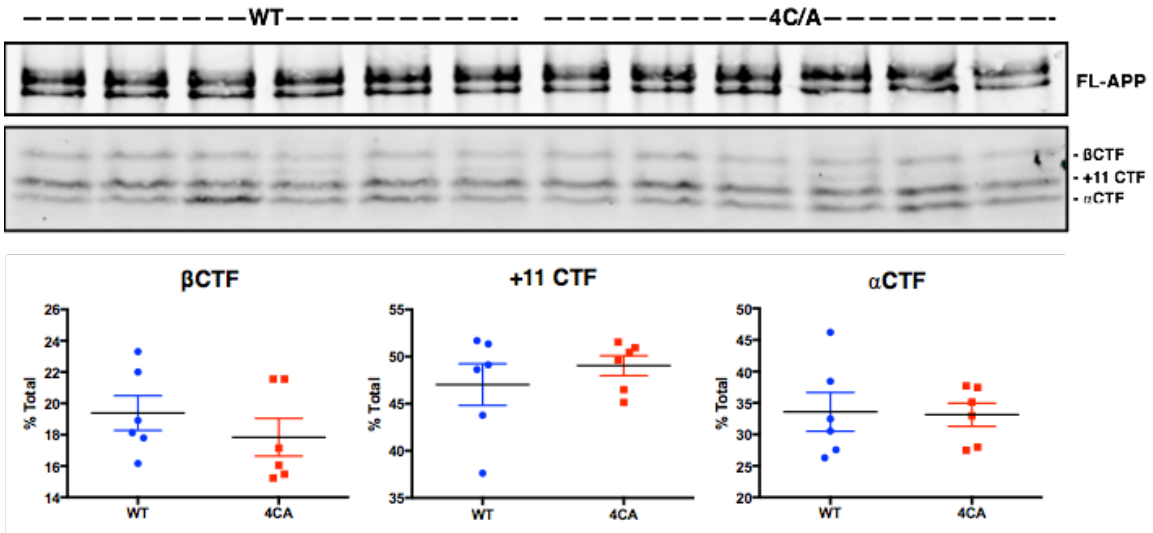

Figure 29. Analysis of APP cleavage products in forebrain lysates from mice expressing either BACEWT or BACE4C/A. 500µg of forebrain lysates were immunoprecipitated using antibody CTM1, which recognizes the C-terminus of APP and therefore will bind to both full-length and APP C-terminal fragments (CTFs). Immunoprecipitates were treated with bacteriophage lambda phosphatase (NEB) as previously described (Buxbaum 1998), washed and eluted by boiling in Laemmli sample buffer before separation on a 16.5% Tris/Tricine gel. Bands were quantified by densitometry and each CTF expressed as a percentage of the total CTFs. Despite slight individual variation, there was no overall difference in the levels of any of the APP CTFs, or in full-length APP.

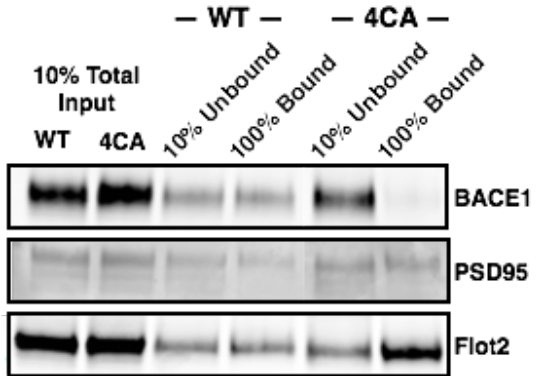

Figure 30. Acyl-RAC assay to determine palmitoylation levels in proteins from brain homogenate purified for membrane proteins. 10% of the total input (crude membrane fraction from brain lysate), 10% of the unbound, and 100% of the protein bound to the acyl-reactive resin were subjected to immunoblot analysis. Comparison of the unbound and bound band intensities indicates that BACE1 is palmitoylated to at least the same extent as PSD95 and Flot2 in mouse brain. However, there is virtually no BACE4C/A present in the unbound fraction, indicating that it does not undergo palmitoylation, as expected.

prepped from forebrain lysates, and used two membrane-associated proteins known to undergo palmitoylation, PSD-95 and Flot2, as a control[121, 122, 135, 154, 159]. Palmitoylation mediates PSD-95 and Flot2 membrane association, therefore ~100% of these proteins should be palmitoylated in the membrane protein preparation, i.e., almost all of the signal should be present in the bound fraction, if the assay is 100% efficient. Because there was some PSD-95 and Flot2, albeit less, detected in the unbound fraction, the assay was clearly not 100% efficient (Fig. 30) However, as expected, virtually no BACE4C/A was detected in the bound fraction, while the BACE1 WT was distributed among both the bound and unbound fractions (Fig. 30). Given the results of the control proteins, the amount of BACE1 WT in the bound fraction might be under-representative of the palmitoylated levels of BACE1 present in the brain. In any case, these results confirm that the 4C/A mutation prevents palmitoylation of BACE1 in vivo.

Palmitoylation targets many classes of proteins to lipid rafts[160]. Previously my lab demonstrated that palmitoylation is required for BACE1 targeting to lipid rafts in transfected non-neuronal cell lines[119]. To confirm that the non-palmitoylatable 4C/A mutant is not targeted to lipid rafts in vivo, freshly extracted forebrain lysates were first fractionated into purified membrane fractions, and then subjected to sucrose density gradient ultracentrifugation. This protocol separates transmembrane and membrane-associated proteins that are present in lipid rafts from those that are targeted to non-raft membranes[119, 161, 162]. In the density gradient, lipid raft components (lipids and raft-associated proteins) float to the interface between the 5% and 35% sucrose layers. When the gradients are

harvested from the top as 1ml fractions, lipid rafts are recovered in fractions 4-6. Flot2 enrichment is used as a marker for the lipid raft fractions. While BACE1 WT is elevated in these raft fractions, the 4C/A mutant is not (Fig. 31). Quantification of samples from three separate WT and 4C/A mice revealed a significant reduction of BACE4C/A in the raft fraction compared to the non-raft fraction (Fig. 31C)[119]. Thus, BACE4C/A does not undergo palmitoylation and is not efficiently distributed to lipid rafts in vivo.

Analysis of in vivo BACE1 localization

As described above, in transfected neurons, BACE4C/A is not targeted to dendritic spines and levels are significantly diminished in axons (Chapter III). Based on this data, I hypothesized that BACE1 localization in axonal tracts in the brain would also be diminished. Endogenous BACE1 is most prominently found enriched in the mossy fibers of the hippocampus, which are axon terminals projecting from the dentate gyrus to the CA3 region. I therefore stained coronal forebrain sections from adult (1.5-2 month old) mice to visualize BACE1 WT and 4C/A localization in the mossy fiber pathway. I used Synapsin1, a presynaptic protein, as a marker to define the dentate and CA3 regions. I also used MAP2 staining as a control for variations in staining due to tissue section thickness. To visualize BACE1, I used the same antibody previously used to stain endogenous BACE1 in non-transfected neuronal cultures (Fig. 11, 12). Contrary to my initial hypothesis, I found clear BACE4C/A staining in the mossy fibers (Fig. 32A). Quantification of BACE1 staining in the specific regions of the mossy fibers – dentate gyrus, suprapyramidal bundle (SPB), infrapyramidal bundle (IPB), and CA3 – revealed no significant differences

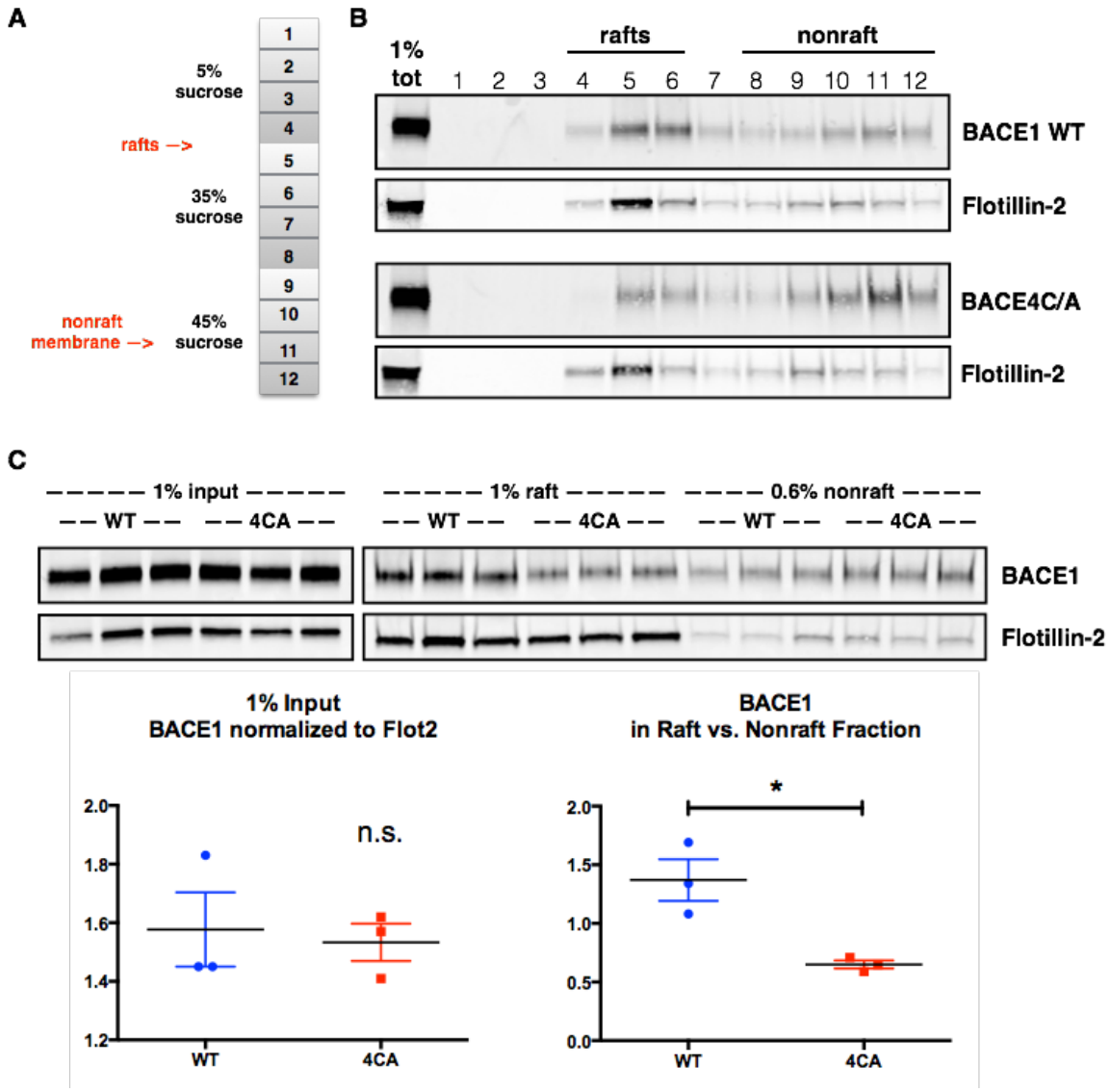

Figure 31. BACE4C/A localization in lipid rafts is significantly reduced compared to BACEWT in mouse brain. A, Schematic illustrating sucrose density gradient used to separate lipid raft-localized proteins from non-raft-localized proteins. The raft fraction separates to the interface between 5% and 35% sucrose, and can be found roughly throughout fractions 4-6 (B), while the non-raft fraction begins at the interface between 35% and 45% sucrose, and can be found roughly throughout fractions 8-12 (B). B, Representative fractions prepared from forebrain membrane proteins from one P7 WT and 4C/A mouse. 1% of the input loaded onto the sucrose gradient was run alongside the fractions for comparison. Blots were probed for Flot2, a membrane protein enriched in lipid rafts. C, Lipid raft (fractions 4-6) and non-raft (fractions 8-12) samples from 3 WT and 3 4C/A mice were run alongside 1% input and quantified. The 1% input BACE1 signal was normalized to Flot2 as a loading control; there was no difference in the amount of BACE1 applied to the sucrose gradients. The level of BACE1 in the raft vs. the non-raft fraction for each mouse was quantified, revealing a significant decrease of BACE4C/A in lipid rafts compared to WT. n=3 per condition. *, $p<0.05$, Student's t-test.

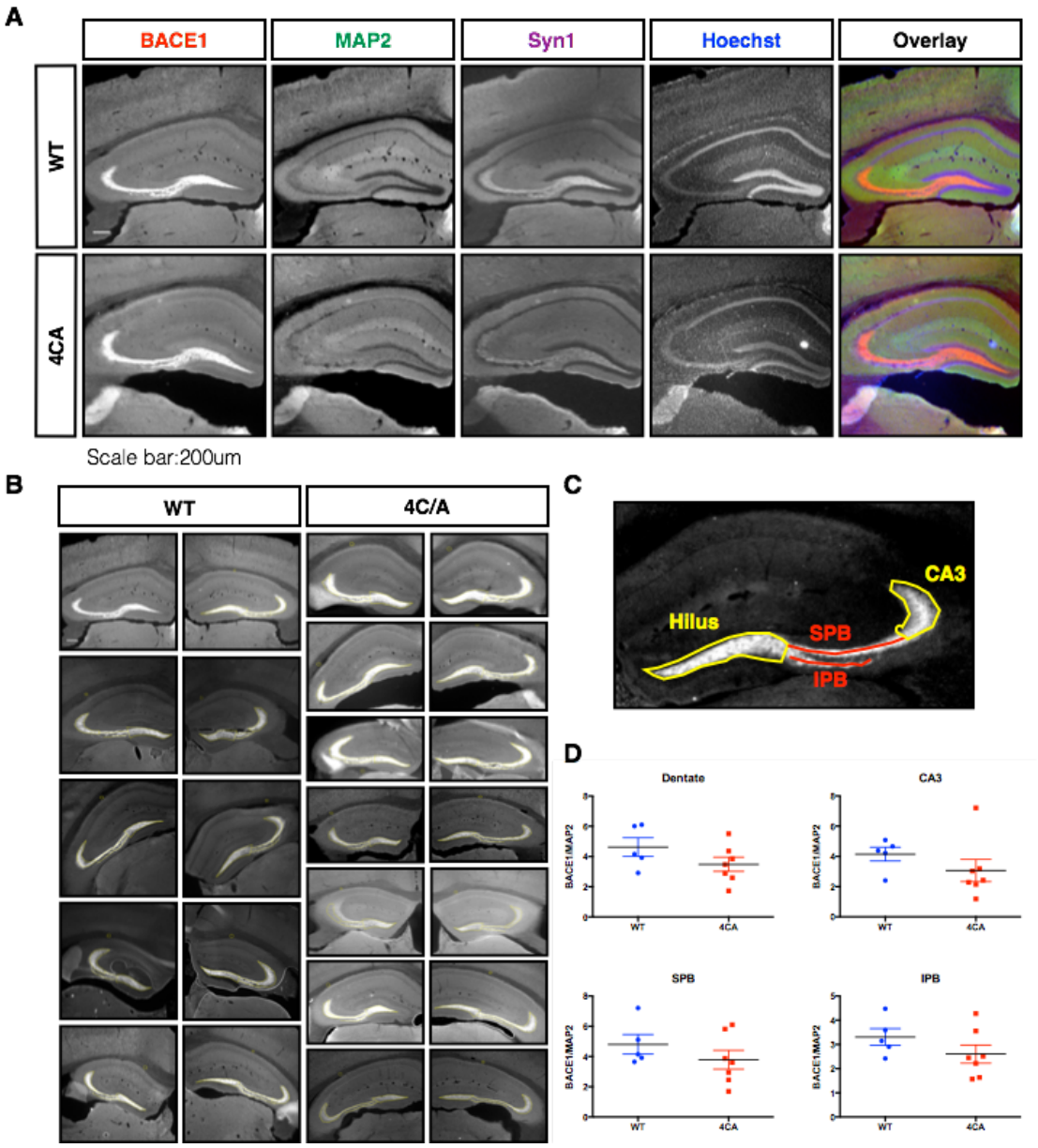

Figure 32. BACE1 localization in mossy fibers. A, Coronal brain sections were stained for BACE1, MAP2, and Synapsin1 (Syn1), a presynaptic marker that allows easy identification of the mossy fibers. There was minor variation in general fluorescence staining between sections, likely due to slight variability in thickness from section to section. This was controlled for in quantifications by first subtracting the background fluorescence intensity and then normalizing the fluorescence of BACE1 by the fluorescence of MAP2 in the same region. Scale bar, 200µm. B-D, BACE1 fluorescence in the mossy fibers was quantified by creating a region around the hilus and CA3 using Syn1 staining as a reference. BACE1 fluorescence was also quantified along the length of the suprapyramidal and infrapyramidal bundles, as defined by Syn1 staining. WT, n = 5; 4C/A, n=7.

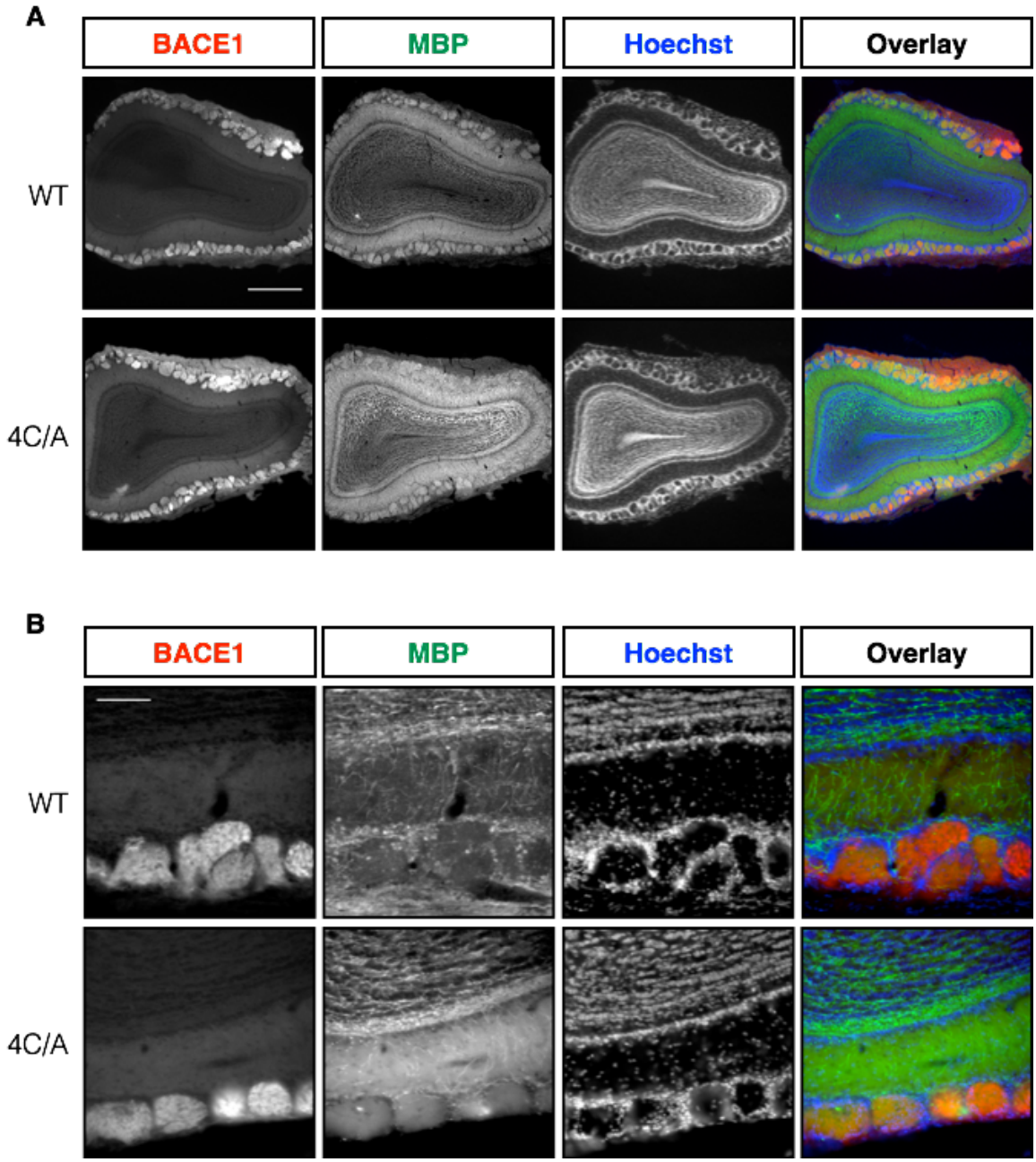

Figure 33. Olfactory bulb in WT and BACE4C/A mice. A, Overall, there were no obvious differences in the morphology of olfactory bulb or the level of BACE1 staining between WT and 4C/A mice, although there did appear to be a slight elevation of MBP staining. Scale bar, 500µm. B, Higher power magnification images of olfactory bulb showed a very slight increase in MBP staining, however only 3 mice in each group were analyzed. There were no large differences in morphology or BACE1 staining. Scale bar, 100µm.

between the WT and the 4C/A (Fig. 32B-D).

BACE1 has been reported to be involved in axon guidance of specific populations of olfactory bulb neurons[74]. Therefore I examined if there were any differences in olfactory bulb morphology between WT and 4C/A mice. I found no obvious differences in BACE1 staining between the two mice, suggesting that BACE1 protein levels were the same (Fig. 33a, b). Higher magnification revealed a possible increase in MBP staining, although only 3 mice were analyzed per group. Although not an issue with analyzing smaller structures, slight variations in the staining intensity across sections, either due to variations in section thickness, would confound analysis or larger structures. Overall morphology and staining of other markers appeared unchanged (Fig. 33b).

My results so far indicate that, while BACE4C/A does not undergo palmitoylation in the brain and does not distribute efficiently to lipid rafts, there are no other apparent differences in the viability or brain localization of BACE1 between mice expressing WT or 4C/A BACE1. Therefore, lack of palmitoylation, and palmitoylation-dependent neuronal targeting, probably does not affect normal BACE1 functioning in healthy animals. However, my main aim in analyzing the BACE4C/A mouse was to assess the affect of palmitoylation in the context of disease, e.g. AD; in the following chapter I describe my analysis of BACE4C/A expression in an AD mouse model, 5XFAD.

CHAPTER V

Mutant BACE4C/A Expression in an Alzheimer's Mouse Model, 5XFAD

In order to determine the effect of the BACE4C/A mutation on APP processing the context of Alzheimer's disease, I turned to a mouse model of early-onset AD, characterized by an aggressive early pathogenesis, the 5XFAD mouse[146]. 5XFAD mice overexpress human APP harboring three mutations (Swedish, London, and Florida) present in familial, early-onset AD, and PS1 mutations (M146L, L286V) that lead to enhanced production of the Aβ42 species specifically. Female 5XFAD mice exhibit an even more aggressive phenotype compared to males[146, 163]; is has been suggested that this is due to the fact that the Thy1 promoter driving transgene expression contains an estrogen response element[163]. However, apparent sex-related differences in amyloid deposition may in fact be due to grouped housing of female mice causing an elevation in cortisol[164], and cortisol administration has been shown to aggravate Aβ production in vivo[165]. To avoid any sex-related confounding variables in this initial study, I chose to restrict my analysis to male 5XFAD mice. 2-3 months is the earliest time point at which plaque burden and increased Aβ becomes apparent[146], but before a dramatic, posttranscriptionally-regulated elevation in BACE1 protein levels[166]; therefore I chose to analyze mice at 3 months of age. This relatively early time point also allows for analysis of initiating pathological mechanisms before widespread synaptic dysfunction and neuronal death occur.

Generation of 5XFAD littermate mice expressing either BACE1WT ("5XFAD") or the BACE4C/A mutant ("5X4CA") resulted from crossing nontransgenic

BACE4C/A heterozygotes with 5XFAD transgenic BACE4C/A heterozygotes (Fig. 10). Analysis of BACE1 protein levels in forebrain lysate indicated no significant differences between 5XFAD and 5X4CA mice (Fig. 34a) similar to results obtained from nontransgenic mice (Fig. 28). In agreement with a previous report, BACE1 levels in this transgenic background at this age, 3 months, were not dramatically different from WT, nontransgenic mice[166], at least by immunoblot detection (Fig. 34a). Analysis of APP CTFs revealed no difference in βCTFs; however, I did find a slight but significant decrease of +11CTF, and an increase of αCTF, in 5X4CA mice compared to 5XFAD (Fig. 34b). Post-hoc analysis revealed a large effect size (>1.0) for both differences, suggesting that there is in fact a decrease in β-cleavage of APP in 5X4CA mice compared to 5XFAD.

Analysis of amyloid burden in 5XFAD and 5X4CA mice by histology

The slight change in APP CTFs that I found in 5X4CA mice suggested that there might, in fact, be a change in BACE1 processing of APP in these transgenic mice. 5XFAD mice display widespread amyloid deposition and behavioral deficits as early as 3 months of age, due to overexpression of mutant human APP and PS1[146]. To determine the levels of amyloid burden in these mice expressing the BACE4C/A mutant, I performed histological staining on serial coronal sections of mouse forebrain (Fig. 35). I used antibody 3D6, which recognizes the first 5 amino acids of the Aβ sequence and thus stains for Aβ. This antibody should also stain βCTFs, which would be expected to have a cellular distribution, rather than the extracellular distribution expected for plaques; βCTFs should also be much less

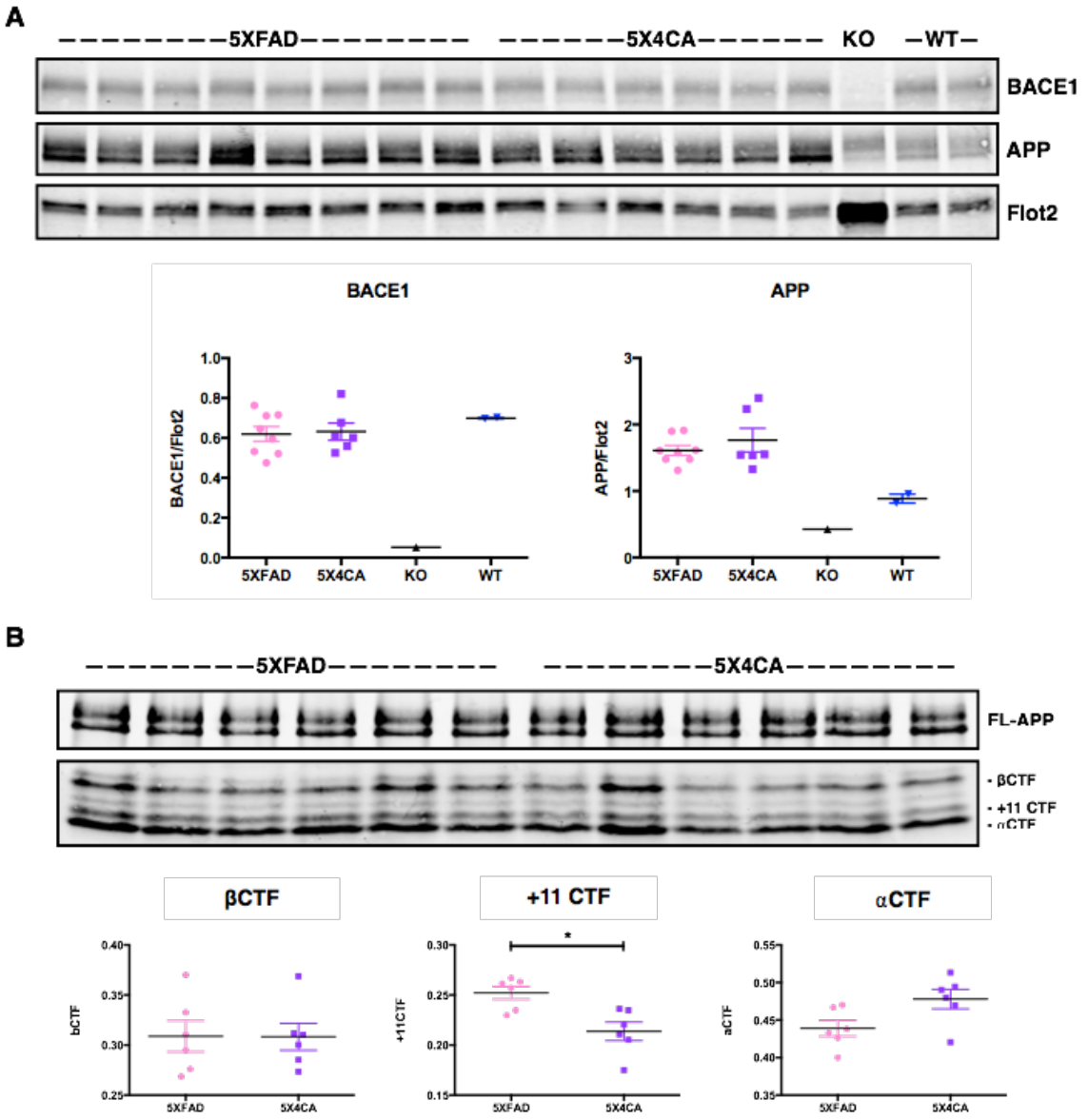

Figure 34. Biochemical analysis of forebrain lysates from 5XFAD and 5X4CA mice. A, Forebrain lysates were immunoblotted for BACE1, APP, and Flot2. There were no detectable differences in BACE1 or APP protein levels. B, Analysis of APP cleavage products in forebrain lysates from 5XFAD or 5X4CA mice. Forebrain lysates were immunoprecipitated using antibody CTM1, and immunoprecipitates were treated with bacteriophage lambda phosphatase. Bands were quantified by densitometry and each CTF expressed as a percentage of the total CTFs. There were no significant differences in full-length APP or βCTFs; however, there was a significant decrease of +11CTFs in 5X4CA mice compared to 5XFAD (post-hoc power analysis: 1.00; effect size, 1.97); there was also a shift toward more αCTFs in 5X4CA mice compared to 5XFAD (post-hoc power analysis: 0.95; effect size, 1.33), suggesting diminished β-secretase cleavage. *, $p < 0.05$, Mann Whitney t-test.

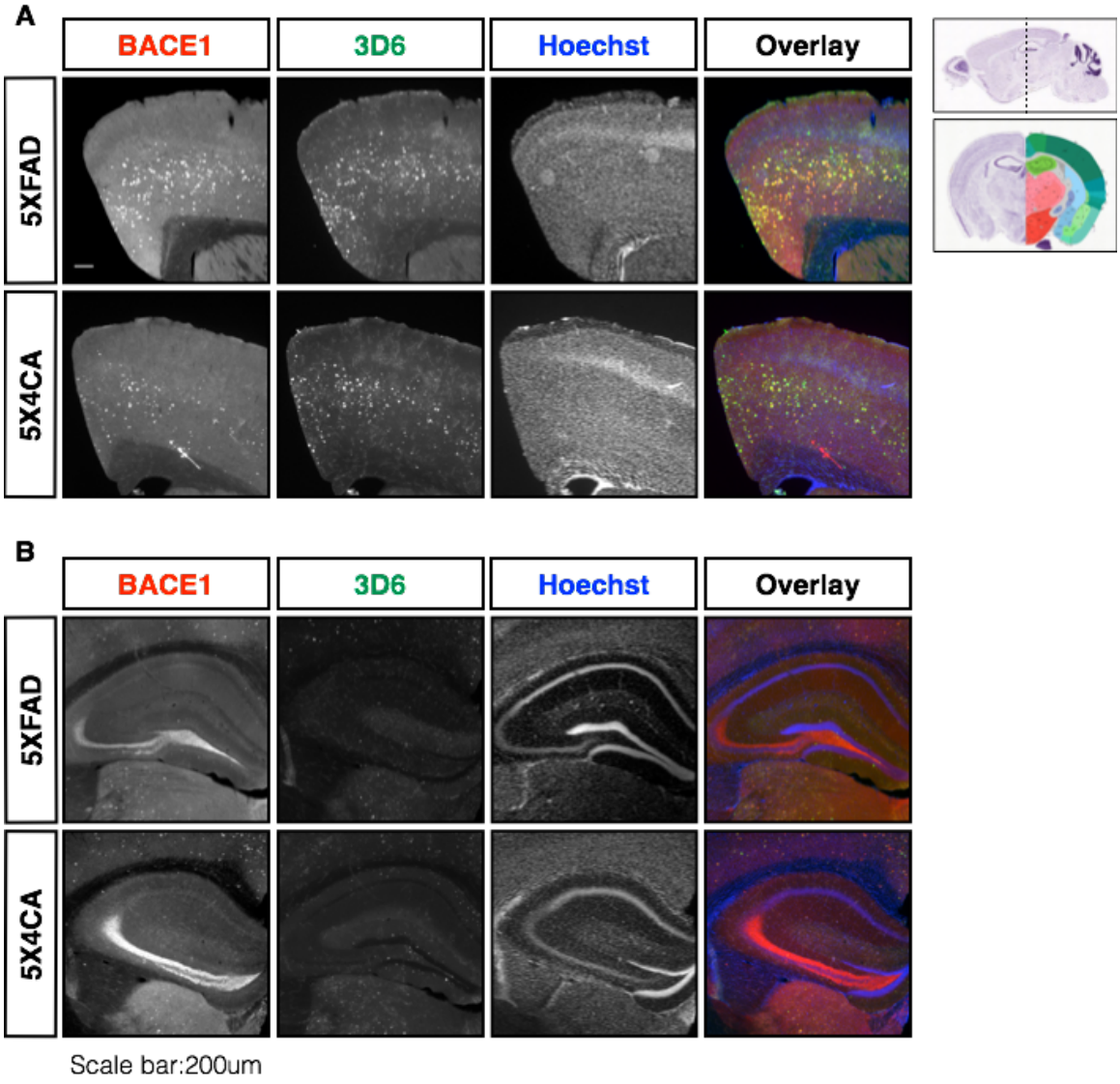

Figure 35. BACE1 and 3D6 staining in 5XFAD mice. In agreement with previous reports, BACE1 can be found prominently in association with 3D6-positive plaques throughout the cortex (A) and in all other areas exhibiting plaques, but less so in the hippocampus (B). There appeared to be a decrease of amyloid deposits and associated BACE1 in 5X4CA mice. Upper right, diagram of coronal section outlining the cortical areas analyzed (from Allen Brain Atlas, http://mouse.brain-map.org). The 5X4CA mouse shown exhibited the most deposits out of the 7 analyzed. Scale bar, 200µm.

prevalent compared to Aβ in these mice, since βCTFs turn over much faster (via conversion to Aβ or degraded in lysosomes) than Aβ in extracellular deposits.

Amyloid deposits appeared most notably throughout the cortex in 5XFAD mice (Fig. 35). Interestingly, I observed fewer 3D6 deposits in transgenic mice expressing BACE4C/A. Co-staining for BACE1 revealed elevated BACE1 levels around these 3D6-positive deposits, as found previously[166]. Although BACE4C/A could still be found in the mossy fibers, similar to non-transgenic mice, BACE4C/A fluorescence levels around amyloid deposits appeared somewhat attenuated compared to BACE1WT in the 5XFAD mice.

To quantify the relative amyloid burden in 5XFAD transgenic mice, I chose to stain using 3,3'-diaminobenzidine (DAB) for detection. Deposits stained by this method are very dark and circular, and are therefore easily distinguishable from any cellular Aβ/APP CTF species (Fig. 36a). Furthermore, DAB staining produces very little background and does not risk photobleaching during image acquisition. All brain sections were scanned simultaneously at the University of Chicago Imaging Core Facility using the Cambridge Research and Instrumentation (CRi) Pannoramic Scan Whole Slide Scanner, thus controlling for any confounding factors relating to variability during image acquisition and allowing for comparison between different sections. Using the Allen Brain Atlas as a reference, I carefully separated each section into specified brain regions, drew a region of interest (ROI) and measured the area as the total area analyzed using ImageJ software (Fig. 36b). Using the WT sections as a negative control for 3D6 staining, I established a threshold across all ROIs around the stained amyloid deposits and measured the area as my amyloid

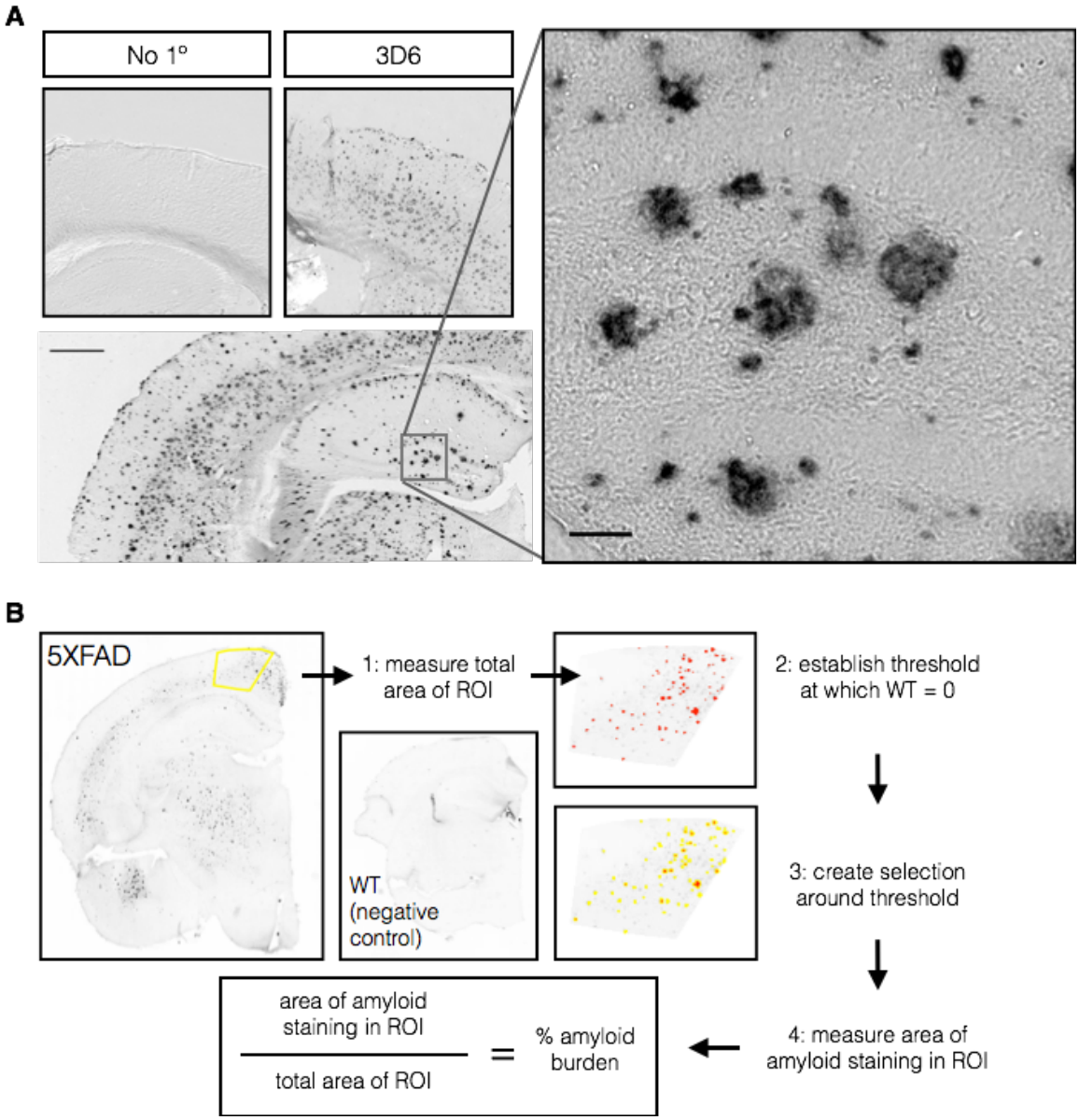

Figure 36. 3D6 staining to assess amyloid burden in an Alzheimer's mouse model, 5XFAD. A, Serial coronal sections spaced 480um apart were stained for Aβ and APP CTFs using antibody 3D6. Staining was performed using DAB, which resulted in almost no background staining as observed in sections using no primary antibody. Amyloid deposits were clearly defined and distinct from any nonspecific staining. Scale bar, 500µm (left), 50µm (right). B, Methodology for image analysis and quantifications. Each region of interest was outlined, the area measured, and a threshold established to create regions around 3D6-positive puncta. The threshold was established using WT as a negative control, and the same threshold was applied to every region analyzed. A new region was created around the area thresholded, and this area was measured to get the area of amyloid burden for each region. For each brain analyzed, the area of amyloid burden in a specified region was divided by the total area of the region of interest to get % area of amyloid burden.

staining. I then divided the area of amyloid staining by the total area for each brain region analyzed to get % amyloid load for each animal. Because different numbers of measurements were taken from each animal, weighted averages were calculated for each group to eliminate any biases due to relative over- or under-sampling. Rather than simply counting the number of plaques in each region of interest, I quantified the area of amyloid deposition to take into account the size of the plaques, which itself is an indicator of disease severity and progression[167].

As stated above, 3 months is an early stage of plaque deposition and amyloid production for 5XFAD mice. Furthermore, this age precedes most behavioral deficits, including fear conditioning, a response that is mediated by the basolateral amygdala, one of the areas that I found to be affected by plaque deposition. Although there was some slight individual variation within each group, I found a significant overall decrease in cerebral amyloid load in 5X4CA mice compared to 5XFAD (Fig. 37). I attempted to separate specific brain areas in which I noticed amyloid deposition (Figs. 38-43). Layer 5 of the cortex and the subiculum had the strongest deposition (Fig. 38, 39), in agreement with a previous report of these mice[146]. The specific cortical areas affected were the motor cortex, anterior cingulate cortex, sensory cortex, retrosplenial cortex, and posterior parietal cortex. I grouped these regions together in my analysis, since amyloid deposition spread across the entire cortex, and was not isolated to specific cortical regions. Regions that did display isolated plaque deposition included the subiculum (Fig. 39), the basolateral amygdala (Fig. 40), the lateral septal nucleus (Fig. 41), and the thalamus (Fig. 42). The hippocampus had some of the least staining at this stage of disease progression,

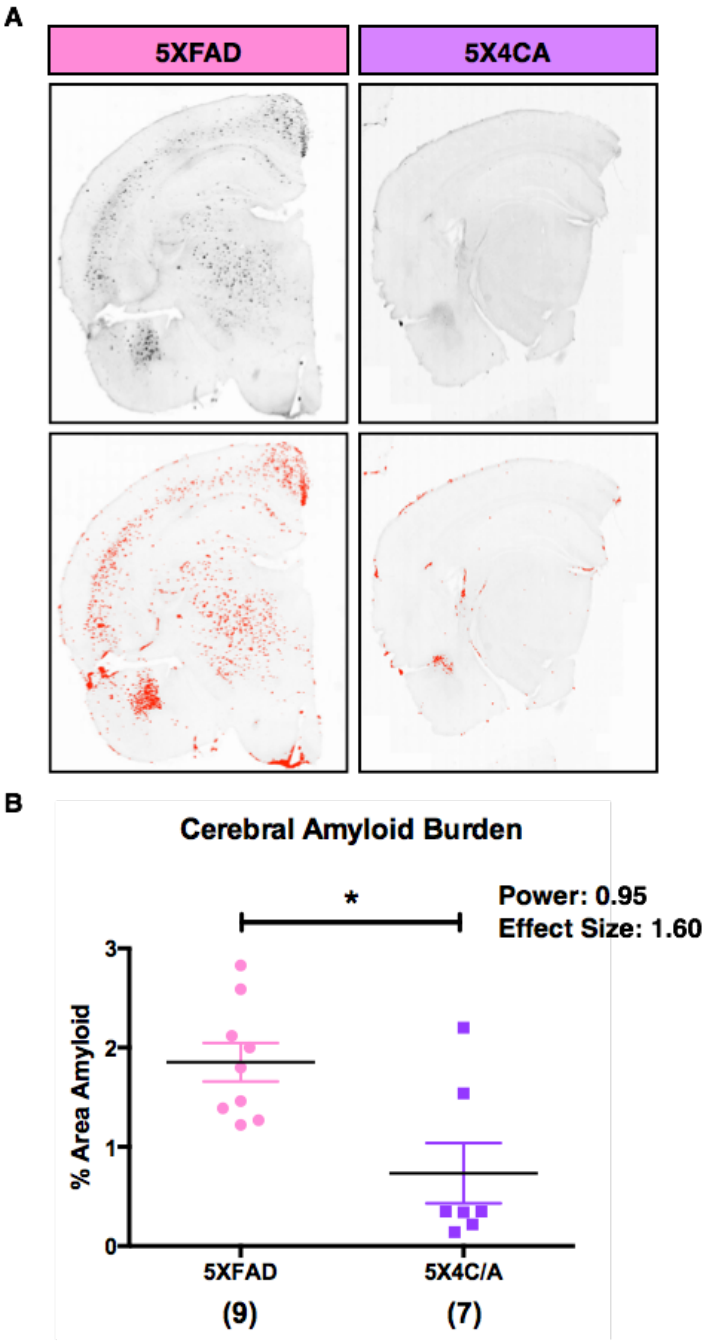

Figure 37. 5XFAD mice expressing BACE4C/A exhibit decreased cerebral amyloid burden compared to 5XFAD mice expressing BACEWT. A, Representative brain sections showing amyloid staining. The same thresholds were applied to each section as described in Fig. 36 and are shown highlighted in red. For quantification, individual regions of interest of roughly equivalent sizes were defined as shown in Figs. 36, 38-43. B, Quantification of % area amyloid. Power analysis and effect size, calculated as Cohen's D, are indicated.

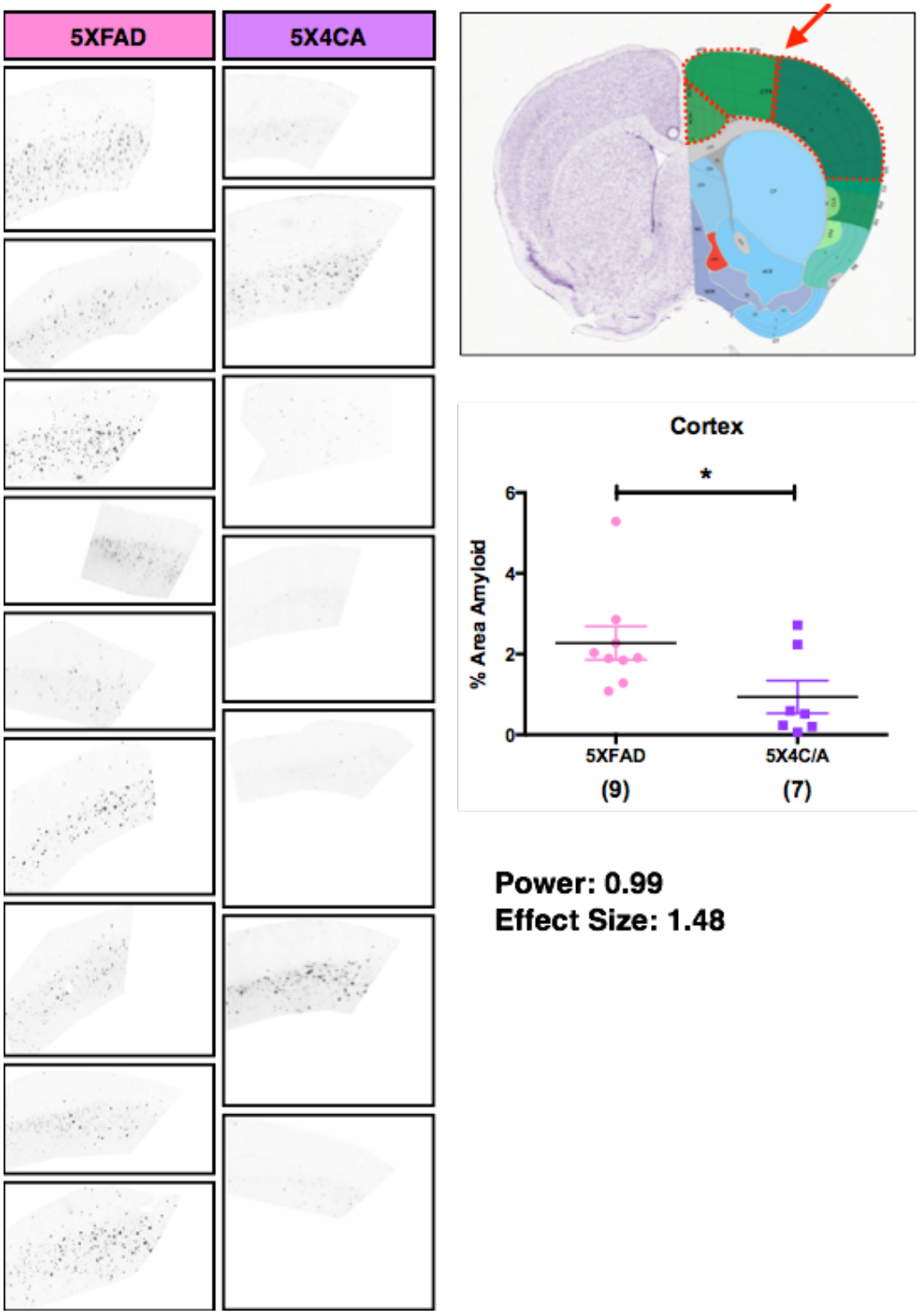

Figure 38. 5XFAD mice expressing BACE4C/A exhibit decreased amyloid burden in the cortex compared to 5XFAD mice expressing BACEWT. Left, representative ROIs quantified in the graph on the right. Upper right, diagram of coronal section outlining the cortical areas analyze (from http://mouse.brain-map.org). Power analysis and effect size, calculated as Cohen's D, are indicated.

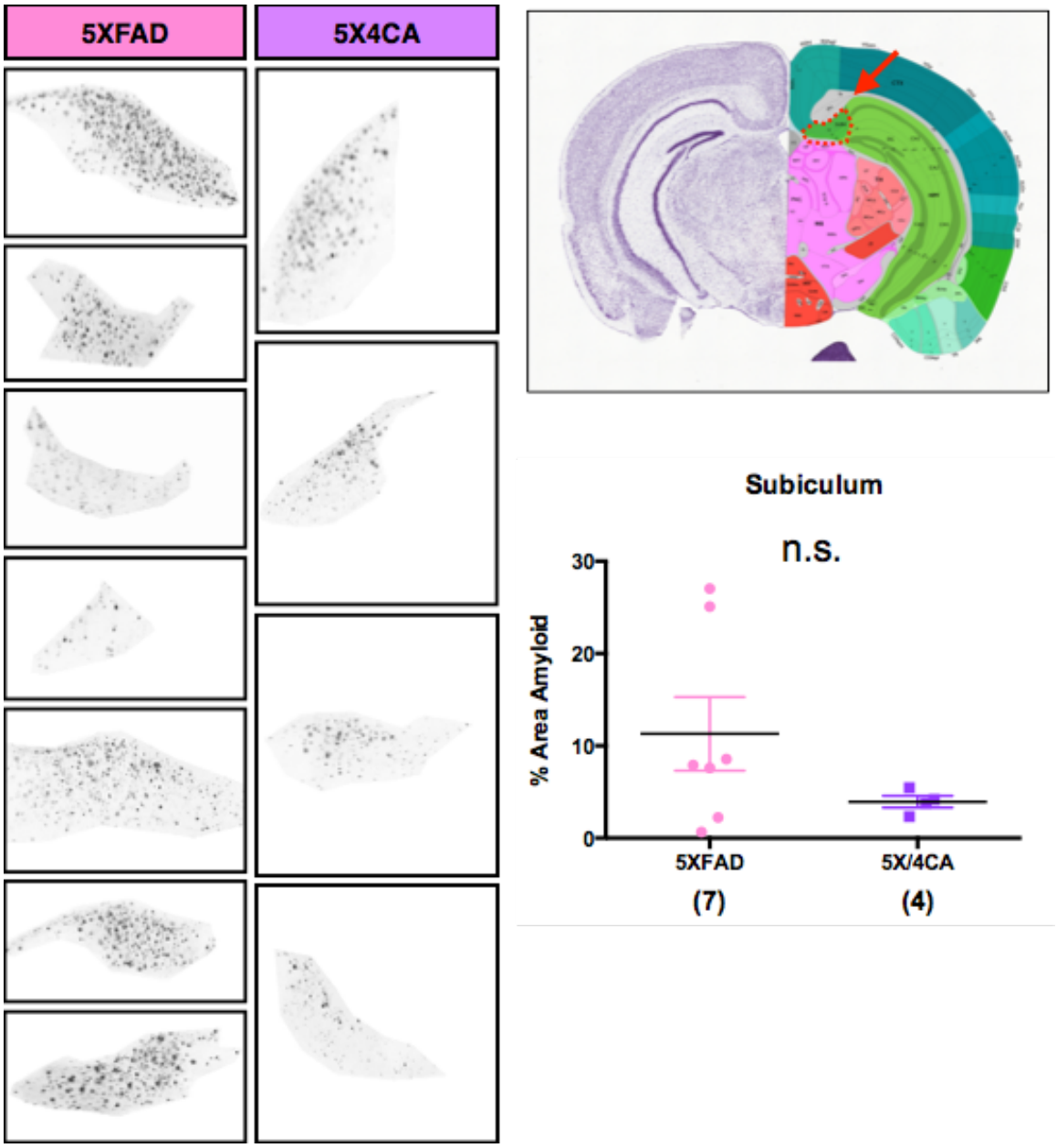

Figure 39. No difference in amyloid burden in the subiculum in 5XFAD mice expressing either BACEWT or BACE4C/A. Left, representative ROIs quantified in the graph on the right. Upper right, diagram of coronal section outlining the area analyzed (from http://mouse.brain-map.org).

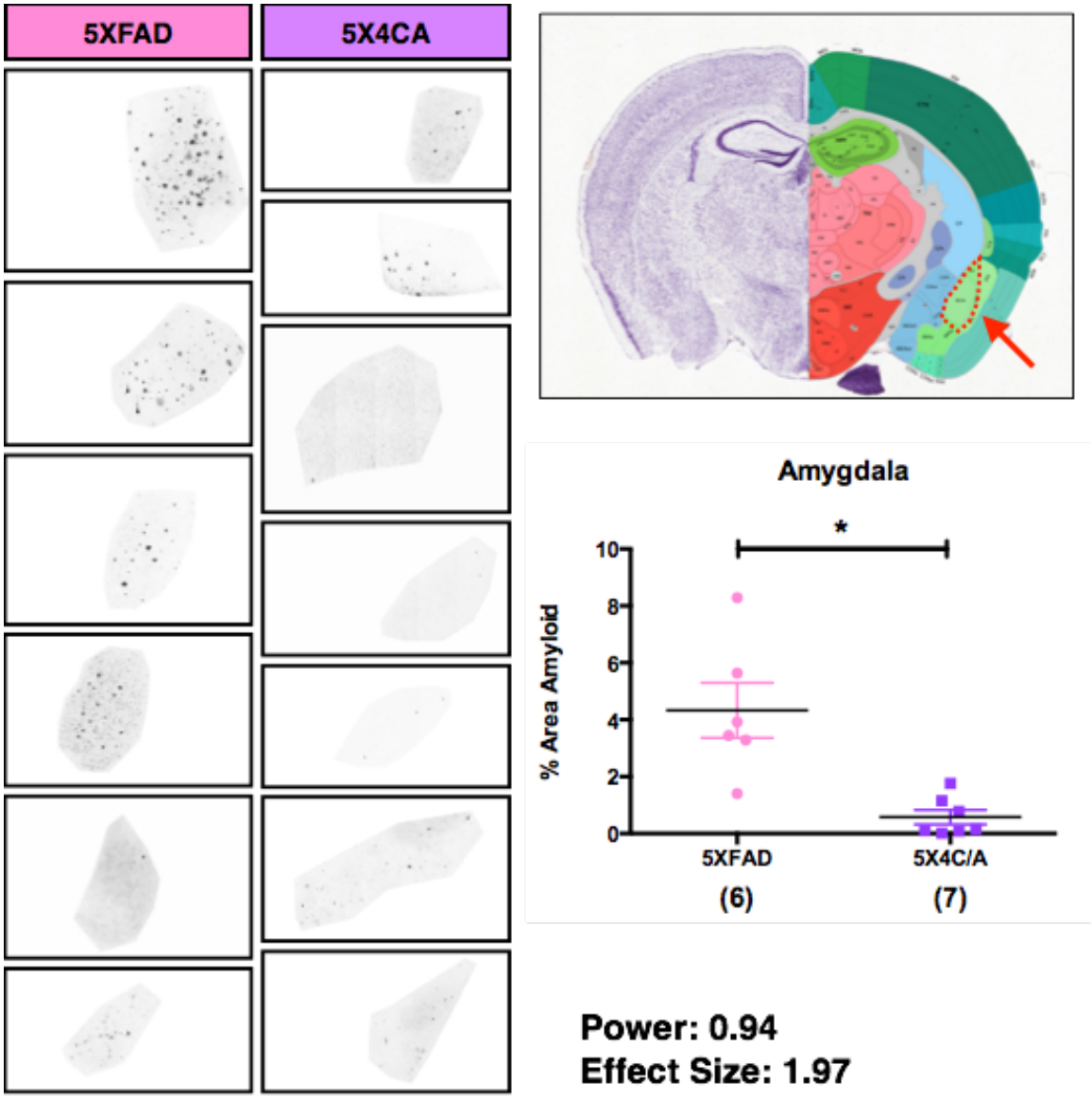

Figure 40. 5XFAD mice expressing BACE4C/A exhibit decreased amyloid burden in the amygdala compared to 5XFAD mice expressing BACEWT. Left, representative ROIs quantified in the graph on the right. Upper right, diagram of coronal section outlining the area analyzed (from http://mouse.brain-map.org). Power analysis and effect size, calculated as Cohen's D, are indicated.

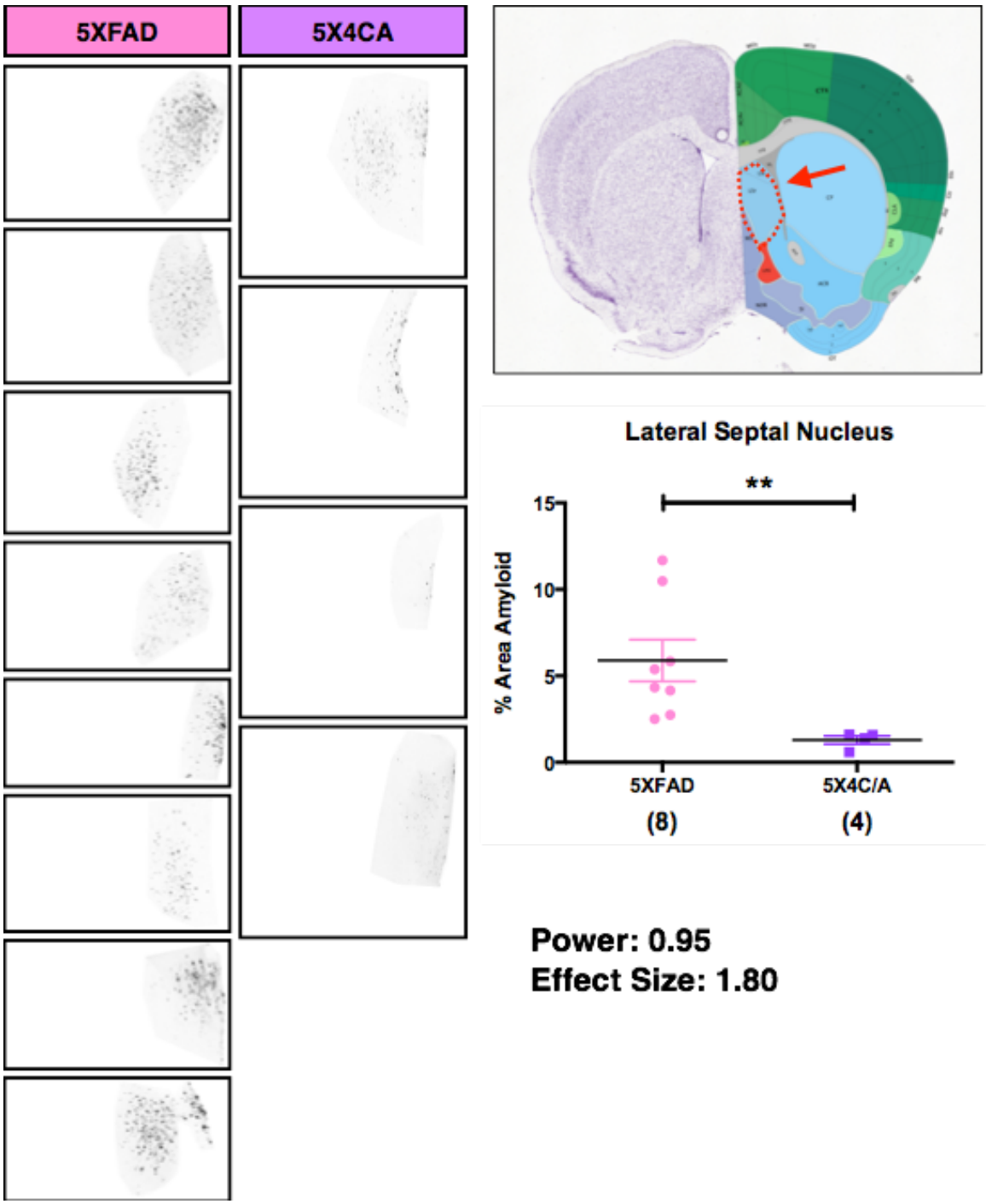

Figure 41. 5XFAD mice expressing BACE4C/A exhibit decreased amyloid burden in the lateral septal nucleus compared to 5XFAD mice expressing BACEWT. Left, ROIs quantified in the graph on the right. Upper right, diagram of coronal section outlining the area analyzed (from http://mouse.brain-map.org). Power analysis and effect size, calculated as Cohen's D, are indicated.

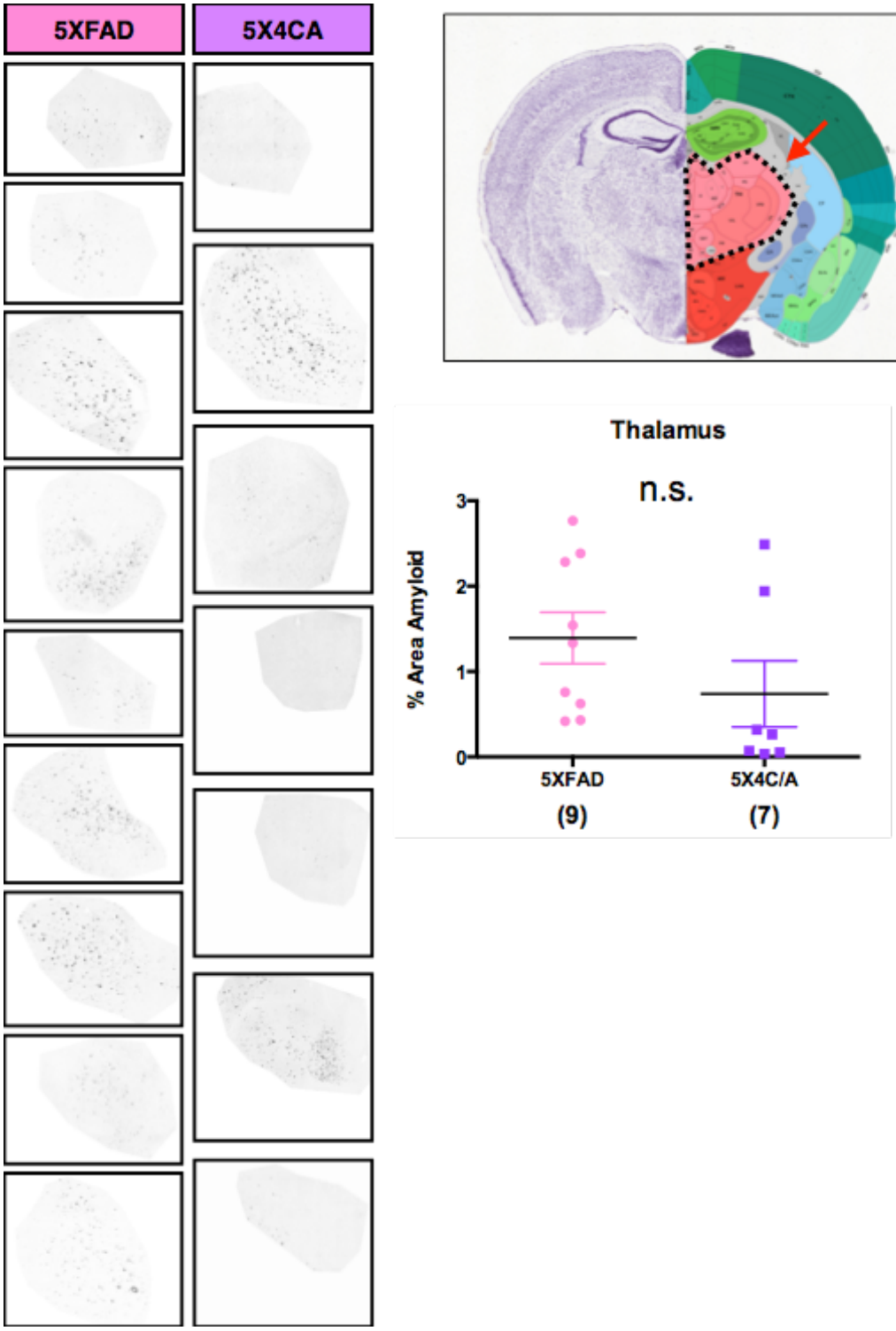

Figure 42. No difference in amyloid burden in the thalamus in 5XFAD mice expressing either BACEWT or BACE4C/A. Left, representative ROIs quantified in the graph on the right. Upper right, diagram of coronal section outlining the area analyzed (from http://mouse.brain-map.org).

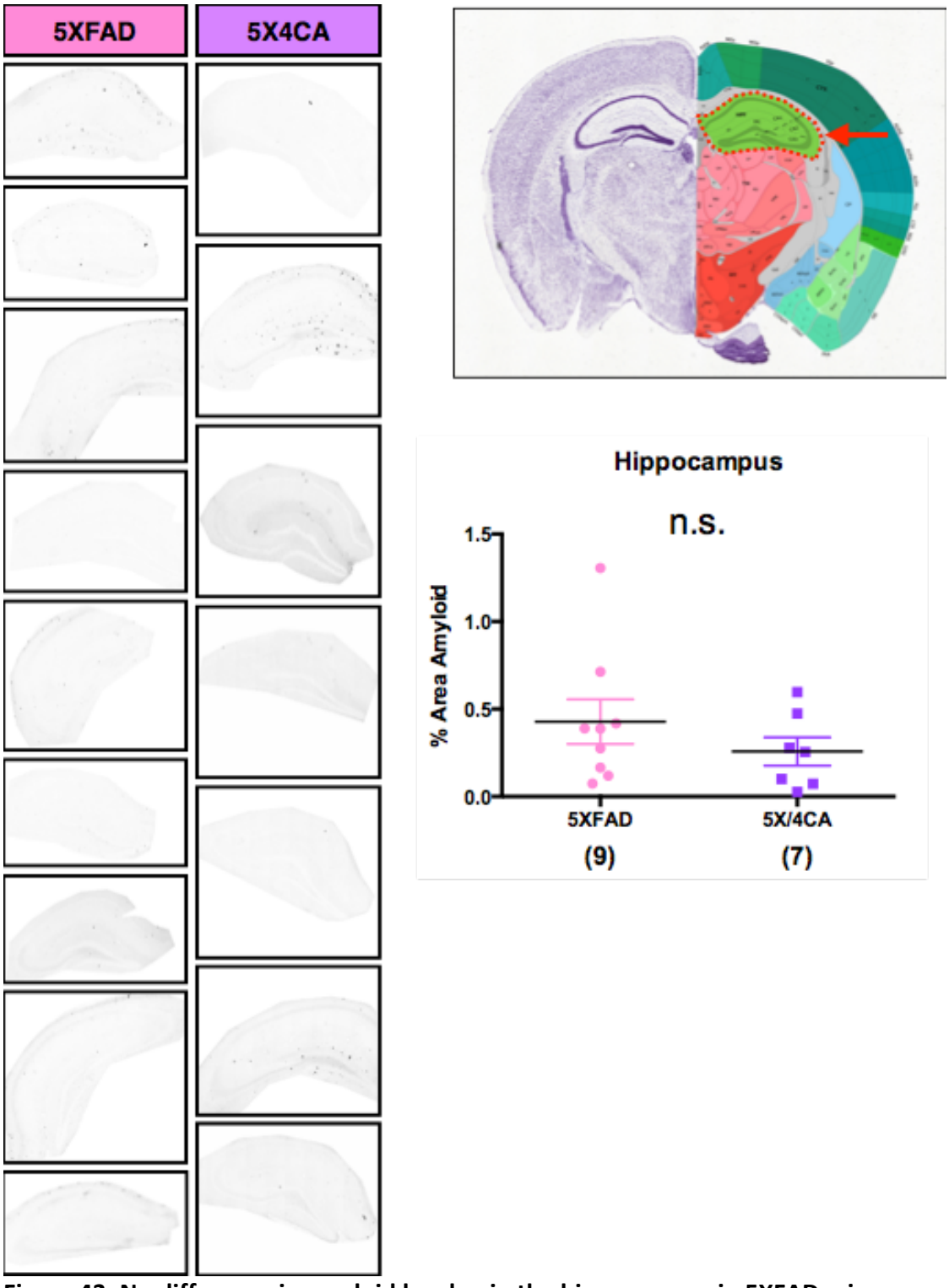

Figure 43. No difference in amyloid burden in the hippocampus in 5XFAD mice expressing either BACEWT or BACE4C/A. Left, representative ROIs quantified in the graph on the right. Upper right, diagram of coronal section outlining the area analyzed (from http://mouse.brain-map.org).

as described previously[146] (Fig. 43). Although there was some individual variability in plaque load within each group, I observed an overall and significant decrease of plaque load in 5X4CA mice compared to 5XFAD mice expressing BACE1WT. The decrease was most striking in cortex, basolateral amygdala, and the lateral septal nucleus. There was no difference between 5XFAD and 5X4CA mice in plaque load in the hippocampus, likely due to the fact that this area had little to no plaque load even in the 5XFAD mice.

BACE1 accumulation in dystrophic neurites in 5XFAD and 5X4CA mice

BACE1 has been found to accumulate in dystrophic neurites, swollen neuritic structures that are found in association with Aβ deposits, in animal models of AD and in human AD patients and aged monkey; these structures appear very soon after the initial formation of plaques, are thought to be primary sites of ongoing local amyloid production, and ultrastructural studies have localized BACE1 to dystrophic neurites that appear to be presynaptic/axonal in origin[97, 166-170]. BACE1 accumulation in these structures is likely due to a post-transcriptional mechanism, specifically protein stabilization due to lack of transport to the lysosome. Given my findings that the 5X4CA mice exhibited fewer plaques than the 5XFAD, and previous findings that 5XFAD mice normally exhibit BACE1 accumulation in dystrophic neurites[166], I sought to determine whether BACE4C/A also accumulates in dystrophic neurites. For this I used immunofluorescence co-staining to analyze the level of BACE1 fluorescence associated with 3D6-positive deposits in the brains of 5XFAD and 5X4CA mice. I again found fewer deposits overall in the brains of mice expressing BACE4C/A. In the deposits that were present, I divided the mean

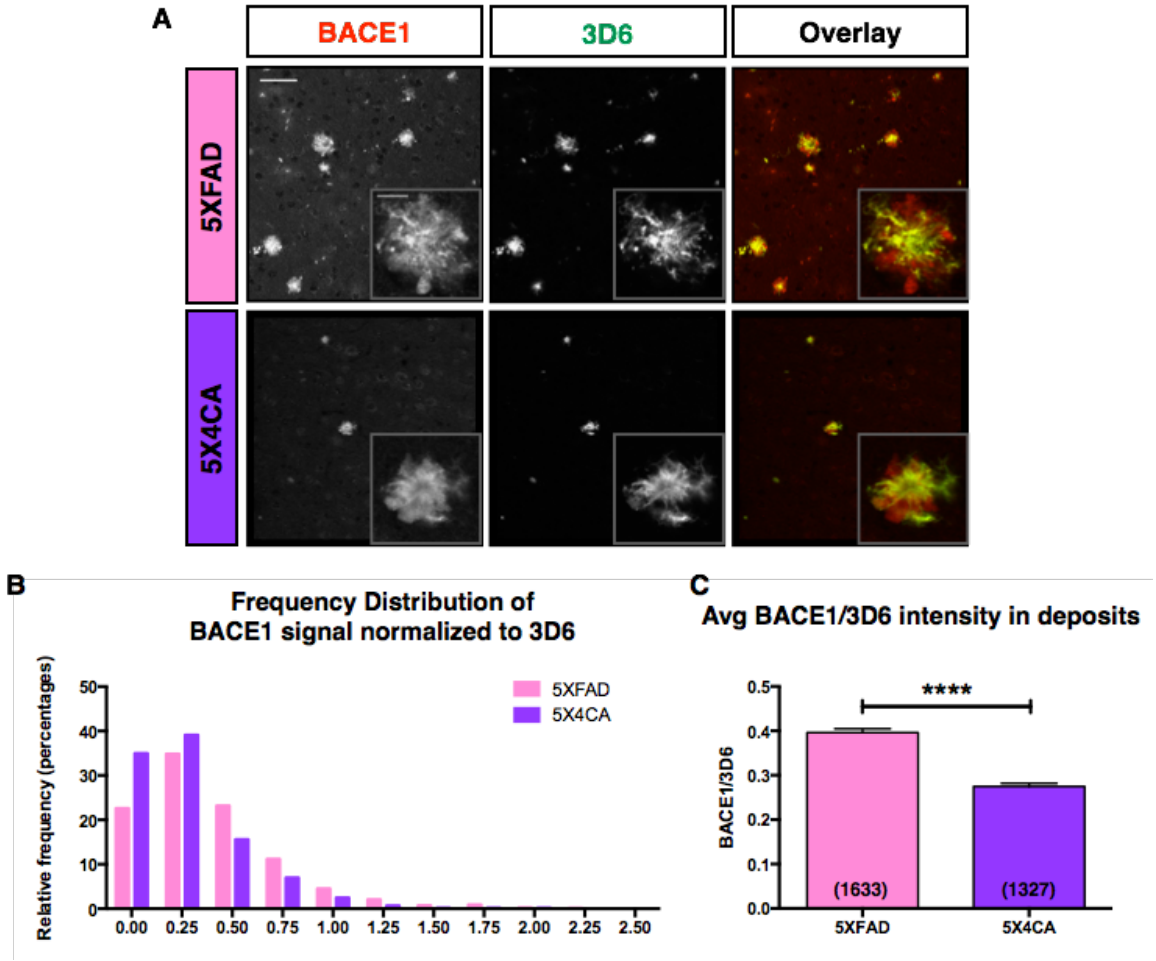

Figure 44. Reduced BACE4C/A accumulation around amyloid deposits compared to BACEWT in 5XFAD transgenic mice. A, BACE1 can be found prominently in association with 3D6-positive deposits, and is higher in 5XFAD deposits. 5X4CA brain tended to have significantly fewer 3D6/BACE1-positive deposits compared to 5XFAD, and the few 5X4CA deposits that were present tended to be smaller, and there tended to be less BACE4C/A accumulation around them compared to BACEWT in 5XFAD brain. Scale bar, 50um; Inset, scale bar, 10um. B, Relative frequency distribution of BACE1 fluorescence normalized to 3D6 fluorescence. The integrated intensity of each was quantified using MetaMorph software, and BACE1 intensity was divided by 3D6 intensity. There were more deposits with little to no BACE4C/A accumulation in the 5X4CA brain compared to BACEWT in 5XFAD brain. C, The average BACE1 fluorescence associated with 3D6 in plaques is significantly diminished in 5XFAD mice expressing BACE4C/A. n = 1633 plaques for 5XFAD, 1327 plaques for 5X4CA, 5 mice each.

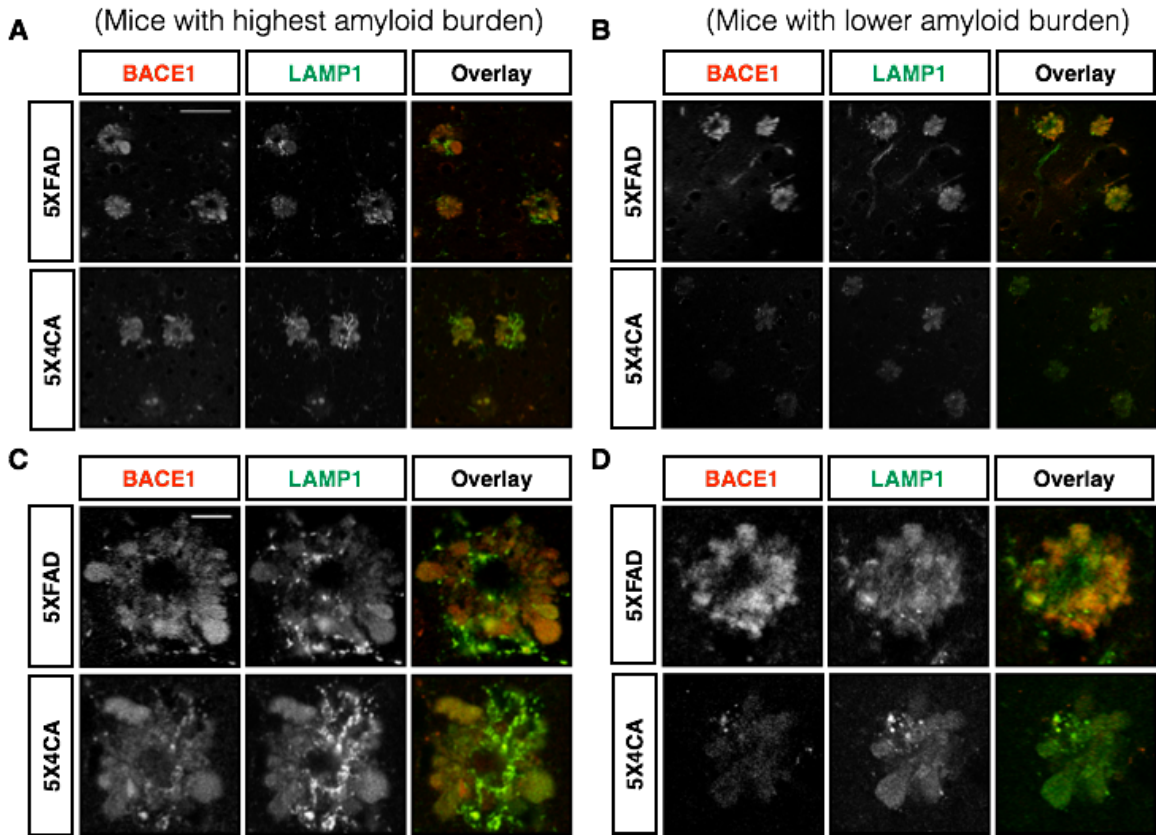

Figure 45. BACE1 is present in LAMP1-positive dystrophic neurites. Representative images from mice with relatively high (A) and low (B) amyloid burden within each group. BACE1 and LAMP1 accumulations form characteristic "donut"-shaped structures. Scale bar, 50um. C & D, Higher power images of dystrophic neurites from A & B. 5X4CA mice exhibited fewer dystrophic neurites, mirroring the decreased amyloid deposition (Fig. 44), and also exhibited somewhat decreased BACE1 fluorescence compared to 5XFAD. Scale bar, 10uM.

fluorescence of BACE1 by that of 3D6 per deposit and plotted the binned data as a histogram. This method controls for any differences in BACE1 fluorescence intensity due to the size of the deposit. The frequency distribution of normalized BACE1 fluorescence associated with 3D6-positive deposits indicated that there were more deposits with no or minimal BACE1 in 5X4CA brain compared to 5XFAD, and there were more deposits with higher levels of BACE1 in 5XFAD brain (Fig. 44a, b). Comparing the average normalized BACE1 fluorescence across all deposits revealed a highly significant decrease of BACE1 fluorescence intensity in BACE4C/A brain (Fig. 44c). These data suggest that the accumulation of BACE1 seen in dystrophic neurites in 5XFAD brain depends on palmitoylation.

To confirm that these amyloid- and BACE1-positive accumulations were truly dystrophic neurites, I co-stained brain sections for BACE1 and LAMP1. LAMP1 is a lysosomal protein elevated in dystrophic neurites, and LAMP1-positive dystrophic neurites are thought to be axonal in origin[169]. Similar to the amyloid-stained deposits, I was able to visualize LAMP1-positive dystrophic neurites as characteristic "donut"-shaped structures, with a hollow core surrounded by BACE1 and LAMP1 fluorescence (Fig. 45). Qualitatively, BACE4C/A levels in dystrophic neurites again appeared reduced when compared to BACE1 WT expressed in 5XFAD brain, even when compared with the 5X4CA mouse exhibiting the highest level of amyloid deposition out of all 5X4CA mice analyzed (Fig. 45a, c). Together, these data suggest that the elevation, i.e. stabilization, of BACE1 that occurs at dystrophic neurites may depend on palmitoylation. The implications of these findings and potential future directions are discussed in the following chapter.

CHAPTER VI

Discussion

I have shown that a palmitoylation-deficient mutant of BACE1 is mislocalized when overexpressed in cultured neurons. Furthermore, I have created a knock-in mouse in which this mutant is expressed at physiological levels and, when crossed with a mouse model of AD, this mutant diminishes Aβ deposition. Specifically, the BACE4C/A mutant is largely, but not completely, excluded from dendritic spines in transfected neurons in culture, and does not undergo axonal enrichment to the extent that the WT does. Levels of BACE4C/A appeared to be diminished overall, and this reduction also occurred by preventing palmitoylation of BACE1 WT by miRNA-mediated knockdown of two palmitoylating enzymes, DHHC-2 and -3. In the knock-in mice, however, the 4C/A mutation did not appear to dramatically affect steady-state BACE1 localization in the brain, despite the lack of palmitoylation. Nevertheless, BACE4C/A expression in a mouse model of AD significantly reduced cerebral amyloid burden. Furthermore, accumulation of BACE1 protein around cerebral amyloid deposits was attenuated in 4C/A knock-in mice, which could explain the reduction of amyloid deposition in these mice. Taken together, these data show that palmitoylation is a post-translational modification that specifically affects BACE1 localization in neurons, and affects APP processing specifically in the context of disease.

BACE1 localization in cultured neurons

I found two main phenotypes of the non-palmitoylatable BACE4C/A when overexpressed in cultured hippocampal neurons. First, I found that the BACE4C/A is

restricted from dendritic spines. I also found that, while BACE1 WT enriched into axons over time in culture, the BACE4C/A mutant did not, and expression of the mutant protein from multiple different constructs and preps was conspicuously and consistently decreased. These latter findings suggest that palmitoylation may play a role in protein stabilization in transfected neurons in culture, although no such difference in protein stabilization was found with the palmitoylation-deficient mutant in non-neuronal cells[119]. Protein turnover rates for palmitoylation-deficient BACE1 may be different in neurons vs. non-neuronal cells; further studies would need to be carried out to demonstrate this.

Lack of non-palmitoylatable BACE1 at the postsynaptic dendritic spine is not unexpected. The dendritic spine is rich in lipid rafts, which are tightly associated with the actin cytoskeleton. As discussed previously, palmitoylation is a common modification among proteins that localize to lipid rafts, and postsynaptically-targeted proteins associate, dissociate, and re-associate with spines via dynamic palmitate cycling in response to synaptic activity. Interestingly, BACE4C/A localization in spines was not completely blocked, showing that palmitoylation-mediated targeting is more efficient, but not an absolute requirement, a common theme throughout this project. It is possible that BACE1 may be important for cleaving postsynaptic proteins, such as Sema4C[64], particularly during the period of synaptogenesis and synapse elimination, when BACE1 expression peaks in the brain.

I, and others in the lab, had made the observation that it was much easier to detect BACE1 in the axon in older transfected neurons. We speculated whether this

was due to specific targeting of BACE1 to the axon, or whether this was an artifact of time after transfection. Arguing against the latter scenario, BACE1 enrichment could not be detected in DIV10 neurons, 5 days after transfection or viral transduction; however, BACE1 axonal enrichment occurred at every time point after transfection in neurons older than DIV12. I have quantified this observation utilizing an axon:dendrite ratio and normalizing to co-expressed Cerulean to account for differences in the level of BACE1 expression due to variable transfection efficiency, and also for differences in fluorescence intensity due to variations in neurite thickness. In both mouse neurons and rat neurons, I have found that BACE1 WT increases localization specifically in the axon, decreasing in the soma and dendrites, while the BACE4C/A never achieves axonal enrichment, and even decreases significantly in all compartments analyzed compared to the WT. I speculate that as neurons mature in culture, more mature synaptic contacts are made, and the increased synaptic activity signals to target BACE1 to the axon; palmitoylation may enhance this process, and so the 4C/A may not respond to synaptic activity as efficiently. An assay to test this theory would be to transfect neurons with either the WT or 4C/A constructs and treat cultures with blockers or inhibitors of synaptic activity for a certain period of time, and then perform axon:dendrite ratio analysis as I have done here. Cultures would need to be sufficiently dense to ensure network activity, and the exact conditions for treatment would need to be worked out on non-transfected neurons to ensure that the neurons stayed healthy; translocation or activation of CamKII or some other synaptic marker would be used as a positive control.

The exact mechanism governing neuron-specific protein targeting to the different polarized compartments (i.e., somatodendritic and axonal) remains to be fully elucidated, and has been an active area of research in neurobiology for a long time. My lab has found compelling evidence that BACE1 undergoes transcytosis, whereby BACE1 is first transported to the dendrite and internalized into endosomes, and is then transported exclusively in the retrograde direction back to the soma, where it is routed selectively to the axon[92, 102, 171]. A significant portion of axon-targeted BACE1 appears to undergo this transcytotic trafficking, and is dependent on EHD1, -3, and Rab11[92, 102]. Given the lack of axon targeting in the non-palmitoylatable BACE4C/A-expressing neurons, I surmised that transcytosis might rely on palmitoylation for efficient transport of internalized BACE1 to the axon. However, attempts to perform live imaging on neurons consistently ended with very low levels of internalized BACE4C/A, below the level necessary for analysis. This is likely not due to any change in the rate of BACE4C/A internalization, since I found comparable levels of internalized BACEWT and 4C/A in neurons, using a FLAG-labeling assay that I developed. BACE4C/A is also found at the plasma membrane of neurons. Interestingly, total BACE4C/A levels, using various different expression constructs, always appeared somewhat decreased, though not always to the level of statistical significance, in contrast to the findings of BACE1 protein stability in non-neuronal cells. In agreement with this notion of neuron-specific diminished BACE4C/A protein stability, knock-down of DHHC-2 and DHHC-3, the palmitoyl transferase enzymes implicated for BACE1 palmitoylation, resulted in decreased BACE1 WT fluorescence throughout the entire neuron compared to

control. DHHC-2 is normally localized to the post-synaptic membrane, while DHHC-3 is a Golgi-resident enzyme; this might explain why the protein level was more drastically reduced with DHHC-3 knockdown compared to DHHC-2 knockdown. Altogether, these data suggest that palmitoylation is important for proper BACE1 intracellular targeting in neurons, and may be necessary for neuron-specific maintenance of BACE1 protein levels.

Phosphorylated BACE1

During the course of my thesis work, I had attempted to perform experiments investigating the localization and role of phosphorylated forms of BACE1, using a phospho-specific antibody that I characterized, PB7. I showed that PB7 is specific only for phosphorylated forms of BACE1, using lysates from HEK293 cells stably expressing BACE1 WT; such lysates treated with phosphatase to remove phosphate groups eliminated the PB7 signal (Fig. 4). Attempts to use PB7 for immunostaining were only successful using cells transfected with BACE1 constructs in which there was no C-terminal tag; BACE1 constructs with N-terminal FLAG-tags stained for PB7 very brightly (Fig. 5). PB7 staining revealed an enrichment of phospho-BACE1 in growth cones of transfected neurons; however, I, and others in the lab, have seen an enrichment of total BACE1 in growth cones, and so an elevated PB7 signal in this compartment is probably due to elevated protein levels overall and not selective for phosphorylated forms of BACE1. Along these lines, BACE S/A, a non-phosphorylatable mutant, is elevated in growth cones, thus the specific role of phosphorylation in this compartment is unclear. Importantly, PB7 did not stain the BACES/A mutant, showing further that the antibody is specific for the

phosphorylated epitope of BACE1. Interestingly, the BACES/A mutant appears to be localized to the surface of neurons, implying that phosphorylation may be necessary for internalization from the neuronal surface in cultured neurons (Fig. 5). Using cultured HEK cells stably expressing various BACE1 constructs, I found that BACEWT and BACE4C/A exhibited a PB7 signal (Fig. 6); hence, the BACE4C/A non-palmitoylatable mutant is capable of undergoing phosphorylation. As expected, the BACES/A mutant did not exhibit a signal, and interestingly, a so-called "phosphomimetic" construct, BACES/D, did not exhibit a signal either, providing further proof of the specificity of the antibody for a phospho-group. Intriguingly, a mutant of BACE1 in which the two leucines in the dileucine motif have been mutated to alanine, "LL/AA", which we have shown does not undergo internalization, also did not exhibit a PB7 signal. It is possible that phosphorylation occurs in an endocytic compartment (since the LL/AA mutant does not appear to be phosphorylated) and facilitates the progression of BACE1 through the endocytic pathway (since the S/A mutant appears to be stuck at the cell surface). Alternatively, it is also possible that the dileucine motif just adjacent to the Ser498 is part of a recognition motif for the enzyme responsible for phosphorylation, or that these two leucine residues are part of the epitope recognized by the PB7 antibody.

The role of BACE4C/A in vivo

From a translational neuroscience perspective, interest in BACE1 biology is ultimately only relevant if it can be traced back to its role in the brain, in health and disease, limiting the usefulness of studies in cultured cells and neurons. I was therefore interested to see if preventing palmitoylation of BACE1, through

expression of the BACE4C/A mutant, would result in the same mislocalization phenotype that I found in cultured neurons, and if this mislocalization would affect APP processing by BACE1. I therefore set out to create a knock-in mouse model, the BACE4C/A mouse. The knock-in mouse allows for a more physiologically relevant analysis of the role that palmitoylation plays in BACE1 biology and APP processing, and based on my data in cultured cells, I hypothesized that BACE4C/A localization would be different compared to BACE1 WT; specifically, I expected that BACE4C/A would be absent from axonal tracts and the presynaptic terminals of the mossy fibers, where BACE1 WT is normally localized. However, histological analysis of brain sections from WT and 4C/A mice revealed no obvious differences in BACE1 localization. In addition to the mossy fibers, I also assessed localization in olfactory bulb sections, as well as the overall morphology of the olfactory glomeruli themselves, since BACE1 is reported to play a role in proper axon guidance of certain specific populations of olfactory neurons. Again, I could not detect any obvious differences in BACE1 localization, or overall morphology, in any brain structures between WT and 4C/A mice. It is possible that, as suggested above, palmitoylation is not absolutely necessary for proper protein targeting, but enhances the efficiency of protein transport. Therefore, while the BACE4C/A may start out less efficiently localized to axons, it may catch up over time. There may also be unknown compensatory mechanisms in place to ensure proper BACE1 targeting, mechanisms that are more obvious in the context of the whole animal rather than simply neurons and glia on a coverslip. In this sense, the discrepancy I find between my in vivo data and my data in cultured cells underscores the importance of

studying protein localization using both methodologies, to get a more complete understanding of how cell biology relates to physiology.

I considered the possibility that there may be biochemically-detectable differences in BACE4C/A expression in the brain. Immunoblot analysis revealed no differences in protein levels at steady state, which is expected for a non-transgenic, gene-targeted mutant expressed by the endogenous promoter and the same protein translational machinery as the WT. I confirmed that the 4C/A does not undergo palmitoylation using an acyl-RAC assay, and also found that the 4C/A is not efficiently targeted to lipid rafts, as expected. Despite this, there were no differences in APP cleavage products, at least by analyzing APP CTFs by immunoblot. Therefore, in healthy mice, palmitoylation, and by extension, lipid raft localization, does not appear to be an absolute requirement for proper BACE1 localization and APP processing in the brain, at least at the levels of analysis studied here.

It is still an open question as to what percentage of BACE1 in the brain undergoes palmitoylation at any given time, and under certain contexts such as health versus stress and disease. I have found that BACE1 localizes to lipid rafts in mouse brain, as a functional assay of BACE1 palmitoylation and subcellular localization, and that the BACE4C/A mutant is significantly reduced in rafts. To optimize detection in this assay, I used forebrain lysates from young (P7) mice, an age at which BACE1 protein levels peak[66] (Fig. 16). The BACE4C/A signal was not completely abolished from rafts; it is possible that this is an artifact of fraction collection starting from the top of the density gradient, resulting in contamination of the upper raft fraction with the lower non-raft proteins, however the gradient

fraction collector that I used is designed to prevent this artifact if used properly. DRM fractionation has been reported to be extremely temperature sensitive[126], and while I performed collections in the cold room, it is entirely possible that, in my hands, the actual temperature of the fractions prior to or during collections was above 4°C. In addition to DRM fractionations, I also performed the acyl-RAC assay to determine palmitoylation state from brain lysates, also from P7 mice. With this assay, I load 100% of the bound fraction, representing palmitoylated protein, and only 10% of unbound, representing non-palmitoylated protein. The fact that I find roughly equivalent band intensities for BACE1 WT in each fraction suggests that roughly 10% of BACE1 in the brain undergoes palmitoylation; however, the binding efficiency of the beads to protein is not 100%, and so this is likely to be an underestimate. Indeed, the assay appears to be inefficient, since all PSD-95 and Flot2 purified in the crude membrane fraction should theoretically be palmitoylated, and yet the PSD95 and Flot2 signals are still detected in the unbound fraction[135, 159]. Regardless, palmitoylation appears to be a modification that is relevant to BACE1 biology in the brain, but the exact effect in healthy brain, beyond mediating lipid raft distribution, is still unclear.

BACE4C/A expression in 5XFAD mice

Despite finding no obvious differences in healthy mice, I wanted to know whether the 4C/A mutation had an effect in the context of AD. I therefore crossed the BACE4C/A mouse line with a transgenic model of AD, the 5XFAD mouse line. Strikingly, these 5X4CA mice expressing the non-palmitoylatable BACE1 mutant exhibited decreased amyloid load compared to the 5XFAD mice expressing

BACEWT. Analysis of BACE1 levels at dystrophic neurites revealed a highly significant decrease of 4C/A compared to WT, providing a possible explanation for the reduced amyloid burden. Intriguingly, while 5X4CA mice showed no differences in the levels of βCTFs, there was a highly significant reduction of +11CTF and concomitant elevation of αCTFs, suggestive of reduced β-cleavage of APP. Treatment of mice with γ-secretase inhibitors would cause an accumulation of βCTF and might make any differences in βCTF production more obvious. However, γ-secretase inhibitors might have other effects that would confound analysis.

Alternatively, if BACE4C/A cleavage is less efficient than BACE1 WT, one might expect that Aβ levels, as measured by ELISA, would be decreased in 5X4CA brain compared to 5XFAD. ELISA analysis of Aβ levels in 5XFAD and 5X4CA was performed by a collaborator, but was deemed unreliable and is currently being repeated by a different group. If there is no significant difference in the level of Aβ between the 5XFAD and 5X4CA, and yet a significant decrease in plaque burden, it might be expected that clearance mechanisms are more efficient in the 5X4CA mice, clearing away soluble Aβ before it has a chance to accumulate in plaques.

To assess BACE1 protein levels in dystrophic neurites, I utilized an anti-BACE1 antibody with its epitope at the C-terminus of the BACE1 protein sequence. Since the C-terminus is also the location of the four Cys to Ala mutations, it is possible that the efficiency of antibody binding depends on the presence of the four cysteine residues, therefore potentially leading to differences in signal due to antibody binding per se and not actually reflective of variable protein levels in a particular compartment. Arguing against this possibility, I used the same antibody

for both biochemical analysis and BACE1 staining in the non-transgenic mice, in which I found comparable levels of BACE1 WT and 4C/A. Yet when I compared the level of BACE1 staining in dystrophic neurites of equivalent size, I consistently found less intense BACE1 staining in mice expressing the BACE4C/A mutant. Staining with anti-BACE1 antibodies that have different epitopes, especially at the N-terminus away from the 4C/A mutation, would resolve this issue more conclusively.

The decrease in BACE4C/A accumulation at dystrophic neurites suggests that palmitoylation is somehow necessary for the BACE1 protein stabilization. Palmitoylation-dependent protein stabilization is a common theme for palmitoylated proteins (reviewed in [172]). For example, palmitoylated lysosomal sorting receptors interact with retromer in endosomes to traffic back to the TGN, while non-palmitoylated receptors will undergo lysosomal degradation[173]. Fas, a signaling receptor involved in cell death and cell survival signaling pathways, reportedly undergoes palmitoylation-dependent protein stabilization due to lack of transport to the lysosome for degradation[174]. It is therefore entirely conceivable that palmitoylation may play a similar role for BACE1 protein stabilization, especially given the consistently lower BACE4C/A levels that I have seen in my experiments with cultured neurons. However, this hypothetical pathway would appear to be a neuron-specific mechanism of BACE1 stability, as no obvious differences were found in BACE4C/A protein stability when expressed in non-neuronal cells[119]. Additionally, the differences in BACE1 protein stabilization due to palmitoylation state were only apparent in dystrophic neurites in the 5XFAD mouse

model, and not in healthy non-transgenic brain, suggesting that stabilization is specific to a cellular context in which the cell is undergoing apoptosis-related stress.

Previous studies have explored the stabilization of BACE1 in dystrophic neurites and linked it to reduced degradation in the lysosome. Activated caspase-3 is elevated in 5XFAD brain[12]. GGA3 is a caspase-3 substrate that undergoes cleavage during apoptosis in a rat model of cerebral ischemia, and this results in stabilization of BACE1 protein levels due to impaired degradation[175]. The impaired degradation is though to be due to decreased transport of BACE1 to the lysosome, in which BACE1 normally undergoes degradation[176]; blocking degradation therefore leads to accumulation in the endosome[177, 178]. These results, taken together with the data from the 5X4CA mouse, support a model in which non-palmitoylated BACE1 undergoes a non-GGA-3-mediated pathway of degradation (Fig. 46), although more experiments would be needed to demonstrate this. Using transfected neurons overexpressing epitope-tagged BACE1 WT and 4C/A, I consistently observed a non-significant decrease of BACE4C/A fluorescence; furthermore, knock-down of the putative enzymes responsible for palmitoylation, DHHC-2 and DHHC-3, resulted in a decrease of BACE1 WT fluorescence throughout the neuron. While this decrease was not striking, and no differences in BACE1 protein levels were detected in healthy WT and 4C/A mice, my results do suggest that a palmitoylation-dependent mode of protein stabilization may exist, but specifically in the context of cellular stress. This alternative degradative pathway is likely not the major pathway taken for BACE1, and would require de-palmitoylation, something that might not occur in the dystrophic neurites of the 5XFAD and AD brain. It would therefore be

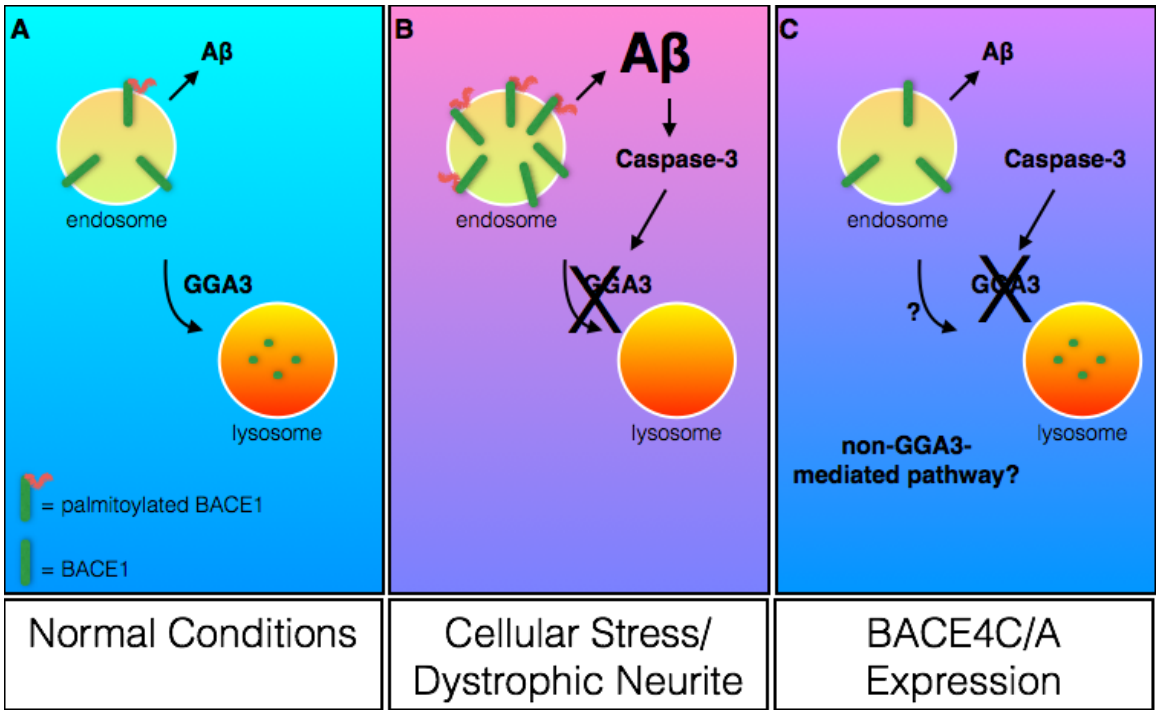

Figure 46. Model for palmitoylation-mediated BACE1 elevation in AD brain. A, Under normal, healthy conditions, BACE1 (green) undergoes palmitoylation (red) and is found at steady-state in the endosome; BACE1 undergoes GGA3-mediated transport to the lysosome where it is degraded. B, Under conditions of cellular stress, for instance at dystrophic neurites, caspase-3 cleaves GGA3, rendering it unable to transport BACE1 to the lysosome; BACE1 therefore accumulates in endosomes where it continues to cleave APP, and Aβ levels become elevated. C, In the 5X4CA mouse, BACE1 levels are not elevated in dystrophic neurites and there is reduced amyloid burden. It is possible that caspase-3 still cleaves GGA3, preventing GGA-3-mediated transport to and degradation in the lysosome; in this case, BACE4C/A may undergo GGA-3-independent transport to the lysosome, thus still enabling degradation in the lysosome and ultimately resulting in less amyloid deposition.

interesting to see if the enzymes that mediate de-palmitoylation are present in dystrophic neurites. Palmitoylation may even interact with another post-translational modification, ubiquitination, which is believed to target transmembrane proteins, including BACE1, to the lysosome[179]. Further studies would need to determine whether the presence of palmitoylation on BACE1 would prevent ubiquitination and ubiquitin-mediated lysosomal targeting.

Conclusion

The findings that very little is changed in the brains of healthy mice expressing the BACE4C/A mutant demonstrates that targeting palmitoylation to subtly alter BACE1 trafficking is a viable strategy to ameliorate APP processing and Aβ production without hampering any of BACE1's other physiological roles. My results also support a model of Aβ-induced BACE1 elevation around plaques that depends on palmitoylation, and that preventing palmitoylation will rescue BACE1 protein degradation.

Bibliography

1. Association, A.s., *2015 Alzheimer's disease facts and figures.* Alzheimers Dement, 2015. **11**(3): p. 332-84.

2. James, B.D., et al., *Contribution of Alzheimer disease to mortality in the United States.* Neurology, 2014. **82**(12): p. 1045-50.

3. Alzheimer, A., et al., *An English translation of Alzheimer's 1907 paper, "Uber eine eigenartige Erkankung der Hirnrinde".* Clin Anat, 1995. **8**(6): p. 429-31.

4. Price, D.L., *New perspectives on Alzheimer's disease.* Annu Rev Neurosci, 1986. **9**: p. 489-512.

5. Jarrett, J.T., E.P. Berger, and P.T. Lansbury, Jr., *The carboxy terminus of the beta amyloid protein is critical for the seeding of amyloid formation: implications for the pathogenesis of Alzheimer's disease.* Biochemistry, 1993. **32**(18): p. 4693-7.

6. Wisniewski, H.M. and R.D. Terry, eds. *Reexamination of the pathogenesis of the senile plaque.* Progress in neuropathology, ed. H.M. Zimmerman. Vol. 2. 1973, Grune & Stratton: New York, London. 1-26.

7. Probst, A., et al., *A special type of senile plaque, possibly an initial stage.* Acta Neuropathol, 1987. **74**(2): p. 133-41.

8. Wisniewski, H.M., et al., *Spectrum of morphological appearance of amyloid deposits in Alzheimer's disease.* Acta Neuropathol, 1989. **78**(4): p. 337-47.

9. Yamaguchi, H., et al., *Diffuse type of senile plaques in the brains of Alzheimer-type dementia.* Acta Neuropathol, 1988. **77**(2): p. 113-9.

10. Yamaguchi, H., et al., *A variety of cerebral amyloid deposits in the brains of the Alzheimer-type dementia demonstrated by beta protein immunostaining.* Acta Neuropathol, 1988. **76**(6): p. 541-9.

11. Serrano-Pozo, A., et al., *Neuropathological alterations in Alzheimer disease.* Cold Spring Harb Perspect Med, 2011. **1**(1): p. a006189.

12. Eimer, W.A. and R. Vassar, *Neuron loss in the 5XFAD mouse model of Alzheimer's disease correlates with intraneuronal Abeta42 accumulation and Caspase-3 activation.* Mol Neurodegener, 2013. **8**: p. 2.

13. Cras, P., et al., *Senile plaque neurites in Alzheimer disease accumulate amyloid precursor protein.* Proc Natl Acad Sci U S A, 1991. **88**(17): p. 7552-6.

14. Glenner, G.G. and C.W. Wong, *Alzheimer's disease: initial report of the purification and characterization of a novel cerebrovascular amyloid protein.* Biochem Biophys Res Commun, 1984. **120**(3): p. 885-90.

15. Glenner, G.G. and C.W. Wong, *Alzheimer's disease and Down's syndrome: sharing of a unique cerebrovascular amyloid fibril protein.* Biochem Biophys Res Commun, 1984. **122**(3): p. 1131-5.

16. Masters, C.L., et al., *Amyloid plaque core protein in Alzheimer disease and Down syndrome.* Proc Natl Acad Sci U S A, 1985. **82**(12): p. 4245-9.

17. Goldgaber, D., et al., *Characterization and chromosomal localization of a cDNA encoding brain amyloid of Alzheimer's disease.* Science, 1987. **235**(4791): p. 877-80.

18. Kang, J., et al., *The precursor of Alzheimer's disease amyloid A4 protein resembles a cell-surface receptor.* Nature, 1987. **325**(6106): p. 733-6.

19. Robakis, N.K., et al., *Molecular cloning and characterization of a cDNA encoding the cerebrovascular and the neuritic plaque amyloid peptides.* Proc Natl Acad Sci U S A, 1987. **84**(12): p. 4190-4.

20. Tanzi, R.E., et al., *Amyloid beta protein gene: cDNA, mRNA distribution, and genetic linkage near the Alzheimer locus.* Science, 1987. **235**(4791): p. 880-4.

21. Goate, A., et al., *Segregation of a missense mutation in the amyloid precursor protein gene with familial Alzheimer's disease.* Nature, 1991. **349**(6311): p. 704-6.

22. Mullan, M., et al., *A pathogenic mutation for probable Alzheimer's disease in the APP gene at the N-terminus of beta-amyloid.* Nat Genet, 1992. **1**(5): p. 345-7.

23. Hardy, J. and D. Allsop, *Amyloid deposition as the central event in the aetiology of Alzheimer's disease.* Trends Pharmacol Sci, 1991. **12**(10): p. 383-8.

24. Selkoe, D.J., *The molecular pathology of Alzheimer's disease.* Neuron, 1991. **6**(4): p. 487-98.

25. Hardy, J.A. and G.A. Higgins, *Alzheimer's disease: the amyloid cascade hypothesis.* Science, 1992. **256**(5054): p. 184-5.

26. Strittmatter, W.J., et al., *Apolipoprotein E: high-avidity binding to beta-amyloid and increased frequency of type 4 allele in late-onset familial Alzheimer disease.* Proc Natl Acad Sci U S A, 1993. **90**(5): p. 1977-81.

27. Corder, E.H., et al., *Gene dose of apolipoprotein E type 4 allele and the risk of Alzheimer's disease in late onset families.* Science, 1993. **261**(5123): p. 921-3.

28. Namba, Y., et al., *Apolipoprotein E immunoreactivity in cerebral amyloid deposits and neurofibrillary tangles in Alzheimer's disease and kuru plaque amyloid in Creutzfeldt-Jakob disease.* Brain Res, 1991. **541**(1): p. 163-6.

29. Wisniewski, T. and B. Frangione, *Apolipoprotein E: a pathological chaperone protein in patients with cerebral and systemic amyloid.* Neurosci Lett, 1992. **135**(2): p. 235-8.

30. Castellano, J.M., et al., *Human apoE isoforms differentially regulate brain amyloid-beta peptide clearance.* Sci Transl Med, 2011. **3**(89): p. 89ra57.

31. Verghese, P.B., et al., *ApoE influences amyloid-beta (Abeta) clearance despite minimal apoE/Abeta association in physiological conditions.* Proc Natl Acad Sci U S A, 2013. **110**(19): p. E1807-16.

32. Miners, J.S., et al., *Abeta-degrading enzymes: potential for treatment of Alzheimer disease.* J Neuropathol Exp Neurol, 2011. **70**(11): p. 944-59.

33. Iwata, N., et al., *Identification of the major Abeta1-42-degrading catabolic pathway in brain parenchyma: suppression leads to biochemical and pathological deposition.* Nat Med, 2000. **6**(2): p. 143-50.

34. Iwata, N., et al., *Metabolic regulation of brain Abeta by neprilysin.* Science, 2001. **292**(5521): p. 1550-2.

35. Hafez, D., et al., *Neprilysin-2 is an important beta-amyloid degrading enzyme.* Am J Pathol, 2011. **178**(1): p. 306-12.

36. Eckman, E.A., et al., *Alzheimer's disease beta-amyloid peptide is increased in mice deficient in endothelin-converting enzyme.* J Biol Chem, 2003. **278**(4): p. 2081-4.

37. Farris, W., et al., *Insulin-degrading enzyme regulates the levels of insulin, amyloid beta-protein, and the beta-amyloid precursor protein intracellular domain in vivo.* Proc Natl Acad Sci U S A, 2003. **100**(7): p. 4162-7.

38. Miller, B.C., et al., *Amyloid-beta peptide levels in brain are inversely correlated with insulysin activity levels in vivo.* Proc Natl Acad Sci U S A, 2003. **100**(10): p. 6221-6.

39. Lambert, M.P., et al., *Diffusible, nonfibrillar ligands derived from Abeta1-42 are potent central nervous system neurotoxins.* Proc Natl Acad Sci U S A, 1998. **95**(11): p. 6448-53.

40. Walsh, D.M., et al., *Naturally secreted oligomers of amyloid beta protein potently inhibit hippocampal long-term potentiation in vivo.* Nature, 2002. **416**(6880): p. 535-9.

41. Lacor, P.N., et al., *Synaptic targeting by Alzheimer's-related amyloid beta oligomers.* J Neurosci, 2004. **24**(45): p. 10191-200.

42. Snyder, E.M., et al., *Regulation of NMDA receptor trafficking by amyloid-beta.* Nat Neurosci, 2005. **8**(8): p. 1051-8.

43. Tang, Y., et al., *Early and selective impairments in axonal transport kinetics of synaptic cargoes induced by soluble amyloid beta-protein oligomers.* Traffic, 2012. **13**(5): p. 681-93.

44. Purro, S.A., E.M. Dickins, and P.C. Salinas, *The secreted Wnt antagonist Dickkopf-1 is required for amyloid beta-mediated synaptic loss.* J Neurosci, 2012. **32**(10): p. 3492-8.

45. Harris, J.A., et al., *Transsynaptic progression of amyloid-beta-induced neuronal dysfunction within the entorhinal-hippocampal network.* Neuron, 2010. **68**(3): p. 428-41.

46. Roberson, E.D., et al., *Amyloid-beta/Fyn-induced synaptic, network, and cognitive impairments depend on tau levels in multiple mouse models of Alzheimer's disease.* J Neurosci, 2011. **31**(2): p. 700-11.

47. Kamenetz, F., et al., *APP processing and synaptic function.* Neuron, 2003. **37**(6): p. 925-37.

48. Allinson, T.M., et al., *ADAMs family members as amyloid precursor protein alpha-secretases.* J Neurosci Res, 2003. **74**(3): p. 342-52.

49. Edbauer, D., et al., *Reconstitution of gamma-secretase activity.* Nat Cell Biol, 2003. **5**(5): p. 486-8.

50. Vassar, R., et al., *Beta-secretase cleavage of Alzheimer's amyloid precursor protein by the transmembrane aspartic protease BACE.* Science, 1999. **286**(5440): p. 735-41.

51. Hussain, I., et al., *Identification of a novel aspartic protease (Asp 2) as beta-secretase.* Mol Cell Neurosci, 1999. **14**(6): p. 419-27.

52. Sinha, S., et al., *Purification and cloning of amyloid precursor protein beta-secretase from human brain.* Nature, 1999. **402**(6761): p. 537-40.

53. Yan, R., et al., *Membrane-anchored aspartyl protease with Alzheimer's disease beta-secretase activity.* Nature, 1999. **402**(6761): p. 533-7.

54. Lin, X., et al., *Human aspartic protease memapsin 2 cleaves the beta-secretase site of beta-amyloid precursor protein.* Proc Natl Acad Sci U S A, 2000. **97**(4): p. 1456-60.

55. Yan, R. and R. Vassar, *Targeting the beta secretase BACE1 for Alzheimer's disease therapy.* Lancet Neurol, 2014. **13**(3): p. 319-29.

56. Cai, H., et al., *BACE1 is the major beta-secretase for generation of Abeta peptides by neurons.* Nat Neurosci, 2001. **4**(3): p. 233-4.

57. Luo, Y., et al., *Mice deficient in BACE1, the Alzheimer's beta-secretase, have normal phenotype and abolished beta-amyloid generation.* Nat Neurosci, 2001. **4**(3): p. 231-2.

58. Ohno, M., et al., *Temporal memory deficits in Alzheimer's mouse models: rescue by genetic deletion of BACE1.* Eur J Neurosci, 2006. **23**(1): p. 251-60.

59. Ohno, M., et al., *BACE1 gene deletion prevents neuron loss and memory deficits in 5XFAD APP/PS1 transgenic mice.* Neurobiol Dis, 2007. **26**(1): p. 134-45.

60. Ohno, M., et al., *BACE1 deficiency rescues memory deficits and cholinergic dysfunction in a mouse model of Alzheimer's disease.* Neuron, 2004. **41**(1): p. 27-33.

61. Giusti-Rodriguez, P., et al., *Synaptic deficits are rescued in the p25/Cdk5 model of neurodegeneration by the reduction of beta-secretase (BACE1).* J Neurosci, 2011. **31**(44): p. 15751-6.

62. Jonsson, T., et al., *A mutation in APP protects against Alzheimer's disease and age-related cognitive decline.* Nature, 2012. **488**(7409): p. 96-9.

63. Hemming, M.L., et al., *Identification of beta-secretase (BACE1) substrates using quantitative proteomics.* PLoS One, 2009. **4**(12): p. e8477.

64. Kuhn, P.H., et al., *Secretome protein enrichment identifies physiological BACE1 protease substrates in neurons.* EMBO J, 2012. **31**(14): p. 3157-68.

65. Lahiri, D.K., et al., *Lessons from a BACE1 inhibitor trial: off-site but not off base.* Alzheimers Dement, 2014. **10**(5 Suppl): p. S411-9.

66. Willem, M., et al., *Control of peripheral nerve myelination by the beta-secretase BACE1.* Science, 2006. **314**(5799): p. 664-6.

67. Hu, X., et al., *Bace1 modulates myelination in the central and peripheral nervous system.* Nat Neurosci, 2006. **9**(12): p. 1520-5.

68. Savonenko, A.V., et al., *Alteration of BACE1-dependent NRG1/ErbB4 signaling and schizophrenia-like phenotypes in BACE1-null mice.* Proc Natl Acad Sci U S A, 2008. **105**(14): p. 5585-90.

69. Zhou, L., et al., *The neural cell adhesion molecules L1 and CHL1 are cleaved by BACE1 protease in vivo.* J Biol Chem, 2012. **287**(31): p. 25927-40.

70. Hitt, B., et al., *beta-Site amyloid precursor protein (APP)-cleaving enzyme 1 (BACE1)-deficient mice exhibit a close homolog of L1 (CHL1) loss-of-function phenotype involving axon guidance defects.* J Biol Chem, 2012. **287**(46): p. 38408-25.

71. Chen, Y., et al., *Alzheimer's beta-secretase (BACE1) regulates the cAMP/PKA/CREB pathway independently of beta-amyloid.* J Neurosci, 2012. **32**(33): p. 11390-5.

72. Cao, L., et al., *The precision of axon targeting of mouse olfactory sensory neurons requires the BACE1 protease.* Sci Rep, 2012. **2**: p. 231.

73. Laird, F.M., et al., *BACE1, a major determinant of selective vulnerability of the brain to amyloid-beta amyloidogenesis, is essential for cognitive, emotional, and synaptic functions.* J Neurosci, 2005. **25**(50): p. 11693-709.

74. Rajapaksha, T.W., et al., *The Alzheimer's beta-secretase enzyme BACE1 is required for accurate axon guidance of olfactory sensory neurons and normal glomerulus formation in the olfactory bulb.* Mol Neurodegener, 2011. **6**: p. 88.

75. Wang, H., et al., *BACE1 knock-outs display deficits in activity-dependent potentiation of synaptic transmission at mossy fiber to CA3 synapses in the hippocampus.* J Neurosci, 2008. **28**(35): p. 8677-81.

76. Wang, H., et al., *Postsynaptic target specific synaptic dysfunctions in the CA3 area of BACE1 knockout mice.* PLoS One, 2014. **9**(3): p. e92279.

77. Cheret, C., et al., *Bace1 and Neuregulin-1 cooperate to control formation and maintenance of muscle spindles.* EMBO J, 2013. **32**(14): p. 2015-28.

78. Thinakaran, G. and E.H. Koo, *Amyloid precursor protein trafficking, processing, and function.* J Biol Chem, 2008. **283**(44): p. 29615-9.

79. Koo, E.H. and S.L. Squazzo, *Evidence that production and release of amyloid beta-protein involves the endocytic pathway.* J Biol Chem, 1994. **269**(26): p. 17386-9.

80. Tomita, S., Y. Kirino, and T. Suzuki, *Cleavage of Alzheimer's amyloid precursor protein (APP) by secretases occurs after O-glycosylation of APP in the protein secretory pathway. Identification of intracellular compartments in which APP cleavage occurs without using toxic agents that interfere with protein metabolism.* J Biol Chem, 1998. **273**(11): p. 6277-84.

81. Malnar, M., et al., *Cholesterol-depletion corrects APP and BACE1 misstrafficking in NPC1-deficient cells.* Biochim Biophys Acta, 2012. **1822**(8): p. 1270-83.

82. Choy, R.W., Z. Cheng, and R. Schekman, *Amyloid precursor protein (APP) traffics from the cell surface via endosomes for amyloid beta (Abeta) production in the trans-Golgi network.* Proc Natl Acad Sci U S A, 2012. **109**(30): p. E2077-82.

83. Okada, H., et al., *Proteomic identification of sorting nexin 6 as a negative regulator of BACE1-mediated APP processing.* FASEB J, 2010. **24**(8): p. 2783-94.

84. Grbovic, O.M., et al., *Rab5-stimulated up-regulation of the endocytic pathway increases intracellular beta-cleaved amyloid precursor protein carboxyl-terminal fragment levels and Abeta production.* J Biol Chem, 2003. **278**(33): p. 31261-8.

85. Cataldo, A.M., et al., *Increased neuronal endocytosis and protease delivery to early endosomes in sporadic Alzheimer's disease: neuropathologic evidence for a mechanism of increased beta-amyloidogenesis.* J Neurosci, 1997. **17**(16): p. 6142-51.

86. Cataldo, A.M., et al., *Endocytic pathway abnormalities precede amyloid beta deposition in sporadic Alzheimer's disease and Down syndrome: differential effects of APOE genotype and presenilin mutations.* Am J Pathol, 2000. **157**(1): p. 277-86.

87. Blanpied, T.A., D.B. Scott, and M.D. Ehlers, *Age-related regulation of dendritic endocytosis associated with altered clathrin dynamics.* Neurobiol Aging, 2003. **24**(8): p. 1095-104.

88. Koo, E.H., et al., *Precursor of amyloid protein in Alzheimer disease undergoes fast anterograde axonal transport.* Proc Natl Acad Sci U S A, 1990. **87**(4): p. 1561-5.

89. Buxbaum, J.D., et al., *Alzheimer amyloid protein precursor in the rat hippocampus: transport and processing through the perforant path.* J Neurosci, 1998. **18**(23): p. 9629-37.

90. Lazarov, O., et al., *Evidence that synaptically released beta-amyloid accumulates as extracellular deposits in the hippocampus of transgenic mice.* J Neurosci, 2002. **22**(22): p. 9785-93.

91. Sheng, J.G., D.L. Price, and V.E. Koliatsos, *Disruption of corticocortical connections ameliorates amyloid burden in terminal fields in a transgenic model of Abeta amyloidosis.* J Neurosci, 2002. **22**(22): p. 9794-9.

92. Buggia-Prevot, V., et al., *A function for EHD family proteins in unidirectional retrograde dendritic transport of BACE1 and Alzheimer's disease Abeta production.* Cell Rep, 2013. **5**(6): p. 1552-63.

93. Cirrito, J.R., et al., *Endocytosis is required for synaptic activity-dependent release of amyloid-beta in vivo.* Neuron, 2008. **58**(1): p. 42-51.

94. Wu, J., et al., *Arc/Arg3.1 regulates an endosomal pathway essential for activity-dependent beta-amyloid generation.* Cell, 2011. **147**(3): p. 615-28.

95. Groemer, T.W., et al., *Amyloid precursor protein is trafficked and secreted via synaptic vesicles.* PLoS One, 2011. **6**(4): p. e18754.

96. Del Prete, D., et al., *APP is cleaved by Bace1 in pre-synaptic vesicles and establishes a pre-synaptic interactome, via its intracellular domain, with molecular complexes that regulate pre-synaptic vesicles functions.* PLoS One, 2014. **9**(9): p. e108576.

97. Kandalepas, P.C., et al., *The Alzheimer's beta-secretase BACE1 localizes to normal presynaptic terminals and to dystrophic presynaptic terminals surrounding amyloid plaques.* Acta Neuropathol, 2013. **126**(3): p. 329-52.

98. Lee, E.B., et al., *BACE overexpression alters the subcellular processing of APP and inhibits Abeta deposition in vivo.* J Cell Biol, 2005. **168**(2): p. 291-302.

99. Shi, Q., et al., *Reduced amyloid deposition in mice overexpressing RTN3 is adversely affected by preformed dystrophic neurites.* J Neurosci, 2009. **29**(29): p. 9163-73.

100. Capell, A., et al., *Apical sorting of beta-secretase limits amyloid beta-peptide production.* J Biol Chem, 2002. **277**(7): p. 5637-43.

101. Sannerud, R., et al., *ADP ribosylation factor 6 (ARF6) controls amyloid precursor protein (APP) processing by mediating the endosomal sorting of BACE1.* Proc Natl Acad Sci U S A, 2011. **108**(34): p. E559-68.

102. Buggia-Prevot, V., et al., *Axonal BACE1 dynamics and targeting in hippocampal neurons: a role for Rab11 GTPase.* Mol Neurodegener, 2014. **9**: p. 1.

103. Deng, M., et al., *Increased expression of reticulon 3 in neurons leads to reduced axonal transport of beta site amyloid precursor protein-cleaving enzyme 1.* J Biol Chem, 2013. **288**(42): p. 30236-45.

104. Das, U., et al., *Activity-induced convergence of APP and BACE-1 in acidic microdomains via an endocytosis-dependent pathway.* Neuron, 2013. **79**(3): p. 447-60.

105. Wang, C.L., et al., *VPS35 regulates developing mouse hippocampal neuronal morphogenesis by promoting retrograde trafficking of BACE1.* Biol Open, 2012. **1**(12): p. 1248-57.

106. Udayar, V., et al., *A paired RNAi and RabGAP overexpression screen identifies Rab11 as a regulator of beta-amyloid production.* Cell Rep, 2013. **5**(6): p. 1536-51.

107. Lefort, R., J. Pozueta, and M. Shelanski, *Cross-linking of cell surface amyloid precursor protein leads to increased beta-amyloid peptide production in hippocampal neurons: implications for Alzheimer's disease.* J Neurosci, 2012. **32**(31): p. 10674-85.

108. Ye, X. and Q. Cai, *Snapin-mediated BACE1 retrograde transport is essential for its degradation in lysosomes and regulation of APP processing in neurons.* Cell Rep, 2014. **6**(1): p. 24-31.

109. Das, S.S. and G.A. Banker, *The role of protein interaction motifs in regulating the polarity and clustering of the metabotropic glutamate receptor mGluR1a.* J Neurosci, 2006. **26**(31): p. 8115-25.

110. Huse, J.T., et al., *Maturation and endosomal targeting of beta-site amyloid precursor protein-cleaving enzyme. The Alzheimer's disease beta-secretase.* J Biol Chem, 2000. **275**(43): p. 33729-37.

111. He, X., et al., *Memapsin 2 (beta-secretase) cytosolic domain binds to the VHS domains of GGA1 and GGA2: implications on the endocytosis mechanism of memapsin 2.* FEBS Lett, 2002. **524**(1-3): p. 183-7.

112. Pastorino, L., et al., *The carboxyl-terminus of BACE contains a sorting signal that regulates BACE trafficking but not the formation of total A(beta).* Mol Cell Neurosci, 2002. **19**(2): p. 175-85.

113. Prabhu, Y., et al., *Adaptor protein 2-mediated endocytosis of the beta-secretase BACE1 is dispensable for amyloid precursor protein processing.* Mol Biol Cell, 2012. **23**(12): p. 2339-51.

114. Walter, J., et al., *Phosphorylation regulates intracellular trafficking of beta-secretase.* J Biol Chem, 2001. **276**(18): p. 14634-41.

115. von Arnim, C.A., et al., *Demonstration of BACE (beta-secretase) phosphorylation and its interaction with GGA1 in cells by fluorescence-lifetime imaging microscopy.* J Cell Sci, 2004. **117**(Pt 22): p. 5437-45.

116. He, X., et al., *Biochemical and structural characterization of the interaction of memapsin 2 (beta-secretase) cytosolic domain with the VHS domain of GGA proteins.* Biochemistry, 2003. **42**(42): p. 12174-80.

117. He, X., et al., *GGA proteins mediate the recycling pathway of memapsin 2 (BACE).* J Biol Chem, 2005. **280**(12): p. 11696-703.

118. Benjannet, S., et al., *Post-translational processing of beta-secretase (beta-amyloid-converting enzyme) and its ectodomain shedding. The pro- and transmembrane/cytosolic domains affect its cellular activity and amyloid-beta production.* J Biol Chem, 2001. **276**(14): p. 10879-87.

119. Vetrivel, K.S., et al., *Alzheimer disease Abeta production in the absence of S-palmitoylation-dependent targeting of BACE1 to lipid rafts.* J Biol Chem, 2009. **284**(6): p. 3793-803.

120. Fukata, Y. and M. Fukata, *Protein palmitoylation in neuronal development and synaptic plasticity.* Nat Rev Neurosci, 2010. **11**(3): p. 161-75.

121. Noritake, J., et al., *Mobile DHHC palmitoylating enzyme mediates activity-sensitive synaptic targeting of PSD-95.* J Cell Biol, 2009. **186**(1): p. 147-60.

122. El-Husseini Ael, D., et al., *Synaptic strength regulated by palmitate cycling on PSD-95.* Cell, 2002. **108**(6): p. 849-63.

123. Huang, K. and A. El-Husseini, *Modulation of neuronal protein trafficking and function by palmitoylation.* Curr Opin Neurobiol, 2005. **15**(5): p. 527-35.

124. Pitto, M., et al., *Palmitic is the main fatty acid carried by lipids of detergent-resistant membrane fractions from neural and non-neural cells.* Neurochem Res, 2002. **27**(7-8): p. 729-34.

125. Pike, L.J., *Rafts defined: a report on the Keystone Symposium on Lipid Rafts and Cell Function.* J Lipid Res, 2006. **47**(7): p. 1597-8.

126. Sonnino, S. and A. Prinetti, *Membrane domains and the "lipid raft" concept.* Curr Med Chem, 2013. **20**(1): p. 4-21.

127. Kuo, Y.M., et al., *Elevated low-density lipoprotein in Alzheimer's disease correlates with brain abeta 1-42 levels.* Biochem Biophys Res Commun, 1998. **252**(3): p. 711-5.

128. Wolozin, B., et al., *Decreased prevalence of Alzheimer disease associated with 3-hydroxy-3-methyglutaryl coenzyme A reductase inhibitors.* Arch Neurol, 2000. **57**(10): p. 1439-43.

129. Refolo, L.M., et al., *Hypercholesterolemia accelerates the Alzheimer's amyloid pathology in a transgenic mouse model.* Neurobiol Dis, 2000. **7**(4): p. 321-31.

130. Fabelo, N., et al., *Altered lipid composition in cortical lipid rafts occurs at early stages of sporadic Alzheimer's disease and facilitates APP/BACE1 interactions.* Neurobiol Aging, 2014. **35**(8): p. 1801-12.

131. Riddell, D.R., et al., *Compartmentalization of beta-secretase (Asp2) into low-buoyant density, noncaveolar lipid rafts.* Curr Biol, 2001. **11**(16): p. 1288-93.

132. Ehehalt, R., et al., *Amyloidogenic processing of the Alzheimer beta-amyloid precursor protein depends on lipid rafts.* J Cell Biol, 2003. **160**(1): p. 113-23.

133. Bhattacharyya, R., C. Barren, and D.M. Kovacs, *Palmitoylation of amyloid precursor protein regulates amyloidogenic processing in lipid rafts.* J Neurosci, 2013. **33**(27): p. 11169-83.

134. Sakurai, T., et al., *Membrane microdomain switching: a regulatory mechanism of amyloid precursor protein processing.* J Cell Biol, 2008. **183**(2): p. 339-52.

135. El-Husseini Ael, D., et al., *Polarized targeting of peripheral membrane proteins in neurons.* J Biol Chem, 2001. **276**(48): p. 44984-92.

136. Leyt, J., et al., *Cholesterol-sensitive modulation of transcytosis.* Mol Biol Cell, 2007. **18**(6): p. 2057-71.

137. Horton, A.C. and M.D. Ehlers, *Neuronal polarity and trafficking.* Neuron, 2003. **40**(2): p. 277-95.

138. Horton, A.C. and M.D. Ehlers, *Secretory trafficking in neuronal dendrites.* Nat Cell Biol, 2004. **6**(7): p. 585-91.

139. Meckler, X., et al., *Reduced Alzheimer's disease ss-amyloid deposition in transgenic mice expressing S-palmitoylation-deficient APH1aL and nicastrin.* J Neurosci, 2010. **30**(48): p. 16160-9.

140. Vetrivel, K.S., et al., *Loss of cleavage at beta'-site contributes to apparent increase in beta-amyloid peptide (Abeta) secretion by beta-secretase (BACE1)-glycosylphosphatidylinositol (GPI) processing of amyloid precursor protein.* J Biol Chem, 2011. **286**(29): p. 26166-77.

141. Thinakaran, G., et al., *Endoproteolysis of presenilin 1 and accumulation of processed derivatives in vivo.* Neuron, 1996. **17**(1): p. 181-90.

142. Kaech, S. and G. Banker, *Culturing hippocampal neurons.* Nat Protoc, 2006. **1**(5): p. 2406-15.

143. Ryan, T.A., et al., *The kinetics of synaptic vesicle recycling measured at single presynaptic boutons.* Neuron, 1993. **11**(4): p. 713-24.

144. Forrester, M.T., et al., *Site-specific analysis of protein S-acylation by resin-assisted capture.* J Lipid Res, 2011. **52**(2): p. 393-8.

145. Wessel, D. and U.I. Flugge, *A method for the quantitative recovery of protein in dilute solution in the presence of detergents and lipids.* Anal Biochem, 1984. **138**(1): p. 141-3.

146. Oakley, H., et al., *Intraneuronal beta-amyloid aggregates, neurodegeneration, and neuron loss in transgenic mice with five familial Alzheimer's disease mutations: potential factors in amyloid plaque formation.* J Neurosci, 2006. **26**(40): p. 10129-40.

147. Hayashi, T., G.M. Thomas, and R.L. Huganir, *Dual palmitoylation of NR2 subunits regulates NMDA receptor trafficking.* Neuron, 2009. **64**(2): p. 213-26.

148. Lin, D.T., et al., *Regulation of AMPA receptor extrasynaptic insertion by 4.1N, phosphorylation and palmitoylation.* Nat Neurosci, 2009. **12**(7): p. 879-87.

149. Gauthier-Kemper, A., et al., *Interplay between phosphorylation and palmitoylation mediates plasma membrane targeting and sorting of GAP43.* Mol Biol Cell, 2014. **25**(21): p. 3284-99.

150. Dotti, C.G., J.A. Esteban, and M.D. Ledesma, *Lipid dynamics at dendritic spines.* Front Neuroanat, 2014. **8**: p. 76.

151. Matus, A., *Actin-based plasticity in dendritic spines.* Science, 2000. **290**(5492): p. 754-8.

152. Kaech, S., et al., *Isoform specificity in the relationship of actin to dendritic spines.* J Neurosci, 1997. **17**(24): p. 9565-72.

153. Fischer, M., et al., *Rapid actin-based plasticity in dendritic spines.* Neuron, 1998. **20**(5): p. 847-54.

154. Fukata, Y., et al., *Local palmitoylation cycles define activity-regulated postsynaptic subdomains.* J Cell Biol, 2013. **202**(1): p. 145-61.

155. Sala, C., et al., *Regulation of dendritic spine morphology and synaptic function by Shank and Homer.* Neuron, 2001. **31**(1): p. 115-30.

156. Hering, H., C.C. Lin, and M. Sheng, *Lipid rafts in the maintenance of synapses, dendritic spines, and surface AMPA receptor stability.* J Neurosci, 2003. **23**(8): p. 3262-71.

157. Hotulainen, P. and C.C. Hoogenraad, *Actin in dendritic spines: connecting dynamics to function.* J Cell Biol, 2010. **189**(4): p. 619-29.

158. Greaves, J., J.A. Carmichael, and L.H. Chamberlain, *The palmitoyl transferase DHHC2 targets a dynamic membrane cycling pathway: regulation by a C-terminal domain.* Mol Biol Cell, 2011. **22**(11): p. 1887-95.

159. Neumann-Giesen, C., et al., *Membrane and raft association of reggie-1/flotillin-2: role of myristoylation, palmitoylation and oligomerization and induction of filopodia by overexpression.* Biochem J, 2004. **378**(Pt 2): p. 509-18.

160. Aicart-Ramos, C., R.A. Valero, and I. Rodriguez-Crespo, *Protein palmitoylation and subcellular trafficking.* Biochim Biophys Acta, 2011. **1808**(12): p. 2981-94.

161. Vetrivel, K.S., et al., *Spatial segregation of gamma-secretase and substrates in distinct membrane domains.* J Biol Chem, 2005. **280**(27): p. 25892-900.

162. Deyts, C., et al., *Novel GalphaS-protein signaling associated with membrane-tethered amyloid precursor protein intracellular domain.* J Neurosci, 2012. **32**(5): p. 1714-29.

163. Sadleir, K.R., et al., *Abeta reduction in BACE1 heterozygous null 5XFAD mice is associated with transgenic APP level.* Mol Neurodegener, 2015. **10**: p. 1.

164. Arndt, S.S., et al., *Individual housing of mice--impact on behaviour and stress responses.* Physiol Behav, 2009. **97**(3-4): p. 385-93.

165. Green, K.N., et al., *Glucocorticoids increase amyloid-beta and tau pathology in a mouse model of Alzheimer's disease.* J Neurosci, 2006. **26**(35): p. 9047-56.

166. Zhao, J., et al., *Beta-site amyloid precursor protein cleaving enzyme 1 levels become elevated in neurons around amyloid plaques: implications for Alzheimer's disease pathogenesis.* J Neurosci, 2007. **27**(14): p. 3639-49.

167. Condello, C., A. Schain, and J. Grutzendler, *Multicolor time-stamp reveals the dynamics and toxicity of amyloid deposition.* Sci Rep, 2011. **1**: p. 19.

168. Zhang, X.M., et al., *Beta-secretase-1 elevation in transgenic mouse models of Alzheimer's disease is associated with synaptic/axonal pathology and amyloidogenesis: implications for neuritic plaque development.* Eur J Neurosci, 2009. **30**(12): p. 2271-83.

169. Gowrishankar, S., et al., *Massive accumulation of luminal protease-deficient axonal lysosomes at Alzheimer's disease amyloid plaques.* Proc Natl Acad Sci U S A, 2015. **112**(28): p. E3699-708.

170. Cai, Y., et al., *beta-Secretase-1 elevation in aged monkey and Alzheimer's disease human cerebral cortex occurs around the vasculature in partnership with multisystem axon terminal pathogenesis and beta-amyloid accumulation.* Eur J Neurosci, 2010. **32**(7): p. 1223-38.

171. Buggia-Prevot, V. and G. Thinakaran, *Significance of transcytosis in Alzheimer's disease: BACE1 takes the scenic route to axons.* Bioessays, 2015. **37**(8): p. 888-98.

172. Linder, M.E. and R.J. Deschenes, *Palmitoylation: policing protein stability and traffic.* Nat Rev Mol Cell Biol, 2007. **8**(1): p. 74-84.

173. McCormick, P.J., et al., *Palmitoylation controls recycling in lysosomal sorting and trafficking.* Traffic, 2008. **9**(11): p. 1984-97.

174. Rossin, A., et al., *Fas palmitoylation by the palmitoyl acyltransferase DHHC7 regulates Fas stability.* Cell Death Differ, 2015. **22**(4): p. 643-53.

175. Tesco, G., et al., *Depletion of GGA3 stabilizes BACE and enhances beta-secretase activity.* Neuron, 2007. **54**(5): p. 721-37.

176. Koh, Y.H., et al., *BACE is degraded via the lysosomal pathway.* J Biol Chem, 2005. **280**(37): p. 32499-504.

177. Kang, E.L., et al., *BACE1 protein endocytosis and trafficking are differentially regulated by ubiquitination at lysine 501 and the Di-leucine motif in the carboxyl terminus.* J Biol Chem, 2012. **287**(51): p. 42867-80.

178. Kang, E.L., et al., *Ubiquitin regulates GGA3-mediated degradation of BACE1.* J Biol Chem, 2010. **285**(31): p. 24108-19.

179. Piper, R.C. and J.P. Luzio, *Ubiquitin-dependent sorting of integral membrane proteins for degradation in lysosomes.* Curr Opin Cell Biol, 2007. **19**(4): p. 459-65.